November 2022

Frequency Domain Diffuse Optics Spectroscopies for Quantitative Measurement of Tissue Optical Properties

Sadhu Moka
University of South Florida

Frequency Domain Diffuse Optics Spectroscopies for Quantitative Measurement of Tissue Optical Properties

by

Sadhu Moka

A dissertation submitted in partial fulfillment
of the requirements for the degree of
Doctor of Philosophy
Department of Electrical Engineering
College of Engineering
University of South Florida

Major Professor: Ashwin B. Parthasarathy, Ph.D.
Andrew Hoff, Ph.D.
Stephen Saddow, Ph.D.
Robert Frisina, Ph.D.
Ann Eddins, Ph.D.

Date of Approval:
November 23, 2022

Keywords: Modulation, Multi-frequency, Blood Oxygenation, Blood Flow

Dedication

To the glory and honor of my Lord and Saviour, Jesus Christ.

To my parents Stephen and Sumitra Moka, my siblings Francis and Shalom who are my constant support.

To my extended family, friends and the body of Christ.

Acknowledgments

This endeavor of mine wouldn't been possible without the help of many. Firstly, I would like to thank my Lord and Savior, Jesus Christ for his unending grace and mercy that sustained me over the years.

I want to extend my deepest gratitude to my Major Professor, Dr. Ashwin Parthasarathy, for believing in me and giving the opportunity to pursue my PhD at TROPICS laboratory. Being the first PhD student in his newly established lab at University of South Florida, I got to have great experiences along with the growth of the lab. I have learned a great deal from Dr. Parthasarathy over the last five years, not just technical and professional skills but also to be a better human. His expertise in biomedical instrumentation is highly appreciable and innovative and has helped me to reshape my research methodologies. I also had the privilege to be teaching assistant for his undergraduate core class, Electromagnetic theory class for ten semesters that helped me to acquire skills in training, mentoring. Altogether, Dr. Ashwin has been a great support throughout my PhD journey.

I would like to thank my committee members - Dr. Andrew Hoff, Dr. Ann Eddins, Dr. Robert Frisina and Dr. Stephen Saddow for providing me inputs and insights in a timely manner. Their feedback during my proposal helped me to realign my perspective on the research approach. I also would like to acknowledge Dr. Supraja Anand for being the chairperson of my defense committee. Dr. Anand and Dr. Eddins have been gracious to me in giving access to use the NIRS instrument in communication sciences and disorders department to validate the systems I built.

During my time at USF, I have met great people. Firstly, I would like to acknowledge Penaz Sultana Parveen Mohammad for all the help and assistance. We both started in the lab at the same time and she has become more like a sister over the years. Her expertise in

data analysis has helped me to learn a lot and I have adapted many of those methodologies in my projects. I appreciate all the help with the experiments and setups. Her support made a lot of things easier during my PhD journey

I would like to thank Abdul Mohaimen Safi for being a great researcher in the lab. Together we have brainstormed many ideas and tried many new approaches. His constant spirit of curiosity has been encouraging to think differently and out of the box. We also had an alternative business plan of starting a restaurant if none of the ideas we tried hadn't worked, but thankfully our projects worked out.

I should mention Steve Sheehy for being a great help in resurrecting the DOS system and helping with system design, wiring and the experiments. Steve was always willing to put in the work and try new methodologies. I would like to thank Arindam Biswas for making my time at lab fun and exciting. I also would like to acknowledge Dillon Buffone, Mitch Harrah, Dheeraj Yalama, Abdallah Atallah, Nikola Otic, Stephen Cini for all the support.

I also would like to acknowledge EE staff - Diana Hamilton, Kristen Brandt, Cherie Dilley and the chair - Dr. Ferekides. I sincerely appreciate all the help from Catherine Burton in guiding me through out the dissertation process.

My family has been a great support during my time at USF. I wouldn't have sustained the journey without the love, prayers and support of my dad - Stephen Vara Prasad, mom - Sumitra Devi, brother - Francis Ebenezer Moka and sister - Shanthi Shalom Moka. I am indebted to them for everything they have done.

I also want to mention my late grandmother, Shantha Leela for taking care of me throughout my childhood and helping me to become the person I am now. I want to thank my aunt, Pallapati Grace Suseela for being a great support to me and my family.

I would like to thank my extended family especially my aunt and uncle Jesse and Krupavaram Chintada, for extending their help whenever needed and always being there for us. I extend my gratitude to Vineela and Vijay Pallapati, Rebecca and Emmanuel Pallapati (late), Jhansi and Sudhakar Pallapati and cousins - Pragna Angel, Honey Marvel, Joshua Prabath,

Joyce, Monami Angelica, Moses Abhishek, Joseph John Vinay and Esther Shobhitha for the consistent support via long group calls.

I also want to thank the members of Christ Church, Kakinada for interceding for me day in and day out. I wouldn't have achieved all that I have without the prayer support of my church back home.

I wouldn't have made it to USA without the relentless pursuit of Mahesh Saka and his family. I would like to thank Mahesh for being a great friend.

I also would like to acknowledge Vishwa Teja Alaparthy, for being a great support when I first arrived in Tampa and guiding me with reaching out to professors.

I am blessed to have Bill and Margie Cooper, senior pastors at Cornerstone Christian Church and the Pastoral team, continually upholding me in their prayer and encouraging me. I want to thank Christian Benecke for being a great mentor personally and spiritually in my personal life and giving counsel whenever needed, Gabriel Cintron for being a great brother in Christ since I've arrived to US.

I deeply appreciate the support of my roommates - Bradley Shaw, for being an encourager, Jonathan Barnett, for being a man of faith, Matthew Wilkinson, for all the deep insights and David Gottwik, for being a man of deep convictions. I started living with them in the first year of my PhD and their constant encouragement have kept me going. I should mention the endless rides from them to campus when I didn't have a car.

I am grateful for Bianca Carolina Guzman, for being a great friend and dreamer over the years, encouraging me with words and actions of Christ's love. I also want to acknowledge Sarah Kasey Boston, for being great sister in Christ and always giving quality advice, Mary Margaret Irene Lumapas for being kind to me, Amber Kay Arnold, Audra Barkwell, Angel Ball and Sarah Burroughs for being great friends.

I also would like to acknowledge Benson Smith, for being a great brother in Christ. Together we had several spontaneous adventures which made my PhD life fun. I want to thank Daniel Osborne for a great brother in Christ and for interceding consistently,

Zachariah Beasley for being a great friend and helping me in both professional and personal life - Conversations over coffee in his office at USF are a great memory.

Ravela Family - Joseph, Deena, Jesvin and Joel were like a second family for me, allowing me to stay at their house to write the dissertation and included me in all the fun stuff along with their family. I sincerely appreciate their support.

Finally I would like to thank Pastor George Matthew and Indian community group at Arise Church, Christian Riveron and the 'In Jesus Name' prayer group, Garret Hopper and Sold family for all the prayers and support.

Table of Contents

List of Tables

List of Figures

Abstract

Tissue oxygen saturation, blood flow and blood volume are physiological bio-markers of tissue health. Diffuse Optical Spectroscopy(DOS) and Diffuse Correlation Spectroscopy (DCS) are two complementary approaches to measure tissue oxygen saturation and blood flow respectively. Quantitative Diffuse Optical Spectroscopy (DOS) uses multi-spectral intensities of near-infrared light that have been modulated at RF frequencies to estimate static tissue optical properties and hence concentrations of oxygenated and de-oxygenated hemoglobin. Diffuse Correlation Spectroscopy estimates tissue dynamics - i.e., blood flow, by measuring temporal intensity auto-correlation function of back scattered light diffusing through the tissue. Conventionally, DCS instruments use coherent light sources with constant intensity. This dissertation focuses on applying frequency domain methods to DOS and DCS to improve measurement fidelity and reduce systemic errors prevalent in current technology. To this end, I introduce a new broadband heterodyne demodulation technique for multi-frequency frequency domain DOS (FD-DOS) and a novel frequency domain DCS (FD-DCS) technique to estimate tissue oxygenation and blood flow index from a single measurement. First, I demonstrate a frequency domain DOS system that measures amplitude and phase of diffuse photon density waves at different source-modulating frequencies and a single source-detector separation. This multi-frequency FD-DOS system reduces measurement errors due to the partial volume effects and overcomes the major drawbacks in the conventional frequency domain DOS instruments that operate at a single modulation frequency. Critically, the (heterodyne) demodulation is performed using off-the-shelf RF components, which decreases instrument size, reduces complexity and increasing the data acquisition rate without requiring large data sets. I validate this new method with controlled experiments on tissue simulating phantoms and *in-vivo* experiments. In the second

part of the dissertation, I extend the multi-frequency aspect to DCS and develop a novel technique - Frequency Domain Diffuse correlation Spectroscopy(FD-DCS). FD-DCS uses intensity modulated light source at RF frequencies to measure frequency dependent intensity auto correlation functions and estimate static and dynamic optical properties of the tissue at a single source-detector separation in a single measurement. FD-DCS system can be easily executed by modifying the source of conventional DCS system to a RF modulated source. I derive a new general photon diffusion model that describes tissue light propagation and a new frequency domain solution for diffuse correlation density waves (DCDW). I built a bench-top prototype, and validated this new theory with experiments on tissue simulating phantom experiments. FD-DCS eliminates the measurement errors caused by differences in tissue sampling volumes and source-detector positions of DOS and DCS systems, thereby eliminating the need for hybrid DOS-DCS system.

Chapter 1: Introduction

1.1 Introduction

Optical methods based on the diffusion of light through tissue, hold the ability to probe a wide variety of tissue types, and measure endogenous bio-markers of tissue health from structures a few centimeters below the surface. [6,36] Optical methods are broadly applicable to any tissue type because they employ non-ionizing radiation, are non-invasive, and are portable. Due to this niche combination of clinical utility and measurement versatility, optical technologies have tremendous potential and power, to be a ubiquitous clinical bedside monitor of tissue function.

Quantitative measurements of tissue function, and technologies that facilitate them, impact all aspects of biomedical research from disease diagnosis and treatment monitoring to physiological modeling of healthy and pathological tissues. Since the discovery of the near infrared 'optical window' in 1977, [59] optical technologies have facilitated niche *in vivo* measurements of deep-tissue hemodynamics, because they are noninvasive, are safe and easy to use, and they offer endogenous sensitivity to two important markers of tissue function – tissue blood flow (oxygen delivery) and tissue oxygen saturation (oxygen consumption) [38,87]. Often, the primary goal of these noninvasive measurements is to elicit the effect of focal changes in tissue function; for example, hemodynamic changes due to localized strokes/brain injuries [20, 39, 40, 44, 48], to image [7, 26, 85, 112] or monitor hemodynamics of localized tumors in the body [21, 27, 30, 31, 36], and functional activation of specific neuronal circuits in the brain. [38, 41, 52, 57, 64, 67, 71, 88, 98, 111] However, the accuracy and fidelity of focal hemodynamic measurements is confounded by systemic biases [15] introduced by instrumentation approaches that require optical detection/measurements at multiple spatial positions

on the surface and heterogeneous tissue geometries. The primary goal of this dissertation is to develop a new class of diffuse optical instruments that will permit robust quantitative monitoring of focal responses in both oxygen saturation and blood flow, with measurements from one source-detector pair.

Currently, two complementary optical technologies are used to quantitatively measure tissue hemodynamics – Diffuse Correlation Spectroscopy (DCS) estimates tissue perfusion by analyzing the temporal fluctuations of highly coherent light that has diffused through tissue [13,14]. Multi-distance Diffuse Optical Spectroscopy (DOS) estimates tissue oxygenation from the differential absorption of light at two or more wavelengths [14,37,42,49,50,107]. In multi-distance DOS, amplitude and phase changes of intensity modulated source are used to obtain the optical parameters at multiple source detector separations. However, these multi-distance measurements suffer from errors due to the partial volume effect; i.e., data recorded at different source-detector separations originate from different tissue regions under the probe (both laterally and in depth). Thus, unless tissue is completely homogeneous, estimates of tissue properties from multi-distance tissue optics measurements are prone to systemic errors. [72, 73] To overcome these limitations, I implement DOS and DCS with intensity modulated sources, and perform frequency resolved measurements of light intensity (DOS) or intensity auto-correlation functions (DCS). Critically, these frequency-resolved measurements can be performed at a single-source detector separation.

In the first part of the dissertation, I develop and validate a 'multi frequency Frequency Domain Diffuse Optical Spectroscopy'(mfFDDOS) system that can estimate the tissue oxygenation at a single source-detector separation. This system introduces a new heterodyne demodulation method to parse amplitude and phase changes from frequency resolved measurements of detected intensity.

The combination of quantitative estimates of tissue hemoglobin concentrations along with blood flow and tissue oxygen saturation measured by these optical techniques, yield important information about the tissue metabolic rate of oxygen, as well as overall tissue

health, function and pathology. Conventional approaches to bedside optical monitoring combine DCS with multi-distance DOS in a bulky hybrid probe to simultaneously measure both static (oxygen concentration) and dynamic (blood flow) tissue properties [4,22,25,43,65, 71, 110]. However, simple combination of these two technologies could result in systematic errors in estimation of tissue hemodynamics and metabolism in heterogeneous tissues, or when monitoring focal changes like functional activation.

The goal of the second part of this dissertation is to address this limitation by adapting DCS to quantitatively and simultaneously measure blood flow and blood oxygenation in a new class of diffuse optics instruments. More specifically, I develop and validate a novel Frequency Domain Diffuse Correlation Spectroscopy (FD-DCS) approach for fast optical bedside monitoring of tissue hemodynamics from a single data set measured at one detector location. In addition, I show that FD-DCS is a general model describing the diffusion of coherent light through tissue, and that conventional DOS and DCS are its special cases.

1.2 Dissertation Organization

Outline of my dissertation is as follows:

Chapter 2 provides a brief introduction to Diffuse Optical methods - DOS and DCS, the underlying theory and various solutions of these two methods with respect to the source types.

In chapter 3, I have introduced a new 'Broadband Frequency Domain DOS system with a heterodyne demodulation at single source-detector separation'. This new system uses off-the-shelf equipment to produce increased data acquisition speeds and throughput while reducing cost and size. In this chapter, I explain the need for multi- distance DOS systems and briefly outlay prior work. I present the instrumentation methods, validation experiments and results.

Chapter 4 introduces a novel 'Frequency Domain Diffuse correlation Spectroscopy(FD-DCS)' system that can estimate blood oxygenation and blood flow in a single measurement at a single source-detector separation. This system eliminates the need for the bulky *in situ* hybrid DOS - DCS system and thereby the systematic errors that arise in the measurement. The new model developed for FD-DCS can be considered as the general photon diffusion model of light transport in the tissue. The chapter includes theory for the new model, characterization experiments, validation experiments and results.

Chapter 5 concludes the dissertation by outlaying the possible future application with the systems I developed.

Chapter 2: Diffuse Optics for Quantitative Tissue Spectroscopy

2.1 Introduction

Optical methods are widely employed in clinical and biomedical research because light is inherently sensitive to a number of tissue physiological properties [35]. In particular, light in near infrared wavelengths exhibit characteristic sensitivity to the concentrations of oxygenated and de-oxygenated hemoglobin and blood flow in the tissue. Generally, these properties are indicative of tissue health and can be used to diagnose and track several critical conditions in medical field. For example, blood flow and blood oxygenation levels in a malignant tumors are different from that of normal tissue, because tumors are typically hypervascularized due to angiogenesis.

Existing non-invasive clinical technologies like Magnetic Resonance Imaging (MRI), Computer Tomography (CT) are used extensively to characterize and image tissue structure. These radiological modalities provide lifesaving information by acquiring images of good spatial resolution of different parts of the body, as appropriate for the disease. However, these imaging modalities are ill-suited for bedside monitoring applications, because they use ionizing radiation (CT), they are expensive, and they often need specialized suites for imaging. On the other hand, optical methods like Diffuse Optical Spectroscopy(DOS) and Diffuse Correlation Spectroscopy(DCS) use non-ionizing light to continuously measure tissue parameters with a portable bedside instrument. Thus, they fill a critical gap in the clinical infrastructure for bedside monitoring of tissue physiology. Optical methods can also measure tissue function, which tells how tissue behaves in response to external stimuli, diseases and other medical condition [103, 105]

Significant development in this field has been made possible with the discovery of optical window by Jobsis in late 1970's [59–61]. Fig. 2.1 shows the a measure of tissue absorption by different components in tissue. The absorption of light in tissue by water and hemoglobin chromophores is relatively low in the near infrared region ($650 - 950$ nm) allowing light to penetrate deep ($2 - 4$ cm) into the tissue. In addition, scattering of light in tissue can be approximated with a negative power law; low average scattering of near-infrared light allows photons to propagate deep into the tissue. Furthermore, light in tissue is mostly forward scattering, which allows photons that have diffused into tissue to reflect back to the surface for detection and analysis. In this regime of relatively, low absorption, and high scattering, light propagation in thick tissues can be modeled as a diffusive process and can be described by a Photon Diffusion Equation [56].

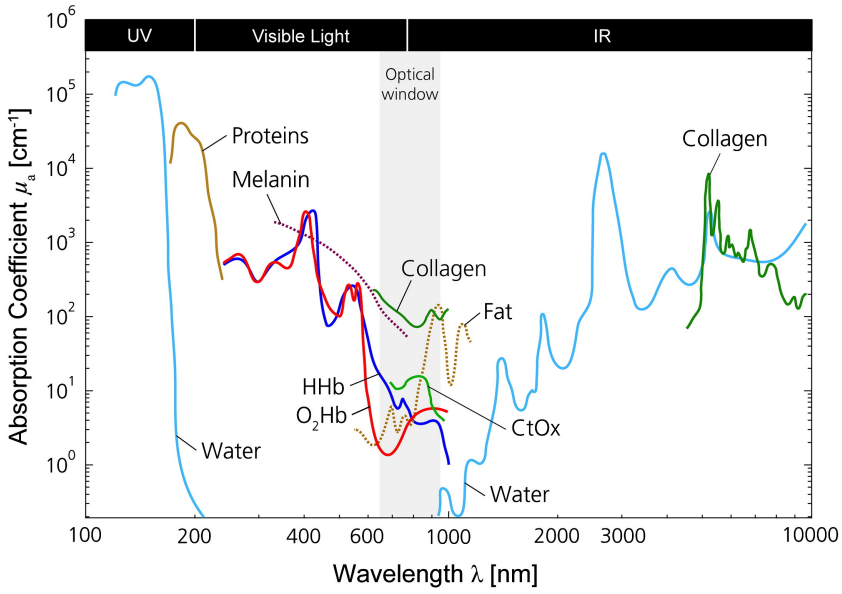

Figure 2.1: Absorption spectra of different chromophores. Figure adapted with permission from [90]

2.2 Light Transport in Tissue

Propagation of light through tissue in the NIR region is primarily characterized by two process - absorption and scattering [56].

2.2.1 Absorption

Absorption refers to the loss of energy by a photon as it propagates/diffuses through tissue. Typically, this energy is converted to heat, but it can also lead to effects such as fluorescence. The light attenuation in the tissue is described by absorption coefficient (μ_a). $1/\mu_a$ is the absorption mean free path, the average distance traveled by a photon in the tissue before it is absorbed. Absorption coefficient is also linearly related to the tissue chromophore concentration. Considering oxy-hemoglobin and de-oxy hemoglobin are the strongest absorbing endogenous tissue chromophores, tissue absorption coefficient can be written as: $\mu_a = \epsilon_{HbO} C_{HbO} + \epsilon_{HbR} C_{HbR}$. Here C_{HbO} and C_{HbR} are the concentrations of oxygenated and de-oxygenated hemoglobin (units of μM), ϵ_{HbO} and ϵ_{HbR} are the corresponding molar extinction coefficients $(cm^{-1}/(moles/liter))$. Typical values of μ_a for tissue at NIR wavelengths are around 0.02 - 0.3 cm^{-1}. Multi-wavelength tissue absorption measurements allow measurement of chromophore concentration by using the spectra of these chromophores.

2.2.2 Scattering

Scattering refers to the deviation in the light path of photons as it interacts with tissue. This deviation occurs due to refraction of light through microscopic refractive index changes in the tissue. Biological tissues vary in the refractive index spatially in the order of the NIR light wavelengths, allowing to probe structural information of tissue molecules and chromophores. The heterogeneous regions of the tissue makes the tissue a highly scattering medium at NIR wavelengths allowing to probe deep tissue lengths.

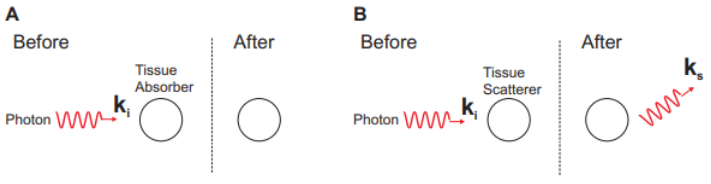

Figure 2.2: Absorption and scattering interaction of photons with tissue chromophores. Figure adapted with permission from [5]

The distance traveled by a photon before it is scattered in the tissue is scattering mean free path and its reciprocal is the tissue scattering coefficient (μ_s). Typical values of μ_s for NIR wavelengths are around 100 - 1000 cm^{-1}. Tissue scattering can be elastic(e.g., Rayleigh and Mie scattering) or inelastic(Raman scattering). Elastic scattering refers to scattering of photons where light energy is conserved while the incident light energy is different than the scattered light energy in the case of inelastic scattering.

While Raman scattering can be used to probe tissue molecular properties, most scattering in tissue is elastic. In this dissertation, we primarily deal with diffusion of light in tissue using relatively low illumination intensities; in this regime, we consider scattering to be elastic.

Absorption coefficient and scattering coefficient, together is called the total attenuation coefficient (μ_t)

$$\mu_t = \mu_a + \mu_s \tag{2.1}$$

The inverse of the total attenuation coefficient is the Mean Free Path (MFP). For the NIR wavelengths, scattering coefficients are higher than the absorption coefficient as scattering is more dominant in those regions.

Although, the scattering coefficient gives information about the scattering in the tissue, it does not include information of the direction of the scattering. The information about the direction of scattering can be obtained by scattering anisotropy factor (g) which is given by $g =< cos\theta >$, a measure of the average scattering angle. g varies from -1 to 1; positive values of g denote forward scattering and negative values of g indicate back scattering. Scattering is isotropic when $g = 0$. Tissue is mostly forward scattering with $g \approx 0.9$. Formal expressions for the anisotropy factor can be obtained from the Heyney-Greenstein phase function [10, 53].

The usage of the scattering phase function allows us to find the length that photon travels before the direction is randomized and loses knowledge of its initial direction. This is called as reduced photon scattering length, random-walk step length, or transport mean free path.

The inverse of the transport mean free path is the reduced scattering coefficient and is given by

$$\mu_s' = \mu_s(1-g) \tag{2.2}$$

Typical values of reduced scattering coefficient in tissue is around $10 cm^{-1}$. The transport attenuation coefficient which is a better indicator of tissue penetration depths than the total attenuation coefficient in biological tissues that are highly anisotropic scattering medium is given by

$$\mu_{tr} = \mu_a + \mu_s' \tag{2.3}$$

2.2.3 Photon Diffusion Equation

Light transport in tissue can be modeled as diffusion process, enabling us to quantitatively measure absorption and scattering in tissue. A full derivation of light diffusion in tissue is beyond the scope of this thesis, and is best covered in numerous text books [10, 38]. Here, we limit our discussion to solutions of the photon diffusion equation, and how they can be leveraged for quantitative tissue spectroscopy. Briefly, the Photon Diffusion Equation (PDE) can be derived from the Radiative Transport Equation (RTE) after applying few simplifying approximations: (a) Light radiation is assumed to be nearly isotropic, (b) tissue is rotationally symmetric (μ_a, μ_s are independent of the direction of light travel), (c) the Radiative Transport Equation is valid, and (d) refractive index between scattering events is homogeneous. With these approximations, the Photon Diffusion equation is given by:

$$\nabla.[D(\vec{r},t)\nabla\phi(\vec{r},t)] - \upsilon\mu_a(\vec{r},t)\phi(\vec{r},t) - \frac{\partial\phi(\vec{r},t)}{\partial t} = -\upsilon S(\vec{r},t) \tag{2.4}$$

Here, $S(\vec{r},t)(Wcm^{-3})$ is the power per unit volume being emitted radially outwards at a time t from a position $\vec{r}$. $D(\vec{r}) \equiv v/(3(\mu_s'(\vec{r}) + \mu_a(\vec{r})))$ is the Photon diffusion coefficient;

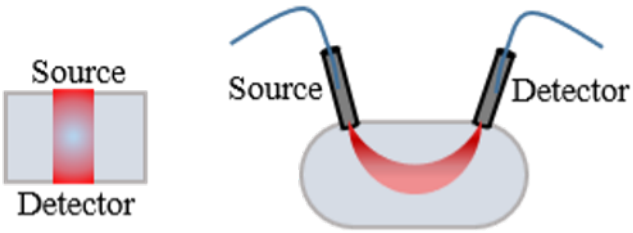

Figure 2.3: Tissue light propagation geometries: Transmission and Reflection

$\phi(\vec{r}, t)(Wcm^{-2})$ is light fluence rate, the power per unit area at point $\vec{r}$ and time t radiating outwards from an element of infinitesimal volume. Photon Diffusion equation is only valid when $\mu_s' \gg \mu_a$, radiance is isotropic, fluence transmitted also has rotational symmetry, source is isotropic, and temporal flux variations are slow compared to the frequency of light.

2.3 Diffuse Optical Spectroscopy/Near Infrared Spectroscopy

Diffuse Optical Spectroscopy (DOS) or Near Infrared Spectroscopy(NIRS) refers to the opto-electronic instrumentation, and analysis methods to practically measure solutions to the Photon Diffusion Equation. [8, 24, 28, 29, 32, 58, 69, 78, 91, 94, 102] The goal of a DOS measurement is to quantitatively estimate tissue absorption and scattering coefficients, and thereby compute tissue oxygen saturation. Practically, DOS signals can be measured from tissue using either transmission geometry or reflection geometry, as seen in Fig. 2.3. Transmission geometry cannot be used in thick tissues ($> 8cm$), as the light is fully absorbed in the tissue over long distances distances. Reflection geometries are more practical for thick tissues, where tissue is assumed to be semi-infinite and homogeneous. In a simple DOS arrangement for semi-infinite homogeneous reflection geometry, NIR light is transmitted into the tissue sample using an optical fiber. A portion of light is reflected back after being absorbed/scattered by multiple cells in the tissue. The reflected light from the tissue is collected by another optical fiber a certain distance away from the source on the tissue surface called the source detector separation (ρ). Reflected light is typically recorded using photo detectors such as a photo diode or a a Photo Multiplier Tube (PMT).

2.3.1 DOS Methods

Practically, three types of solutions to the Photon Diffusion Equation can be realized with DOS depending on the sources. 1. Frequency Domain Diffuse Optical Spectroscopy (FD-DOS). 2. Continuous Wave NIR Spectroscopy /Diffuse Optical Spectroscopy (CW NIRS/DOS). 3. Time Domain Diffuse Optical Spectroscopy (TD-DOS). This thesis focuses on frequency domain methods for diffuse optics, and hence I discuss FD-DOS approaches in detail below. Continuous wave and time-domain methods are discussed briefly for completeness.

2.3.1.1 Frequency Domain Diffuse Optical Spectroscopy

In Frequency Domain Diffuse Optical Spectroscopy (FD-DOS), tissue is illuminated with light, whose intensity is modulated at RF frequencies. The propagation of the intensities through tissue forms a photon diffusion wave which can travel up to 2 - 4 cm deep into the tissue. These are called Diffuse Photon Density Waves (DPDW) and have been shown to have wave properties. [17,38] The photon diffusion wave experiences a decrease in amplitude and changes in phase as it travels through the tissue. Amplitude and phase of the reflected diffusion wave at a given source-detector separation forms a frequency domain solution to the Photon Diffusion Equation. Practically, an analytical (or computational) solution (i.e., amplitude and phase of detected light power) to the Photon Diffusion Equation in a homo-

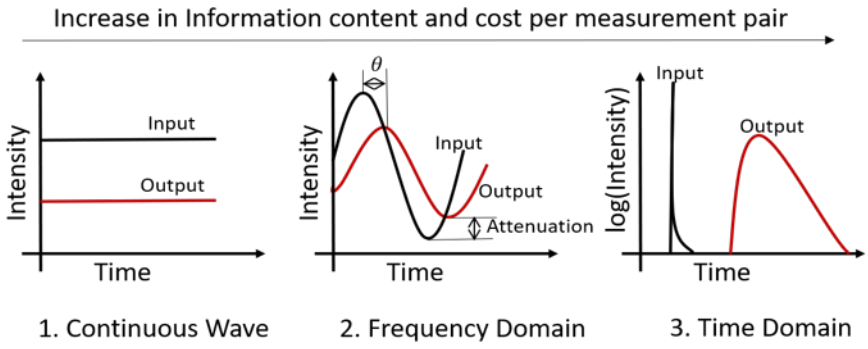

Figure 2.4: DOS methods - different sources. Figure adapted with permission from [72]

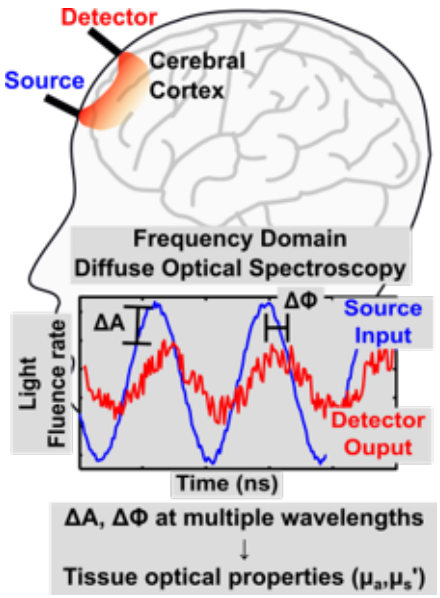

Figure 2.5: A typical cerebral FD-DOS measurement

geneous, semi-infinite medium is compared to measured quantities to compute tissue optical properties.

In FD-DOS, the intensity of source is modulated at radio frequencies. The source term in FD-DOS contains ac and dc components and is given by equation 2.5.

$$S(\vec{r}, t) = S_{dc}(\vec{r}) + S_{ac}(\vec{r})e^{-i\omega t} \tag{2.5}$$

Here, $\omega = 2\pi f$ is the angular frequency of modulation, where f is the frequency of modulation. At a position $\vec{r}_s$ in the tissue, the source fluence rate is given by equation 2.6, where $\delta(\vec{r} - \vec{r}_s)$ is three-dimensional Dirac delta function.

$$S(\vec{r}, t) = S_o(1 + e^{i\omega t})\delta(\vec{r} - \vec{r}_s) \tag{2.6}$$

This intensity modulated light source will produce a continuous wave component and an oscillating component with the same modulation frequency. Light fluence rate at a distance

r and time t is given by equation 2.7.

$$\phi(\vec{r}, t) = \Phi_{dc}(\vec{r}) + \Phi_{ac}(\vec{r})e^{-i\omega t} \tag{2.7}$$

Substituting the source term and the light fluence rate in the Photon Diffusion Equation 2.4,

$$\nabla.(D(\vec{r})\nabla\Phi_{dc}(\vec{r})) - \upsilon\mu_a\Phi_{cw}(\vec{r}) = -\upsilon S_d c(\vec{r} - \vec{r}_s) \tag{2.8}$$

$$\nabla.(D(\vec{r})\nabla\Phi_{ac}(\vec{r})) - \upsilon\mu_a(\vec{r}) + i\omega)\Phi_{ac}(\vec{r}) = -\upsilon S_a c(\vec{r} - \vec{r}_s) \tag{2.9}$$

For homogeneous media, equation 2.8 and 2.9 simplify to

$$(\nabla^2 - \kappa_0^2)\Phi_{dc}(\vec{r}) = -\frac{S_d c\upsilon}{D}\delta(\vec{r} - \vec{r}_s) \tag{2.10}$$

$$(\nabla^2 - \kappa^2)\Phi_{ac}(\vec{r}) = -\frac{S_a c\upsilon}{D}\delta(\vec{r} - \vec{r}_s) \tag{2.11}$$

$\kappa_o^2 = \upsilon\mu_a/D$, $\kappa^2 = (\upsilon\mu_a - i\omega)/D$ and κ is the wave vector. The solution for equation 2.11 is fluence rate in the form of a damped wave and is called Diffuse Photon Density Wave (DPDW). DPDW is given by equation

$$\Phi(\vec{r}, t) = A(\vec{r})exp[i(\omega t - \theta(\vec{r}))] \tag{2.12}$$

$A(\vec{r})$ and $\theta(\vec{r})$ are the amplitude and phase of the wave and relate to the real (κ_r) and complex imaginary (κ_i) parts of the wave vector. To obtain the optical parameters with the DPDW, amplitude and phase are measured either at multiple source detector separations or multiple frequencies.

$$A(\vec{r}) = \frac{S_0\upsilon}{4\pi Dr}[exp(-\kappa_r\vec{r})] \tag{2.13}$$

$$\theta(r) = \kappa_i\vec{r} \tag{2.14}$$

Table 2.1: Table defining terms in semi-infinite solution to PDE

Symbol	***Quantity***
S_o	Input Power
$\upsilon = c/n$	Speed of light in tissue
$Z_b = \frac{2}{3} l_t r \frac{1+R_eff}{1-R_eff}$	Location of 'image' source; extrapolated zero boundary
R_eff	Fresnel reflection coefficient
$l_{tr} \approx 1/\mu_s'$	Transport mean free path
$\kappa^2 = (\mu_a - i\omega)/D$	Wave vector
$r_1^2 = \rho^2 + l_{tr}^2$; $r_b^2 = \rho^2 + (2z_b + l_{tr})^2$;	

The solution of Photon Diffusion Equation for semi-infinite homogeneous medium in reflection geometry is given by equation 2.15, obtained by solving semi-infinite frequency domain Green's function for extrapolated – zero boundary condition.

$$\Phi(\rho, \omega, \lambda) = \frac{S_0 \upsilon}{4\pi D} \left[\frac{exp(-\kappa r_1)}{r_1} - \frac{exp(-\kappa r_b)}{r_b} \right] \tag{2.15}$$

Here, $\Phi(\rho, \omega, \lambda)$ is fluence rate at source-detector separation (ρ), intensity modulation frequency (ω) and wavelength (λ). Other parameters are described in Table 2.1

κ_r and κ_i are related to μ_a and μ_s as shown in equation 2.16 and equation 2.17

$$\kappa_r = \left(\frac{\upsilon^2 \mu_a^2 + \omega^2}{D^2} \right)^{1/4} cos \left[\frac{1}{2} arctan(\frac{\omega}{\upsilon \mu_a}) \right] \tag{2.16}$$

$$\kappa_r = \left(\frac{\upsilon^2 \mu_a^2 + \omega^2}{D^2} \right)^{1/4} sin \left[\frac{1}{2} arctan \frac{\omega}{\upsilon \mu_a} \right] \tag{2.17}$$

Finally, tissue absorption coefficient is linearly related to the concentration of chromophores and is dependent on wavelength.

$$\mu_a(\lambda) = \sum_i \varepsilon_i(\lambda) c_i \tag{2.18}$$

where, $\varepsilon_i(\lambda)$ is the extinction coefficient of the i^{th} chromophore, and c_i is the concentration.

Practically, a FD-DOS system is realized as shown in the Fig 2.6. Laser diodes having wavelengths in the near infrared region are used as light sources. To drive the laser, a current driver is employed. In FD-DOS this current is modulated at RF frequencies ranging from 0.05– 1 GHz using a bias tee. A reference signal is generated by splitting the optical signal with a $90-10$ fiber splitter; 90% is used to illuminate the tissue. Alternatively, the reference signal can be obtained by splitting the RF signal. To transport the light from the source to the tissue, optical fibers of 0.5 – 3 mm core diameter are used. A custom probe is built to hold the optical fibers onto the tissue. The system shown in the Figure 2.5 shows DOS implemented to measure cerebral tissues. Light travels through the tissue as diffuse photon density waves and the back-reflected light is collected using a detector at source – detector separation ($2 \sim 5$ cm). Typically, the back-reflected light is detected using a photo diode or a photo multiplier tube. The output from the detector is an electrical current, proportional to the detected intensity, which is converted to a voltage signal and amplified using a trans-impedance amplifier. The amplitude and phase of this amplified signal are measured to estimate the optical parameters.

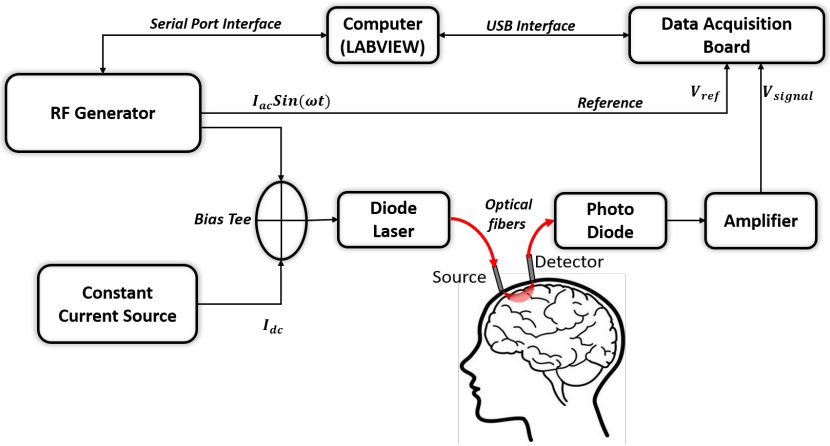

Figure 2.6: FD-DOS instrumentation

Amplitude (A) and phase (θ) of the detected fluence rate at the tissue surface can be estimated with different demodulation techniques. Demodulation and extraction of these parameters can be performed using either analog or digital methods. Analog demodulation

approaches use discrete radio frequency components like mixers and filters. The most common analog demodulation method is IQ demodulation, which is shown in figure 2.7. Here, the detected intensity (modulated at RF frequencies) is directed to the RF ports of two mixers. A reference signal is directed to the Local Oscillator (LO) port of one mixer, and a 90° phase shifted reference signal is directed to the second mixer. The in-phase (I) and quadrature (Q) components, which represent $A\cos\phi$ and $A\sin\phi$ are attained at the Intermediate Frequency (IF) ports after low pass filtering, which are used to compute the Amplitude (A) and phase (ϕ). If the frequency of the reference signal is the same as signal frequency, the demodulation is referred to as Homodyne. Heterodyne demodulation refers to the mixing of the signal with that of a slightly different frequency to 'down convert' the amplitude and phase to a lower 'beat' frequency. While homodyne systems use fewer RF components, heterodyne systems can be more sensitive because the phase detection is performed at a lower frequency. In either case, care should be taken to properly shield RF elements to avoid signal leakage, and prevent noise contamination. Analog methods are also not flexible to implement; scaling the system would require multiple discrete components for larger systems. Alternatively, digital demodulation methods use Analog to Digital Converters (ADC) to directly sample the reference and detected signals simultaneously. ADC's digitize the analog signal, which is stored in a computer for post processing with software like MATLAB (Mathworks, MA) or LabVIEW (National Instruments, Austin, TX), to retrieve Amplitude and Phase. Off-the-shelf ADC devices are extensively available at different sampling rates, to satisfy the Nyquist sampling rule.

Note that FD solutions to the Photon Diffusion Equation vary with both source detector separation (ρ) and frequency of modulation (ω). So far, most FD-DOS systems have used a multi-distance approach – i.e., they measure amplitude and phase at different source detector separations to estimate tissue optical properties. To implement this multi distance approach, amplitude and phase measurements must be made at each separation which may require the use of multiple sources and detectors (increase in cost and complexity) or the use of an optical

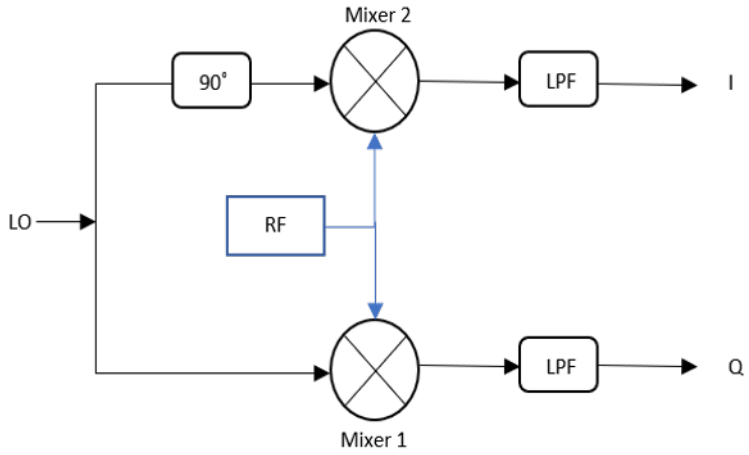

Figure 2.7: IQ demodulation

switch (increase in measurement time). Critically, light measured at different source detector separations sample different depths of tissue, and hence multi-distance measurements are systemically affected by tissue heterogeneities. Alternatively, some studies have recently suggested FD-DOS measurements at multiple modulation frequencies and at a single source-detector separation. These multi-frequency FD-DOS measurements can be performed with instruments that are simpler. Critically, measurements made at different frequencies are less affected by tissue heterogeneities because measurements at different frequencies sample the same tissue volume. I detail the state-of-the art multi-frequency FD-DOS instruments, and advances I have made to this technology in Chapter 3.

2.3.1.2 Continuous Wave

In Continuous Wave Near Infrared Spectroscopy (CW NIRS), constant intensity of near infrared light is used to illuminate the tissue and the reflected diffuse light is detected at a specified source detector separation $(1 \sim 3)$ cm. Thus, continuous wave measurement is the easiest to implement. Measured intensity at the detector is attenuated in comparison to the source intensity due to absorption of light by tissue chromophores such as oxy-hemoglobin(HbO) and de-oxy-hemoglobin(HbR) [33, 45, 92]. Changes in these concentrations, e.g., due to functional activation, impart changes in the measured intensity, which

can be analyzed using the modified Beer-Lambert Law. [5] CW NIRS only measures changes in concentrations and cannot estimate absolute values because we cannot separate light attenuation due to absorption from those due to scattering. This is evident by realizing that the light detected at the detector can be expressed as a special case of the frequency domain solution to the Photon Diffusion Equation (equation 2.8), with $(\omega = 0)$

$$\Phi_{cw}(\vec{r}) = \frac{\upsilon S_0}{4\pi D\vec{r}} \left[exp(-\left[\frac{\upsilon \mu_a}{D}\right]^{1/2} \vec{r}) \right] \tag{2.19}$$

In CW-NIRS measurement performed at one source-detector separation, the detected intensity change is due to a combination of the absorption coefficient, μ_a, and the diffusion coefficient, $D = \upsilon/3(\mu_a + \mu_s')$. If a CW-NIRS measurement is performed at different source detector separations, the measured fluence as a function of source-detector separation r would follow a negative exponential trend, which can be fit to Equation 2.8 to estimate the effective attenuation coefficient $\mu_{eff} = \sqrt{3\mu_a(\mu_a + \mu_s')}$.

2.3.1.3 Time Domain

Time-Domain Diffuse Optical Spectroscopy (TD-DOS) uses light pulses of very short duration (≈ 100 ps) to illuminate the tissue. Time domain systems track their arrival times of these photon pulses at a detector placed on the surface to estimate the photon diffusion time-of-flight (DTOF) curves. Practically, TD-DOS is the impulse response of tissue, and its solution is the inverse Fourier transform of frequency domain solution.

$$\Phi(\vec{r}, t) = \frac{\upsilon S_0}{(4\pi Dt)^{3/2}} exp\left[-\frac{r^2}{4Dt} - \mu_a \upsilon t \right] \tag{2.20}$$

where, t is the time. These theoretical models for light propagation in tissue enable estimation of absolute values of absorption co-efficient μ_a and scattering co-efficient μ_s and thereby, oxy and deoxy-hemoglobin concentrations. TD-DOS systems are difficult to implement because of the high-power short duration pulses, need for fast electronics, high-speed

detection, and the need to accurately characterize the instrument response function. Recent advancements in the photonics and semiconductor industry is promising for increased usage of TD-DOS systems [55, 81, 83].

2.4 Diffuse Correlation Spectroscopy

Diffuse Correlation Spectroscopy(DCS) is a complementary optical method to measure tissue dynamics, specifically blood flow (F). DCS measures temporal intensity fluctuations of highly coherent laser light scattered through tissue. Light diffuses through the tissue via multiple path-lengths from the source to the detector. At the detector, electric fields of the multiply scattered light via multiple path-lengths interfere causing a 'speckle' pattern to develop at the detector. When the scattering agents are dynamic (red blood cells in our case), the speckle pattern, and the intensities, fluctuate in time. To quantify blood flow, the auto-correlation functions of these fluctuating intensities are calculated, and fit to a diffusion model. Fast decay of the intensity auto-correlation function implies high flow while slower decay implies low flow. The normalized intensity auto-correlation function that is measured at the detector is given by equation 2.21

$$g_2(\tau) = \frac{\langle I(t)I(t+\tau)\rangle_t}{\langle I(t)\rangle^2} \tag{2.21}$$

Here, $I(t)$ is intensity at the detector at time t and $I(t+\tau)$ is the time shifted intensity with a delay time τ.

The diffusive process in DCS is modeled by correlation diffusion equation (CDE) which is given by

$$[\nabla^2 D - \upsilon\mu_a - 2\upsilon\mu_s'\kappa_o^2 F\tau]G_1(\tau) = -\upsilon S_o \tag{2.22}$$

Here, $G_1(\tau)$ is the electric field auto-correlation function, μ_a and μ_s' are the tissue absorption and scattering coefficients, D is photon diffusion coefficient, υ is the speed of light in tissue,

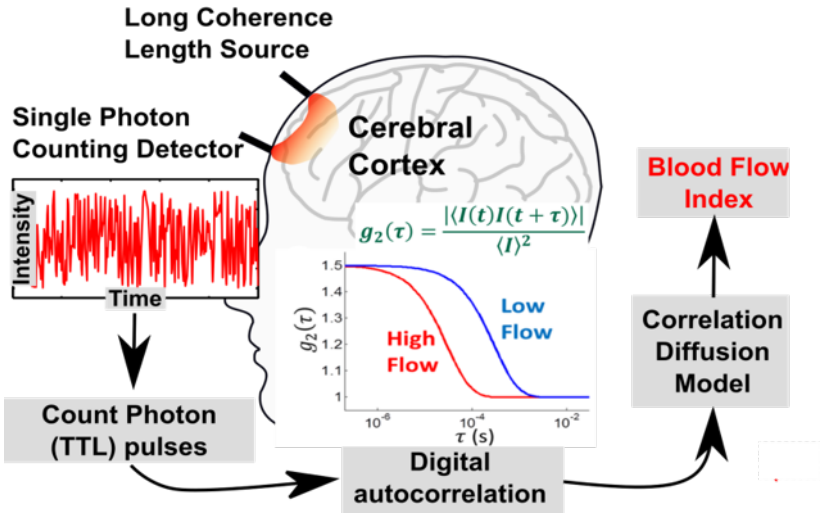

Figure 2.8: DCS measurement

$\kappa_o = 2\pi/\lambda$ is the wave number of input light, τ is the correlation lag, S_o is the source power and F is the tissue blood flow index.

The solution to the CDE is dependent on the source type and the geometry. The intensity auto-correlation function is related to the electric field auto-correlation function using the Siegert's relation, given by

$$g_2(\tau) = 1 + \beta|g_1(\tau)|^2 \tag{2.23}$$

$g_1(\tau)$ is the normalized electric field auto-correlation function, given by

$$g_1(\tau) = \frac{\langle E(t)E(t+\tau)\rangle_t}{\langle E(t)\rangle^2} \tag{2.24}$$

Formally, intensity I is related to the electric field E by $I = |E|^2$

2.4.1 DCS Methods

Diffuse Correlation Spectroscopy (DCS) can be realized in different ways depending on the source type. Conventional implementations of DCS utilize illumination sources of constant intensity. Recently Sutin. et. al., [97], Pagliazzi et. al., [80] and Samaei. et. al., [89] have demonstrated time domain diffuse correlation spectroscopy by using high coherence pulsed

laser as source. The solutions to the CDE vary with respect to the source type which I discuss in the following sections. In Chapter 4, I describe a new implementation of DCS, Frequency Domain DCS, which used intensity modulated light sources.

2.4.1.1 Continuous Wave

Continuous wave DCS uses a long coherence laser source of constant intensity. The coherence of the light source preserves the phase of the light wave, allowing for de-correlations to be sensitive to flow. The coherence length of the light source should be greater than the difference between the longest and shortest path-length in the tissue. The solution of CDE for a continuous wave semi-infinite geometry is given by

$$G_1(\rho,\tau) = \frac{\upsilon S_o}{4\pi D}\left[\frac{exp(-\kappa_D(\tau)r_1)}{r_1} - \frac{exp(-\kappa_D(\tau)r_b)}{r_b}\right] \tag{2.25}$$

Here,

$G_1(\rho,\tau)$ is the un-normalized electric field auto-correlation function

S_o is the continuous wave source

D = Diffusion coefficient ($\frac{1}{3(\mu_a+\mu_s')}$

ρ - Source - Detector Separation

τ = Decay time

$\kappa_D(\tau) = [(\upsilon\mu_a - 2\upsilon\mu_s'\kappa_o^2 F\tau)/D]^{1/2}$ - dynamic wave vector

$r_1 = (l_{tr}+\rho^2)^{1/2}$; $r_b = ((2z_b + l_{tr})^2 + \rho^2)^{1/2}$

$l_t r \approx 1/\mu_s'$ - Transport mean free path

$Z_b = \frac{2}{3} l_{tr}\frac{1+R_{eff}}{1-R_{eff}}$ - Extrapolated zero boundary for index matched boundaries.

2.4.1.2 Time Domain

Time domain DCS uses high-powered, long coherence length pulsed lasers to resolve the temporal point spread function at the detector. The slope of the time of flight curve gives the optical properties. The intensity auto-correlation functions at different pulse widths of the

source can give blood flow at different optical path-lengths in the tissue. Figure 2.9 illustrates the time domain DCS approach. The time domain solution for correlation diffusion equation is given by equation 2.26

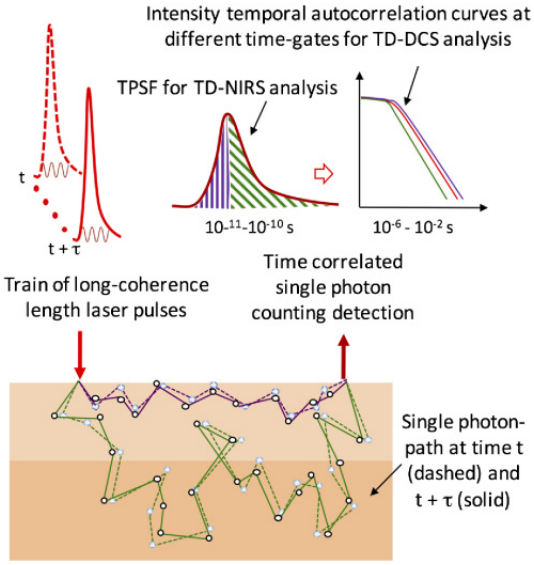

Figure 2.9: TD-DCS approach. Figure adapted with permission from [97]

$$G_1(\rho, z=0, t) = c\left(\frac{3\mu_s'}{4\pi ct}\right)^{3/2} exp[-\mu_a + 2\mu_s' D_B \kappa_o^2 \tau)ct] exp\left(-\frac{3\mu_s'\rho^2}{4ct}\right) \left[exp\left(-\frac{3\mu_s' z_o^2}{4ct}\right) - exp\left(-\frac{3\mu_s'(z_o+2z_b)^2}{4ct}\right)\right] \tag{2.26}$$

Here, t is the arrival time of the photons and c is the speed of light,

Chapter 3: Multi-frequency Frequency Domain Diffuse Optical Spectroscopy

3.1 Introduction

[1]In chapters 1 and 2, I described the motivations for developing a new frequency domain instrument for tissue spectroscopy, and the theory of the photon diffusion process. Briefly, Diffuse Optical Spectroscopy (DOS) can be realized in three different ways depending on the the type of source used - continuous wave (CW), time domain(TD) and frequency domain(FD) - which refer to light sources that use constant intensity, pulsed light sources, and intensity modulated light sources respectively. Frequency domain DOS(FD-DOS) systems have gained popularity as they can measure absolute values compared to the CW systems and are easier to implement compared to the time-domain systems. Specifically multi-distance FD-DOS systems are being used widely for research and clinical studies [1,5,36,38,46,47,51,51,54,63,66,70,79,82,84,86,99–101,101,104,106,113]. Multi-distance FD-DOS measures amplitude and phase of the detected intensity modulated light as a function of source-detector separation. To realize this system, multiple source detector pairs are needed which not only increases the instrument complexity and probe size, but also introduces partial volume effects. Alternatively, amplitude and phase can be measured at one source-detector separation, but as a function of source modulation frequency. These multi-frequency FD-DOS systems eliminate the need for multiple source-detector pairs, reduce the instrument complexity and cost.

In this chapter, I implement and validate a new multi-spectral, multi-frequency FD-DOS system with a broadband heterodyne demodulation to recover amplitude and phase of the diffuse photon density wave, at a single source-detector separation. This system uses of

[1] *This chapter is adapted from [77]. Permission is included in Appendix A*

off-the-shelf components and can support data acquisition rates up to 20Hz. Furthermore, I demonstrate a low-cost phase synchronized dual signal generation system and a broadband heterodyne demodulation technique that down converts RF signals to KHz range for easy data acquisition and phase measurement. I validate the system using tissue simulating phantoms and *in vivo* arm-cuff occlusion experiments in humans.

3.2 Need for Multi-frequency Methods

CW-DOS is extensively used for functional activation and clinical research because of the simplicity in its instrumentation. While CW-DOS systems can be configured to image blood oxygenation over large tissue volumes, they can only measure relative changes of concentrations of oxygenated and de-oxygenated hemoglobin (ΔC_{HbO} and ΔC_{HbR} respectively). TD-DOS systems can perform quantitative depth sensitive measurements of tissue optical properties (and hence concentrations of oxygenated and de-oxygenated hemoglobin, C_{HbO} and C_{HbR}), but the instrumentation is complex to realize. TD-DOS systems need very fast (pico second) high power pulses to measure photon diffusion time of flight (DTOF), to estimate absolute values of absorption coefficient (μ_a) and scattering coefficients (μ_s). FD-DOS systems can also estimate absolute values of absorption coefficient (μ_a) and scattering coefficients (μ_s), and they are easy to implement when compared to TD-DOS with respect to instrumentation, size and complexity. FD-DOS measures amplitude and phase changes of intensity modulated light that travels through the tissue as Diffuse Photon Density Wave(DPDW). The slope of the amplitude and phase changes of the DPDW at the detector are used to estimate absorption coefficient (μ_a) and scattering coefficients (μ_s).

Although, multi-distance FD-DOS is easy to realize compared to TD-DOS, it needs amplitude and phase measurements to be performed in at least three different source-detector positions. Figure 3.1 demonstrates a typical multi distance probe [72, 74]. Alternatively, FD-DOS can estimate the static optical properties at a single source-detector separation by varying modulation frequencies in the RF range using multiple wavelength

sources which we refer to as multi-frequency FD-DOS. Using multi-frequency FD-DOS method to acquire static optical properties eliminate the need for multiple source detector separations. Figure 3.2, [5] demonstrates that there is a significant change in the detected signal amplitude with respect to the modulating frequency(part (A) of the figure). Also, the DPDW's having modulating frequencies up-to 400MHz travel almost the same tissue (B). (C) shows the fraction of photons detected that are visiting tissue depths greater than 1 cm. The simulations shown in this figure are for a semi-infinite medium with properties $(\mu_a = 0.1cm^{-1}, \mu_s = 10cm^{-1}, \eta = 1.4, \eta_o ut = 1.0)$ and a source detector separation of $2.5cm$.

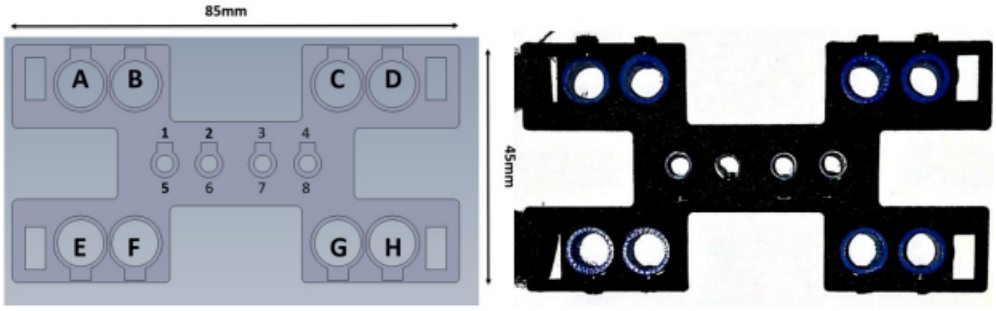

Figure 3.1: A typical multi-distance FD-DOS probe. Figure adapted with permission from [72]

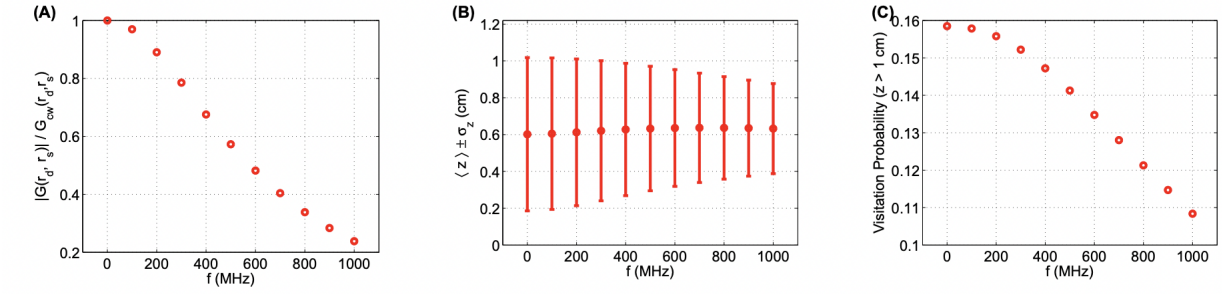

.

Figure 3.2: Modulation depth(A), Mean depth of detected photon visitation(B), fraction of detected photons with sitting tissue depths greater than 1 cm, vs modulating frequency. Figure adapted with permission from [5]

3.2.1 Partial Volume Effects

One significant issue with the multi-distance FD-DOS is the partial volume effects. As discussed earlier, most FD-DOS systems are implemented to measure amplitude and phase changes as a function of the source-detector separations (ρ). Multi-distance approaches to optical spectroscopy inherently assume that the measurements made at different source-detector separations are equally sensitive to changes in tissue optical properties. Unfortunately, this assumption is almost always invalidated by heterogeneous tissue compositions, and in focal hemodynamic changes such as functional activation. Fig 3.3 highlights how sensitivities of measured optical signal (FD amplitude, as an example) to changes in tissue absorption is spatially distributed for multiple source-detector separations (left column), using finite element simulations (NIRFAST [34, 68, 108]) of homogeneous semi-infinite tissue. Thus, a focal change in absorption (e.g., due to functional activation/tumor) at a depth of 10-15 mm below the surface, would elicit a larger change in measured FD amplitude at 2.5 cm vs. 1.5 cm, resulting in systemic biases. It has been also recently shown that partial volume effects inherent in multi-distance spectroscopy could lead to an underestimation of hemodynamic changes during functional activation. [72] This issue is exacerbated in tissues, which are heterogeneous. Taking cerebral measurements as an example, the measurement volume would consist of scalp, skull, cerebrospinal fluid, and cerebral cortex, all with different tissue optical properties. Multi-frequency FD-DOS methods eliminates the system complexity and reduced the influence of partial volume effects from the multi-distance methods. The advancement of the digital circuits in the semiconductor industry allow fast switching of the modulation frequencies making the multi-frequency methods more desirable.

3.3 Prior Work

Over the years, the instrumentation of DOS systems have evolved to decrease cost, decrease complexity and increase measurement rates and accuracy. For example, a network analyzer costing a few hundred thousand dollars has been replaced by an ADC which costs

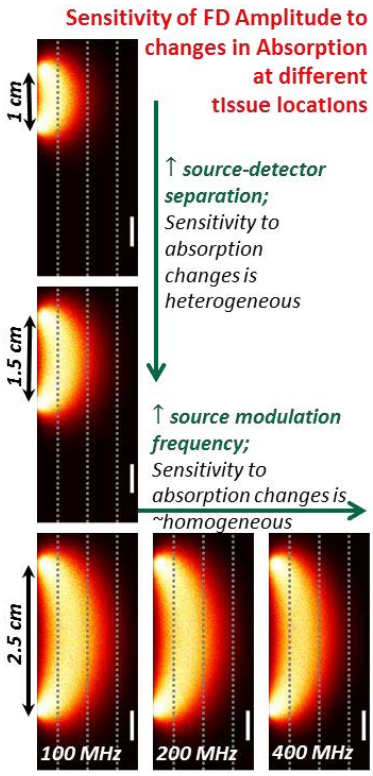

Figure 3.3: Partial volume effects illustration: Photon travel in tissue with varying source-detector separation and varying source modulating frequency. Figure credit: Penaz Parveen Sultana Mohammad

less than thousand dollars. Here, I discuss prior implementations of multi-frequency DOS systems.

Tromberg. B. J., et. al. [100] used the multi-frequency FD DOS approach for the first time in 1996, to record optical properties of tissue and thereby resolve physiological property differences between normal and malignant tissues. The system uses a network Analyzer analyzer (HP 8753C) to modulate the intensity of light at frequencies (300 KHz to 1 GHz). Laser diodes of wavelengths 674 nm, 811 nm, 849 nm, 956 nm were used as sources. A $200\mu m$ diameter fiber was used to illuminate the tissue, and a $100\mu m$ diameter gradient-index fiber was used on the detector. The detector, an APD (Hamamatsu – C5658), was biased at 12 V. The optical power at the tissue was $30mW$. Amplitude and phase data were acquired for a few seconds over the frequency range sweep using the network analyzer. Acquisition of data and control of the network analyzer was driven by a computer (MacIntosh Quadra)

and LabVIEW. Data obtained clearly showed difference in normal and malignant tissues. μ_a, μ_s' values for the normal tissue were around $0.1cm^{-1}$, $10.5cm^{-1}$ and for the malignant tissue(tumor) were found to be around $0.2cm^{-1}, 10cm^{-1}$.

B. Yu. et al. [109] used a multi-frequency FD DOS instrument to invasively measure optical properties of breast tissue during biopsy. To measure optical properties at the same position as the biopsy, a a $200\mu m$ diameter source fiber and $600\mu m$ diameter detector fiber was fit into a $2.4mm$ diameter biopsy needle. The measurements were repeated at 12 different angular positions encompassing a full circle. At each scan position, tissue was extracted and the biopsy results are compared with the results obtained from the DOS system. Laser diodes at three wavelengths, 660 nm, 811 nm, and 849 nm were controlled using a current driver (LDC-3908, ILX Lightwave). A network analyzer (Agilent 8712) was used as the RF source supplying -11.3 dBm RF power. An APD (C5658, Hamamatsu Japan) was used to detect the light, followed by a 19 dB AC amplifier (ZFL – 500 HLN, Minicircuits). Heterodyne detection at frequency 15 Hz was realized using the Network Analyzer. Each single scan which measures fluence at frequencies from 50-150 MHz took 8 seconds to complete and the total scan at a tissue point was finished in a minute. DOS measurements were converted to concentrations of adipose, fibroglandular and blood content at different wavelengths. These properties were compared with the pathological results of adipose, fibroglandural and blood content percentages. Positive correlation with age for adipose was recorded in the study and it was observed that fibroglandular and blood contents were not dependent on the age.

In 2000, Pham et al. [82] built a multi-frequency FD-DOS system to measure fluence at frequencies up to 500 MHz with 201 discrete frequencies. The time taken for the frequency sweep is 675 ms. Similar to the previous two approaches, a network analyzer was used in the receiver electronics. $100\mu m$ diameter source fibers and 1 mm diameter detector fibers were used to illuminate and receive light from the tissue. An APD (C5658-S6045-03, Hamamatsu Corporation) with 3dB cutoff bandwidth of 500 MHz was used as detector. In this study, several measurements were performed to characterize the phase and amplitude of the DOS

measurements. The accuracy of amplitude and phase estimates was observed to increased with RF power. The paper also discussed that the the source of noise in the measurements were amplifiers and back ground light, which could be reduced by proper shielding. Simulations fitting phase only, amplitude only and both amplitude and phase were performed. Simultaneous fitting of both amplitude and phase was successful in retrieving optical properties with high accuracy.

Jung, J. et. al. [63] performed multi-requency FD-DOS using digital demodulation and under sampling. Here, the intensity was modulated from 50 to 300 MHz in steps of 4 MHz. An RF transmitter (Rhode/ Schwartz - SMIQ03B) is used to generate a 7.8 dBm RF signal. The measured DC outputs ranged from 10 - 20 mW for the 5 measurement wavelengths (690, 785, 808, 830, and 850 nm) used. Optical fiber for the source was $400\mu m$ in diameter and while a 3mm core diameter fiber was used for detection. Light detection was realized using a APD (S11519-30, Hamamatsu) having 3 mm diameter sensitive area. The system used a 14 bit, 250 MSPS ADC with a 700 MHz 3 dB cutoff bandwidth, and a low cost data capture board (TSW1405EVM) to record data up to 64 kilobytes on the computer. Measurements are performed at a source detector separation of 2 cm. Per data analysis, integer multiples of Nyquist frequencies were discarded and a phase correction was implemented to account for under sampling effects. Specifically, in even Nyquist zones, phase was reversed and corrected using the formula ($0.5 \times F_{sampling} - F_{sampling}$). In the odd Nyquist zone phase was not reversed but altered using formula ($F_{sampling} - 1.5 \times F_{sampling}$) The results were compared with standard Measurements and following errors were recorded - amplitude: 4.42%, phase: 0.023%, absorption coefficient : 4.87%, and scattering coefficient: 1.90%.

D. Robyler, et. al. [86] developed a Multi-frequency FD-DOS system using a Direct Digital Synthesis signal generator (AD9910, Analog Devices) which is a 1 GSPS, 14-bit Digital to Analog converter (DAC). A 400 MHz low pass filter was used to avoid high frequency harmonics and 10dB amplifier was used to provide boost the modulation depth. A current driver (LDC 3900) was used to produce a 20 mw laser output. Optical fiber for the

source was $400\mu m$ in diameter and while a 3mm core diameter fiber was used for detection. A 3 mm diameter active area Avalanche Photo diode (APD S6045-05, Hamamatsu) was used as the detector. Data acquisition was done in digital domain with an ADC. A 12 bit, 3.6 GSPS and an 800 mv peak to peak ADC (ADC12D1800, National Instruments) was used to directly record the intensity modulated fluence output following Nyquist sampling criteria. Intensity data was recorded while modulation frequency varied from 150 – 400 MHz in steps of 1 MHz. At each frequency 2048 samples were recorded for post processing with MATLAB. The amplitude was found to be affected by the bit depth, signal strength, signal to noise ratio while phase was affected if the data was sampled at peaks and troughs of the signal. Amplitude and Phase precision decreased with modulation frequency because diffuse media acts as a low pass filter. Also, harmonic distortion and signal to noise ratio worsened when modulation frequency was low. When compared to a gold standard network analyzer, the precision was found to be 1.02% for amplitude and 0.59° for phase. Errors for absorption coefficient was $\approx 1.5\%$ and $\approx 0.5\%$ for scattering coefficient.

Finally, Torjesen et al. [99] recently developed a multi-frequency FD-DOS device using digital demodulation and under sampling at six wavelengths. This system used a direct digital dynthesis based signal generator (AD9910, Analog Devices) to provide RF power to laser diodes at wavelengths 658, 690, 785, 808, 830, and 850 nm, driven by an eight channel current driver (Newport Inc.), through an RF splitter (Mini Circuits). DOS intensities were recorded with when source modulation frequencies varied from 100 - 400 MHz in steps of 1 – 7 MHz. 0.5mm area diameter APD (C5658, Hamamatsu) was used as the detector. A 14-bit ADC sampling at 250 MSPS was used to digitize the samples with a max output of 2 v peak to peak. A high pass filter was used after the output of APD to remove any harmonics. In the system, all signals above 125 MHz were aliased. A MATLAB program was used to remove the aliasing frequency bins. Cuff Occlusion test was performed with this system and was compared with ECG. The results were found to be consistent with the cuff occlusion procedure.

In the above systems, it can be noticed that the instrumentation simplified to a great extent. Tromberg. B. J., et al. [100] B. Yu. et al., [109] Pham et al [82] used a network analyzer as the RF source and also for the data acquisition and demodulation. Network analyzers are bulky and cost up to few hundred thousand dollars. More recent work by D. Robyler., et al [86] used a digital direct synthesis board as signal generator and ADC for data acquisition. These developments have decreased the size and cost of the device and increased the efficiency. Jung, J. et al, [62] Torjesen et al. [99] have used demodulation techniques based on under sampling which allowed them to record DOS data at lower frequencies reducing the cost, data size and increasing the speed of the system. Although the basic construction of the system is similar, these new techniques both on the detection and illumination sections have been used off- the-shelf equipment to simplify the instrumentation.

3.4 Theory

The goal of a multi-frequency FD-DOS measurement is to measure the amplitude and phase of the detected intensity modulated light as a function of modulation frequency. Following equation 2.3.1.1, for a homogeneous semi-infinite geometry, the frequency domain solution to the photon diffusion equation is given by:

$$\phi(\rho,\omega) = \frac{S_o \upsilon}{4\pi D}\left[\frac{exp(-\kappa(\omega)r_1)}{r_1} - \frac{exp(-\kappa(\omega)r_b)}{r_b}\right] \tag{3.1}$$

The terms are defined in Table 3.1 The measured fluence rate ϕ is modeled as $\phi(\omega,\rho) = A(\omega,\rho)exp(i(\omega t - \theta(\omega,\rho)))$, where A and θ are the amplitude and phase of the detected intensity. Figure 3.4 plots the solution for A and θ as a function of modulation frequency, from the forward model (Equation 3.1), for a source-detector separation $(\rho = 2cm)$.

Table 3.1: Table defining terms in semi-infinite solution to PDE

Symbol	***Quantity***
ϕ	Fluence Rate
ρ	Source - detector separation
ω	Modulation frequeny
D	Diffusion Coefficient
S_o	Input Power
$\upsilon = c/n$	Speed of light in tissue
$Z_b = \frac{2}{3} l_{tr} \frac{1+R_eff}{1-R_eff}$	Location of 'image' source; extrapolated zero boundary
R_eff	Fresnel reflection coefficient
$l_{tr} \approx 1/\mu_s'$	Transport mean free path
$\kappa^2 = (\mu_a - i\omega)/D$	Wave vector
$r_1^2 = \rho^2 + l_t r^2;$ $r_b^2 = \rho^2 + (2z_b + l_t r)^2;$	

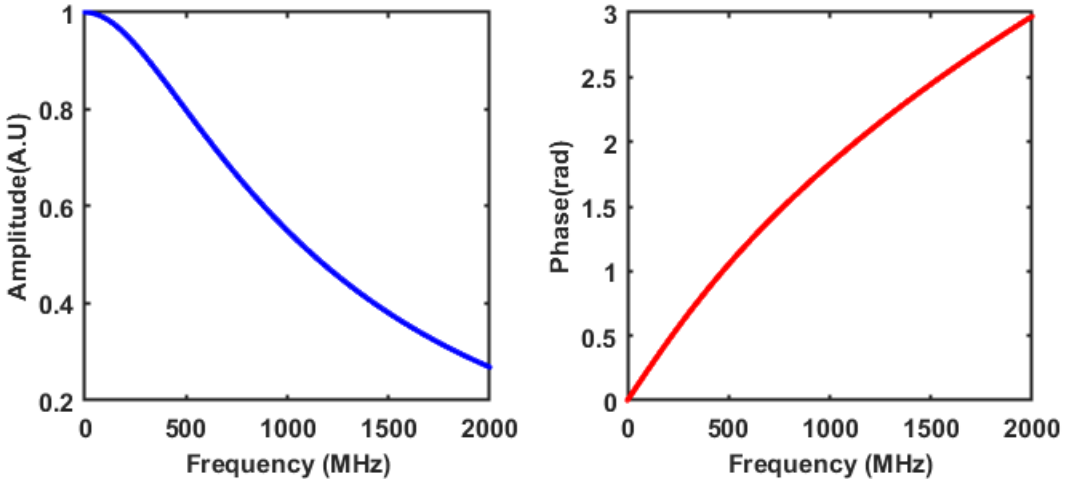

Figure 3.4: Amplitude and frequency as a function of modulation frequencies

3.5 Instrumentation

Instrumentation for multi-frequency FD-DOS has been executed in two stages. Initial validation experiments were conducted with a bench-top set-up for single wavelength measurements which I will refer to as mfFD-DOS(V1). After the preliminary results, this setup was updated to mfFD-DOS(V2) with stand-alone components and extended to multiple wavelengths for *in vivo* experiments.

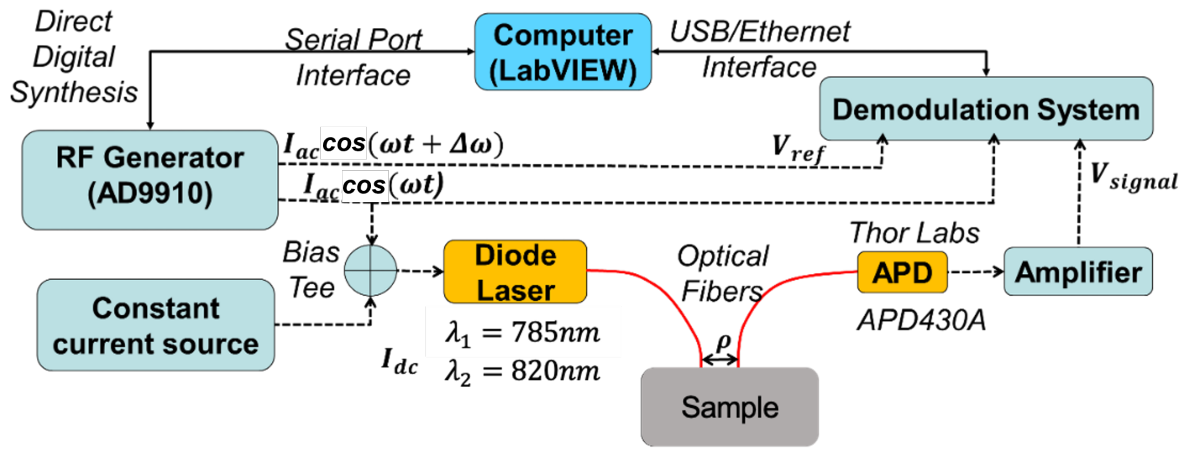

Figure 3.5: Multi-frequency FD-DOS block diagram

Fig. 3.5 shows the schematic of broadband multi-frequency FD-DOS system with heterodyne demodulation. The bench-top version, mfFD-DOS(V1), uses a laser diode (L785P090, $785nm$, $90mW$ max power, Thorlabs, Newton, NJ) as the light source. The laser diode was mounted on temperature controlled mount (LDM9T, Thorlabs, Newton, NJ) and driven at its operating current by a constant current source (LDC205, Thorlabs, Newton, NJ). The intensity of the laser was modulated at RF frequency ($\omega_1 = 200 - 400MHz$) using a digital frequency synthesizer (AD9910, Analog Devices) and interfaced to the laser diode mount using a Bias-Tee. The digital frequency synthesizer was controlled by custom software (LabVIEW, National Instruments, Austin, TX) via a serial port interface (USB-8451, National Instruments, Austin, TX). A second phase synchronized RF frequency synthesizer (AD9910, Analog Devices) was used to generate a frequency shifted RF wave at $\omega_2 = \omega_1 + \Delta\omega$, where $\Delta\omega = 300KHz$ is the beat frequency used for heterodyne demodulation. The signal generation system is described in more detail in Section 3.5.1. Illumination of the sample was realized using $400\mu m$ diameter multi-mode fiber. The diffuse reflected light was collected $1-3$ cm away from the source using a $1000\mu m$ diameter multi-mode fiber, and was directed to a silicon variable gain avalanche photo detector (APD430A, Thorlabs, Newton, NJ). The output of the photo detector was amplified (ZFL -1000LN+, Mini Circuits, 18dB gain), and low pass filtered ($400MHz$ cut-off frequency) to pre-process the signal for demodulation. The

demodulation process, described in more detail in Section 3.5.2, down converts the RF signal from MHz to the beat frequency $300KHz$. A lock-in amplifier (MFLI, Zurich Instruments, Zurich, Switzerland) recorded the down converted signal to estimate amplitude and phase. Amplitude and Phase values were stored on the computer with custom software (LabVIEW, National Instruments, Austin, TX).

For mfFD-DOS(V2), the system was extended to two NIR wavelength sources. Two SM fiber-pigtailed laser diodes (LP785-SF100, $785nm$, $100mW$ max power, Thorlabs, Newton, NJ) and (LP820-SF80, $820nm$, $80mW$ max power, Thorlabs, Newton, NJ) were mounted on compact laser Diode/temperature controller with TO-can Mount (CLD1011LP, Thorlabs, Newton, NJ). An optical switch (OSW12-780E, Thorlabs, Newton, NJ) was used to switch between lasers. The signal generation system was the same as in mfFD-DOS(V1). Amplifiers at signal generation and detectors were replaced with low noise amplifiers (ZX60-P103LN+, Mini Circuits). To increase the data acquisition speed, amplitude and phase were recorded via auxiliary outputs of the lock-in-amplifier (MFLI, Zurich Instruments). This improved the acquisition speed of mfFD-DOS(V2) to $612kSa/s$ compared to $200kSa/s$ in mfFD-DOS(V1). These values were recorded on the computer using 1 MS/s ADC (NI-9223, National Instruments, Austin, TX) with custom software (LabVIEW, National Instruments, Austin, TX).

3.5.1 Signal Generation Subsystem

Two phase synchronized RF signals with frequencies $(\omega, \omega + \Delta\omega)$ are required to execute heterodyne demodulation in the mfFD-DOS system. These frequencies were generated using the multi-chip synchronization feature of AD9910 (Analog Devices). AD9910 is a CMOS direct digital synthesizer capable of producing analog signals up to $400MHz$ via its Digital to Analog Converter (DAC). Two AD9910s were used to generate RF signals at frequencies (ω and $\omega + \Delta\omega$). Synchronization of these RF output signals was achieved by matching the clock states and the transitions between the clock states of both AD9910s. The rising edge

of the master clock for both the DACs were matched to have a coincident reference clock. A synchronization timing signal (*sync_clk*) was produced by the master DAC and distributed to both master and slave DACs. A coincident CMOS TTL logic signal (*ioUpdate*) was sent to all the DACs to produce a synchronized state across the devices. For two or more AD9910s to be synchronized, the reference clock, the *sync_clk* and *ioUpdate* on all the DACs need to be coincident. ADCLK846 (Analog Devices), a LVDS/CMOS, fanout buffer optimized for low jitter and low power operation, was used to distribute the *sync_clk* signals. A D-flipflop (74LVC74A, Texas Instruments) was used to produce a coincident *ioUpdate* that was synchronized with the rising edge a clock with a frequency signal that is 4× the *sync_clk* to both the DACs. A custom printed circuit board with all the IC's (AD9910, ADCLK846, 74LVC74A) can be designed to implement the synchronization with a minimal footprint.

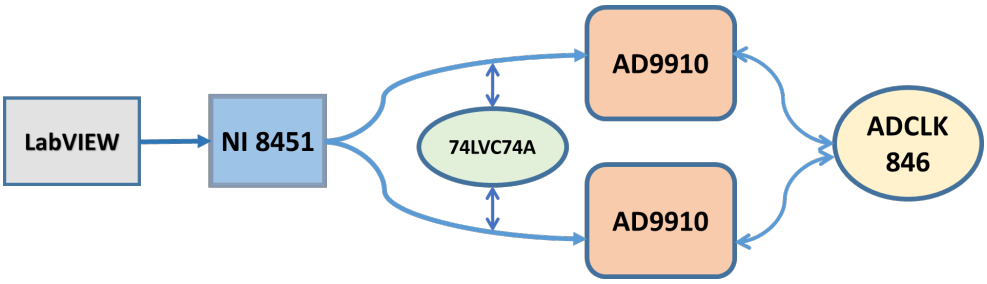

Figure 3.6: Multi-frequency FD-DOS signal generation

3.5.2 Detection and Demodulation

Fig 3.7 shows the RF broadband heterodyne demodulation approach to measure amplitude and phase of the photon fluence rate as a function of modulation frequency. Photon fluence rate measured from the sample was mixed with phase synchronized, frequency shifted reference wave to produce a down converted (low frequency) signal at the beat frequency. The amplitude/phase of the down-converted signal is proportional/equal to the amplitude/phase of the detected fluence rate. A second down conversion circuit generates a low frequency reference signal for a lock-in amplifier (MFLI, Zurich Instruments) to estimate the amplitude and phase of the fluence rate.

To better understand this, consider two signals

$$\begin{aligned} V_1(t) &= A_1 cos(\omega_M t + \theta_1) \\ V_2(t) &= A_2 cos((\omega_M + \Delta\omega)t + \theta_2) \end{aligned} \tag{3.2}$$

where A_1, A_2 are the amplitudes, ω_M is the modulation frequency, $\Delta\omega$ is the beat frequency and θ_1, θ_2 are the phases of the respective signals.

Both the signals are split two ways using an RF splitter. The laser is modulated with $(V_1(t))$ and the modulated optical signal travels as diffuse photon density waves through the sample (tissue) with amplitude attenuation and phase lag given by

$$V_3(t) = A_3 cos(\omega_M t + \theta_3) \tag{3.3}$$

where A_3 is the attenuated amplitude, and θ_3 is the phase of the signal.

This 'message' signal is multiplied to the reference signal $V_2(t)$ using a mixer giving rise to harmonic frequency components in multiples of the modulating frequency. The undesired frequencies are filtered out to have the down-converted signal at beat frequency.

$$V_3(t) \times V_2(t) = A_3 cos(\omega_M t + \theta_3) \times A_2 cos((\omega_M + \Delta\omega)t + \theta_2) \tag{3.4}$$

Here the trignometric identity $2cos(M) \times cos(N) = cos(M - N) + cos(M + N)$ is used resulting in

$$\begin{aligned} V_3(t) \times V_2(t) = \frac{A_3 A_2}{2} [&cos(\omega_M t + \theta_3 - \omega_M t - \Delta\omega t - \theta_2) \\ &+ cos(\omega_M t + \theta_3 + \omega_M t + \Delta\omega t + \theta_2)] \end{aligned} \tag{3.5}$$

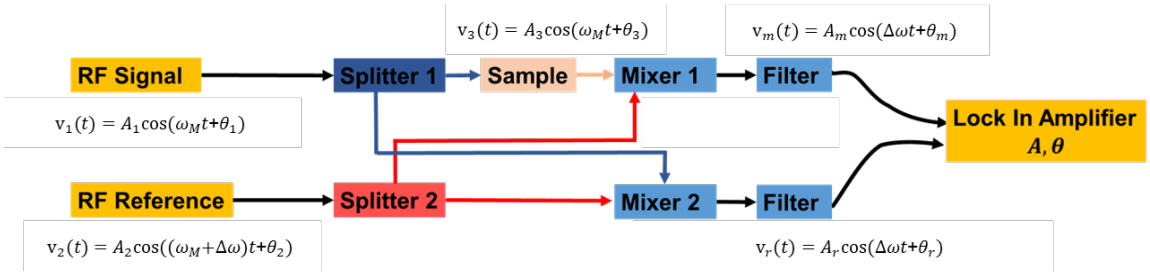

Figure 3.7: Heterodyne demodulation methodology for multi-frequency FD-DOS system

$$V_3(t) \times V_2(t) = \frac{A_3 A_2}{2}[cos(\Delta\omega t + \theta_3 - \theta_2) + cos(2\omega_M t + \Delta\omega t + \theta_3 + \theta_2)] \tag{3.6}$$

The down converted 'message' signal after filtering the second term in Equation 3.6 is given by

$$V_m(t) = A_m cos(\Delta\omega t + \theta_m) \tag{3.7}$$

where $A_m = \frac{A_3 A_2}{2}$ and $\theta_m = \theta_3 - \theta_2$

Similarly, the signals $V_1(t), V_2(t)$ are mixed bypassing the sample to get the reference signal

$$V_r(t) = A_r cos(\Delta\omega t + \theta_r) \tag{3.8}$$

where $A_r = \frac{A_1 A_2}{2}$ and $\theta_r = \theta_1 - \theta_2$

The signals $V_m(t), V_r(t)$ are down-converted signals at the beat frequency and are input to the lock-in-amplifier to retrieve the amplitude and phase changes. The lock-in-amplifier uses IQ demodulation method to estimate the amplitude and phase.

3.6 Results and Discussion

3.6.1 Validation of mfFD-DOS System Using Systematic Experiments

I validated the new mfFD-DOS system with experiments on tissue simulating phantoms and demonstrated that the system can be used *in vivo* in humans. For experimental validation, frequency dependent amplitude $(A^m(\rho,\omega))$ and phase $(\theta^m(\rho,\omega))$ were recorded for a given wavelength (λ). Here, the superscript m indicates measured data. The measured data were fit to the frequency dependent amplitude ($A^{th}(\rho,\omega)$) and phase ($\theta^{th}(\rho,\omega)$) from the forward model (Equation 3.1). Here, the superscript th indicates theory. The fit was used to estimate tissue optical properties $\mu_a(\lambda_1)$, $\mu_s(\lambda_1)$. The data is solved as a multivariate nonlinear optimization problem, wherein parameter $\chi^2 = \Sigma_M\{|A^{th}(\rho,\omega) - A^m(\rho,\omega)|^2 + |\theta^{th}(\rho,\omega) - \theta^m(\rho,\omega)|^2\}$ is minimized over M modulation frequencies using *fminsearch* (MATLAB, Mathworks Inc., Natick, MA). For *in vivo* experiments, concentrations C_{HbO}, C_{HbR} are estimated from measured μ_a, μ_s and molar extinction coefficients $\epsilon(\lambda)$. To elaborate, we solve the linear system of equations given by $\mu_a(\lambda) = \epsilon_{HBR}(\lambda)C_{HbR} + \epsilon_{HbO}(\lambda)C_{HbO}$ where the suffix HbO, HbR corresponds to oxy- and de-oxy- hemoglobin. Finally, tissue oxygen saturation is $StO_2 = C_{HbO}/(C_{HbO} + C_{HbR})$, and the metabolic rate of oxygen will be calculated from the oxygen concentrations and blood flow.

For initial validation experiments using mfFD-DOS(v1), 1000 amplitude and phase measurements were performed and averaged with the lock-in amplifier for each modulation frequency (150 - 400 MHz with 1 MHz interval). The source-detector separation was 1.3 cm and the source wavelength was 785nm. The frequency dependent amplitude and phase were fit to a semi-infinite solution to the Photon Diffusion Equation (Equation 3.1), after phantom calibration to account for source-detector fiber coupling coefficients and instrument frequency [5] . The setup was tested on a liquid phantom (20% Intralipid, India ink and distilled water). Fig 3.8 shows representative data and fit of measured amplitude and phase

(after calibration with phantom of known optical properties). The estimated tissue optical properties were within 10% error when compared to the theoretical values.

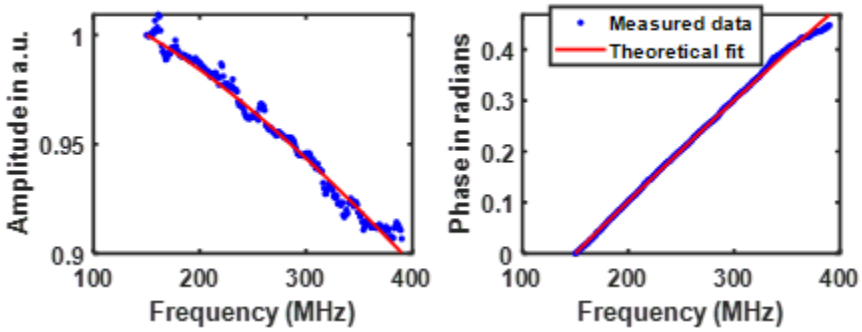

Figure 3.8: Amplitude and phase acquired by mfFD-DOS(v1) by varying modulation frequencies from 150 - 200 MHz and fit to the semi-infinite solution of the photon diffusion equation. Representative data and fit from a tissue simulating liquid phantom.

To verify the sensitivity of the instrument to absorption and scattering changes, I performed a series of experiments on different tissue simulating liquid phantoms, where the phantom (μ_a) was varied from 0.04 to $0.1 cm^{-1}$ in steps of $0.02 cm^{-1}$ by changing the concentration of India ink in the phantom while keeping the (μ_s') constant. In another set of experiments, the phantoms' (μ_s') was varied from 8 to $10 cm^{-1}$ in steps of $1 cm^{-1}$ by changing the intralipid volume in the phantom while keeping (μ_a) constant. Fig 3.9 demonstrates the sensitivity of mfFD-DOS(v1) system to absorption and scattering changes in the tissue simulating phantoms. The sensitivity is shown to be linear for both absorption and scattering changes with $R^2 > 0.97$. The red dashed line indicate the linear fit and blue dots indicate the retrieved estimates of absorption and scattering coefficients.

3.6.2 Liquid Phantom Experiments

The second part of more extensive liquid phantom experiments were performed using the mfFD-DOS(v2) system. Here, the system is validated for accuracy at two wavelengths(785 nm and 820 nm) and two source-detector separation (2 cm and 2.5 cm). Data was also acquired at three different sampling time per modulation frequency - 5ms, 10ms and 100

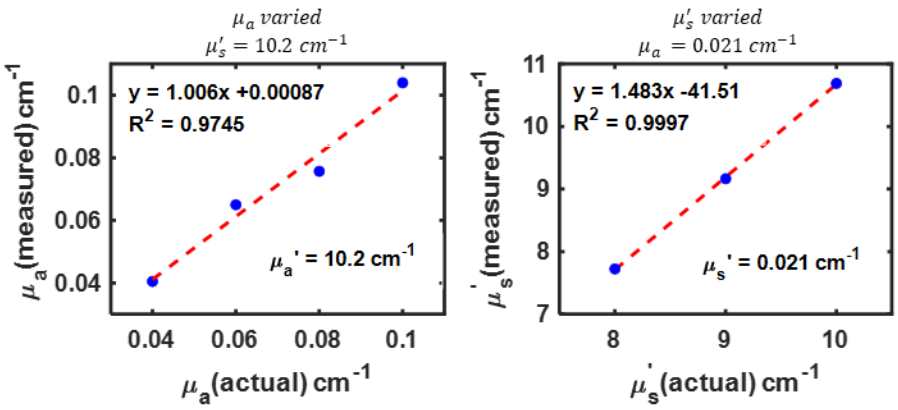

Figure 3.9: Graph demonstrating sensitivity of mfFD-DOS(v1) to absorption and scattering changes.

ms(see appendix C). Here, (μ_a) was varied from 0.02 to $0.1cm^{-1}$ in steps of $0.02cm^{-1}$ by changing the concentration of India ink in the phantom while keeping the (μ_s') constant. (μ_s') was varied from 6 to $12cm^{-1}$ in steps of $2cm^{-1}$ by changing the Intralipid volume in the phantom while keeping (μ_a) constant. Figures 3.10 - 3.17 demonstrate the sensitivity of mfFD-DOS(v2) system to absorption and scattering changes in the tissue simulating phantoms at wavelengths 785 nm and 820 nm and two source-detector separation 2 cm and 2.5 cm) for a sampling time per modulation frequency of 5 ms. To describe the results, we consider for example Fig 3.10. Here, the plot on the left shows the tissue absorption coefficient measured with the mfFD-DOS system along the y-axis, and the actual tissue absorption coefficient along the x-axis. The blue line is a fit of the data to a linear regression model - here the slope of the line is 1.008 indicating that the measured and actual absorption coefficients have a close to 1:1 correspondence ($R^2 = 0.87$). The two dashed black lines represent 95% confidence bounds of the linear regression line. All data is within the confidence limits. The plot on the right shows the measured tissue scattering coefficients in these phantoms. Recall that the scattering coefficients were held fixed. The blue dashed line represent the true μ_s' values and the red diamond markers represent the estimates retrieved by the mfFD-DOS system. The other graphs present the data in a similar manner. The slope of the fit, uncertainty in slope, and R^2 for all the fits are summarized in table 3.2

Table 3.2: Fit characteristics of absorption and scattering changes

λ	ρ	Varying Parameter	Slope	Uncertainty in slope	R^2
785 nm	2.0 cm	μ_a	1.008	(0.8421, 1.173)	0.873
785 nm	2.0 cm	μ_s'	0.943	(0.8303, 1.057)	0.878
785 nm	2.5 cm	μ_a	1.034	(0.6915, 1.376)	0.240
785 nm	2.5 cm	μ_s'	0.971	(0.8734, 1.07)	0.980
820 nm	2.0 cm	μ_a	1.179	(0.9953, 1.364)	0.908
820 nm	2.0 cm	μ_s'	0.972	(0.9037, 1.0041)	0.970
820 nm	2.5 cm	μ_a	0.958	(0.7337, 1.183)	0.892
820 nm	2.5 cm	μ_s'	0.980	(0.9427, 1.017)	0.992

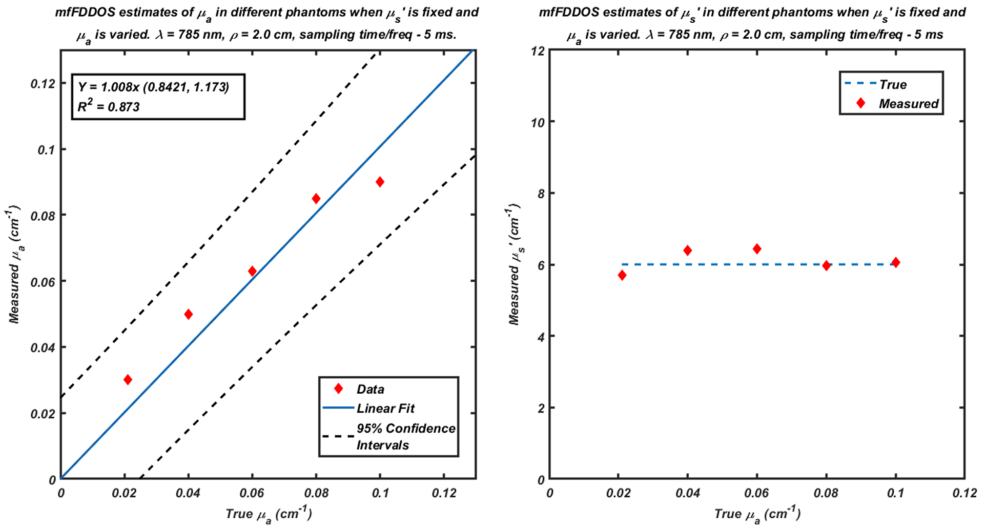

Figure 3.10: Sensitivity of mfFD-DOS to measuring absorption changes at 785 nm at source-detector separation of 2.0 cm

3.6.3 In Vivo Measurements

To check the feasibility of the mfFD-DOS system for in-vivo measurements, I performed an arm cuff occlusion experiment. *In vivo* experiments were performed based on a protocol approved by the Institutional Review Board at the University of South Florida. Briefly, the protocol for arm cuff occlusion experiments included two minutes baseline time, followed by occlusion of blood flow to the arm for a minute by using pressure cuffs over the bicep as shown in Fig 3.18 and two minutes of recovery. Frequency dependent amplitude and phase were recorded continuously using the mfFD-DOS(v2) system, for a source detector separation of 2

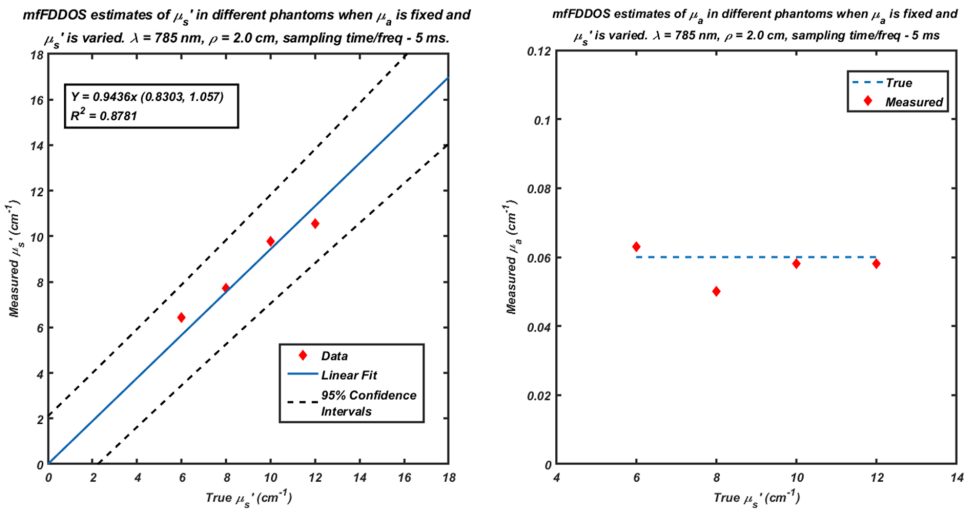

Figure 3.11: Sensitivity of mfFD-DOS to measuring scattering changes at 785 nm and source-detector separation of 2.0 cm

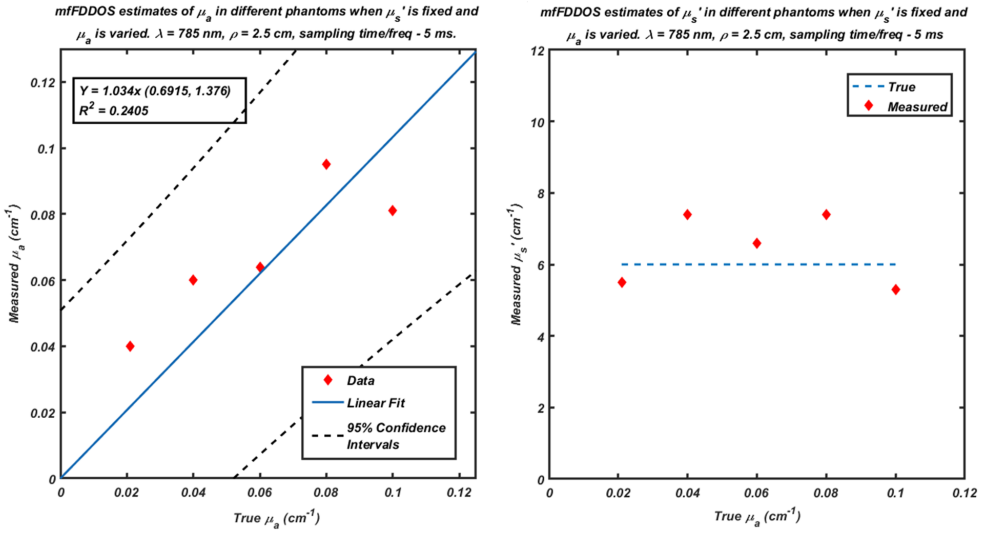

Figure 3.12: Sensitivity of mfFD-DOS to measuring absorption changes at 785 nm and source-detector separation of 2.5 cm

cm and at wavelengths 785 nm and 820 nm. In the cuff occlusion test, it is expected to see a decrease in oxygenated hemoglobin concentration and increase in de-oxygenated hemoglobin concentration during disruption in the blood flow to the arm.

Fig 3.19 shows the change in AC amplitude as the FD DOS system, at $785nm$, during the baseline of the arm cuff-occlusion. The plot on the left clearly demonstrated the pulsatility of the amplitude, which is due to dynamic changes in tissue absorption due to blood flow

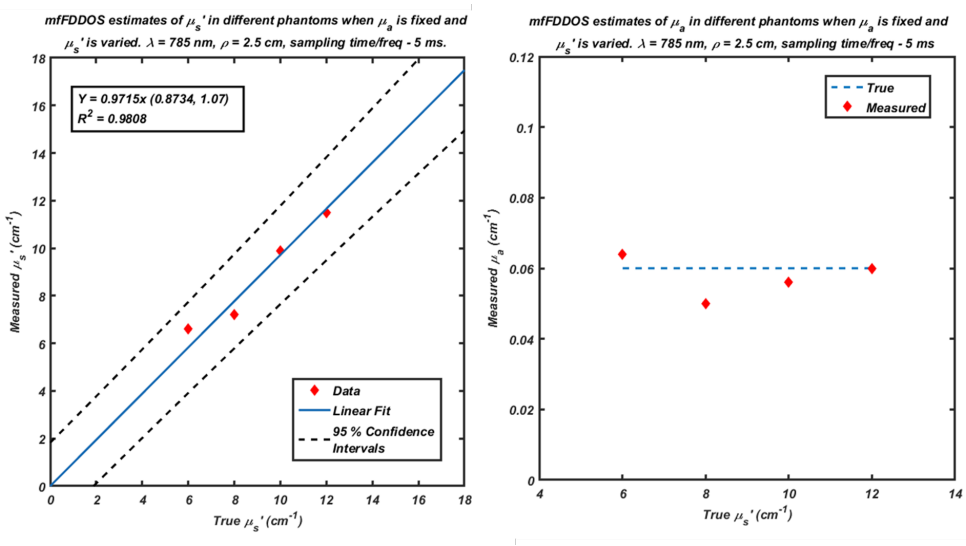

Figure 3.13: Sensitivity of mfFD-DOS to measuring scattering changes at 785 nm and source-detector separation of 2.5 cm

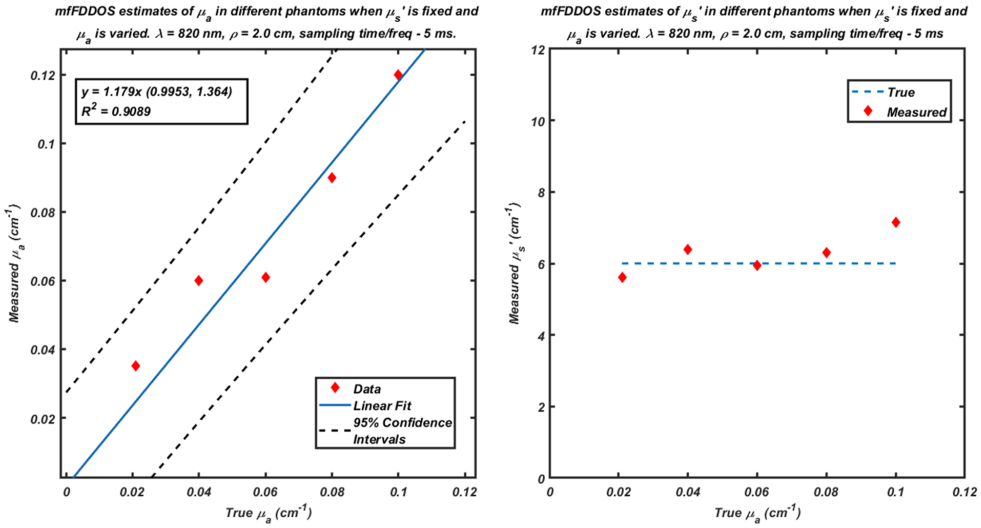

Figure 3.14: Sensitivity of mfFD-DOS to measuring absorption changes at 820 nm and source-detector separation of 2.0 cm

pulsatility. AC amplitude was recorded at high sampling rate for this measurement. The corresponding frequency spectrum on the right shows a clear peak around $\approx$ 1 Hz. Figures 3.20 and 3.21 display the absorption and scattering coefficients retrieved at $\lambda = 785nm$, while figures 3.22 and 3.23 display the absorption and scattering coefficients retrieved at $\lambda = 820nm$ during the baseline measurement of arm cuff-occlusion. Here, the average values are in the expected range for a healthy subject.

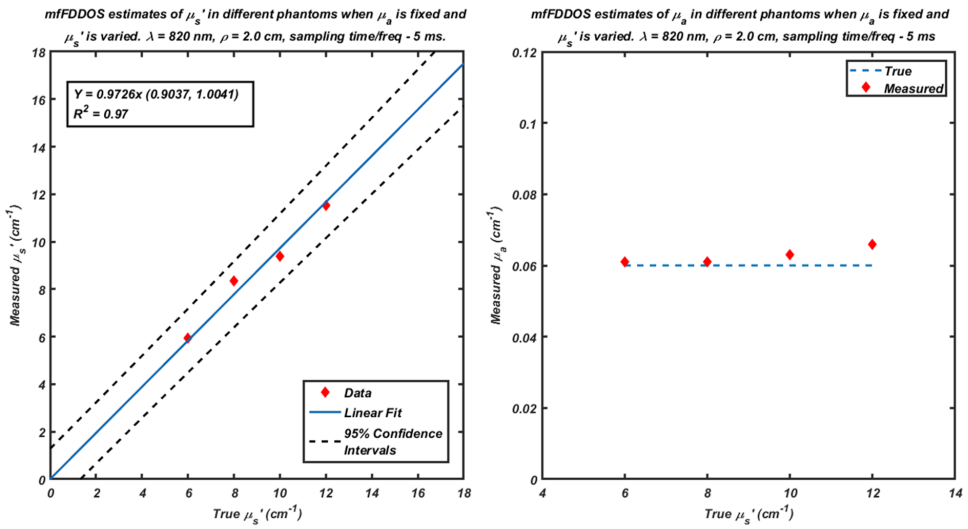

Figure 3.15: Sensitivity of mfFD-DOS to measuring scattering changes at 820 nm and source-detector separation of 2.0 cm

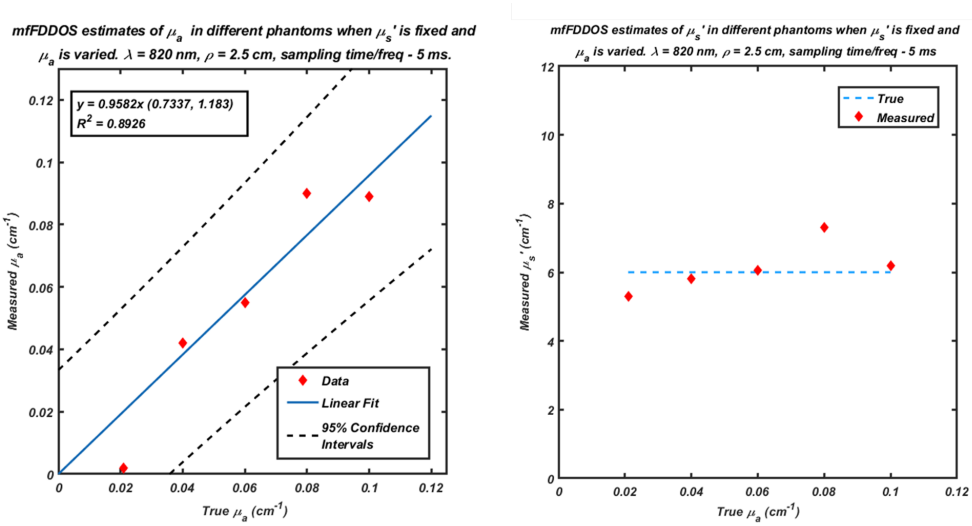

Figure 3.16: Sensitivity of mfFD-DOS to measuring absorption changes at 820 nm and source-detector separation of 2.5 cm

Fig. 3.24 shows the absolute (right) and relative (left) concentrations of oxygenated hemoglobin (red curve) and de-oxygenated hemoglobin (blue curve) during the arm cuff occlusion experiment. As expected with normal physiology, cuff occlusion causes a $20 \approx 30\%$ reduction in oxygenated hemoglobin - this is due to restriction of blood supply to the arm. At the same time, the concentration of de-oxygenated hemoglobin increases proportionally, as the oxygenated hemoglobin in the sample volume is consumed by tissue metabolism. The

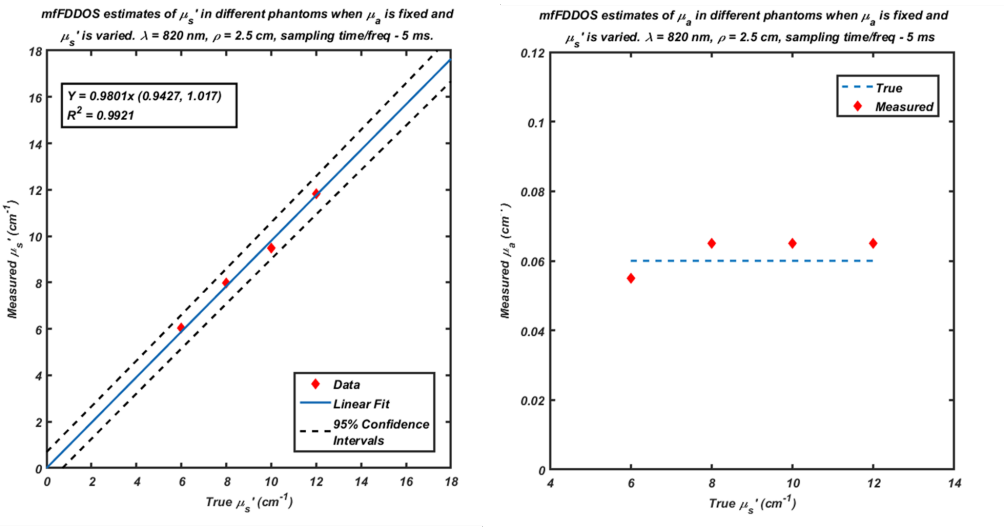

Figure 3.17: Sensitivity of mfFD-DOS to measuring scattering changes at 820 nm and source-detector separation of 2.5 cm

trends are reversed immediately after recovery. These experiments clearly demonstrate the sensitivity and dynamic range of the mFFD-DOS system to measure tissue oxygenation.

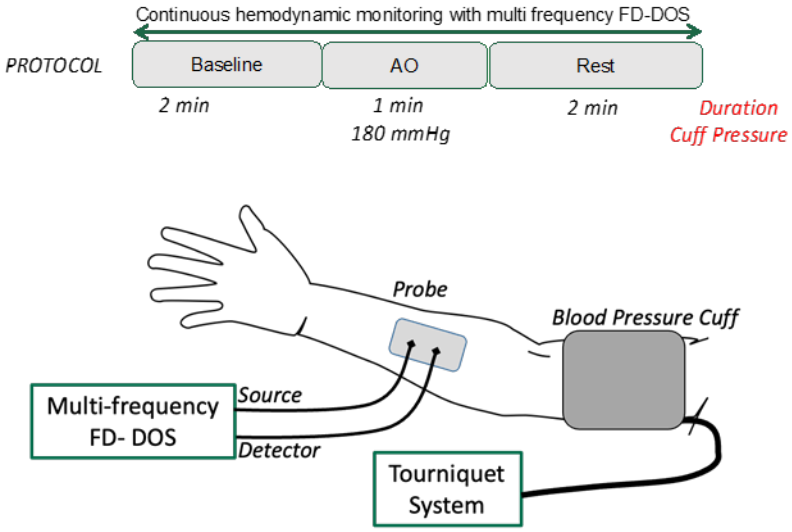

Figure 3.18: Arm cuff-occlusion protocol

3.6.4 Discussion

The results presented above clearly show that the new FD-DOS system with heterodyne demodulation is capable of estimating absorption coefficient and scattering coefficient with

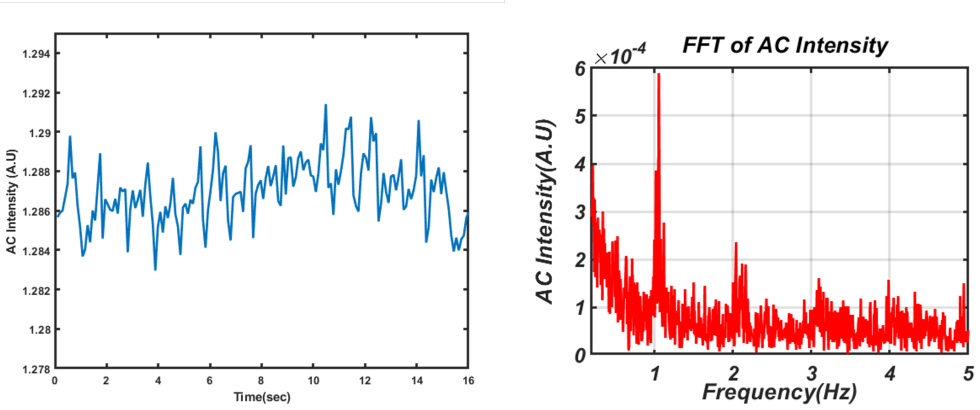

Figure 3.19: In-vivo measurement showing pulsatility

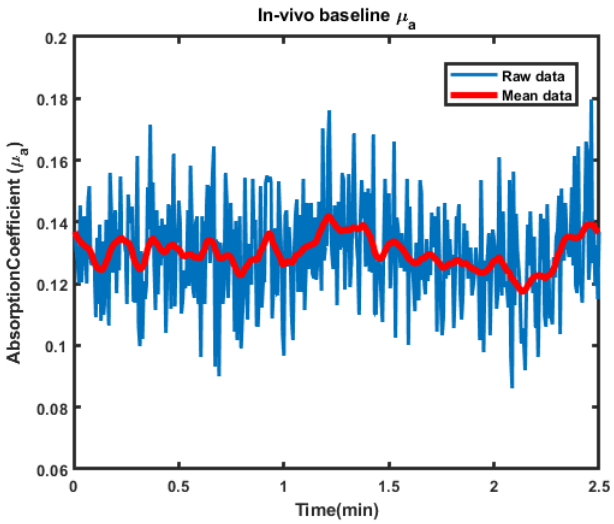

Figure 3.20: In-vivo baseline μ_a at $\lambda = 785nm$

minimal errors. The system has been tested for accuracy at source-detector separations 2.0 cm and 2.5 cm. Figures 3.10 - 3.17 demonstrate that the system follows the same trend in estimation of the static optical properties at both the distances. At longer source-detector separations, photon travel deep in the tissue ($1 \approx 2$ cm) allowing us to probe deeper tissue. [96] This system can be used to perform functional studies on brain and other deeper tissues.

The data proves that the system can obtain data with sampling rate as small as 2ms per modulation frequency. The signal generation circuit needs a delay of 3ms at every modulation frequency change. Even with this limitation, the system can acquire data with a rate of 10

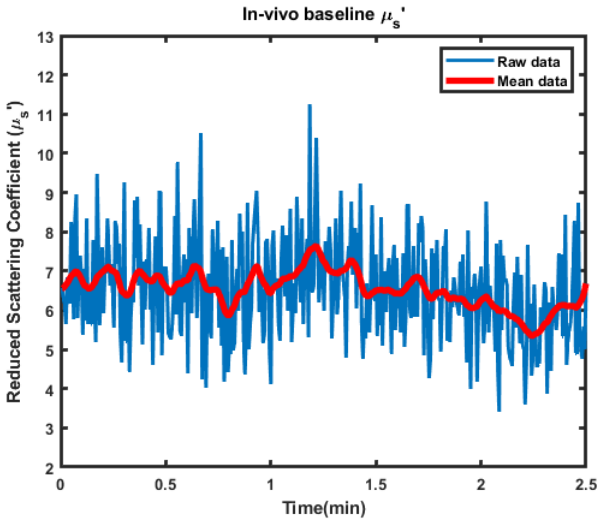

Figure 3.21: In-vivo baseline μ_s' at $\lambda = 785nm$

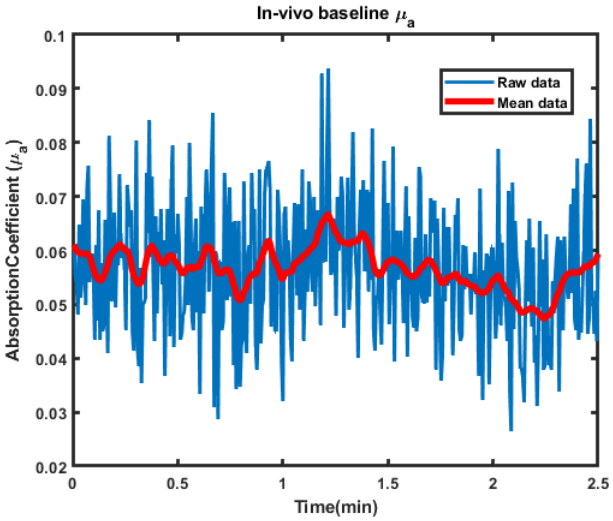

Figure 3.22: In-vivo baseline μ_a at $\lambda = 820nm$

Hz of frequency sweep (200 - 400 MHz in steps of 10 MHz), and 210 Hz for a modulating frequency. The system can achieve speeds up-to 30 Hz per frequency sweep and 630 Hz per modulation frequency if the delay is eliminated. High sampling rate up to 1 MHz can be achieved for continuous wave measurement using the acquisition system. The *in-vivo* data shows that the multi-frequency FD-DOS system can measure absolute values of absorption and scattering coefficient and is sensitive to changes in tissue oxygen concentration.

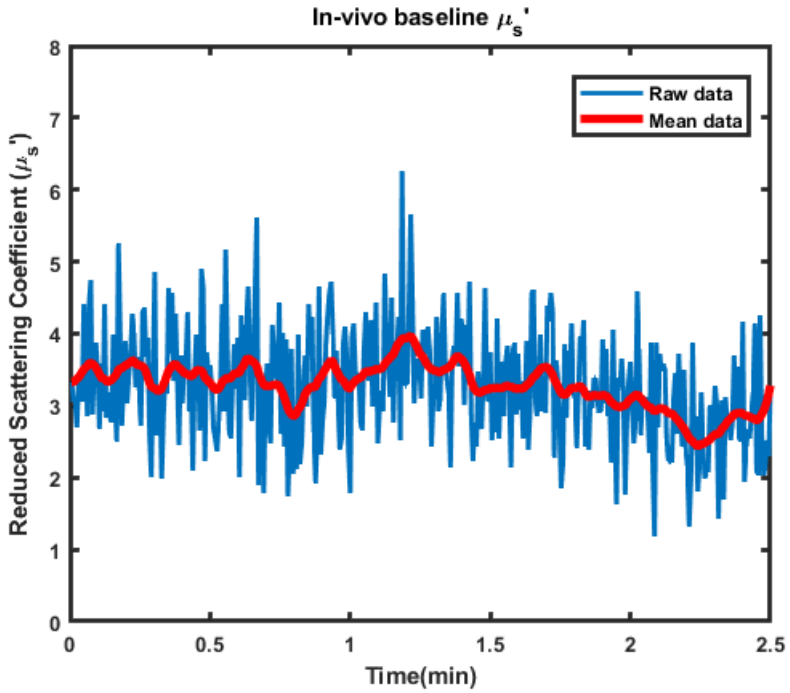

Figure 3.23: In-vivo baseline μ_s' at $\lambda = 820nm$

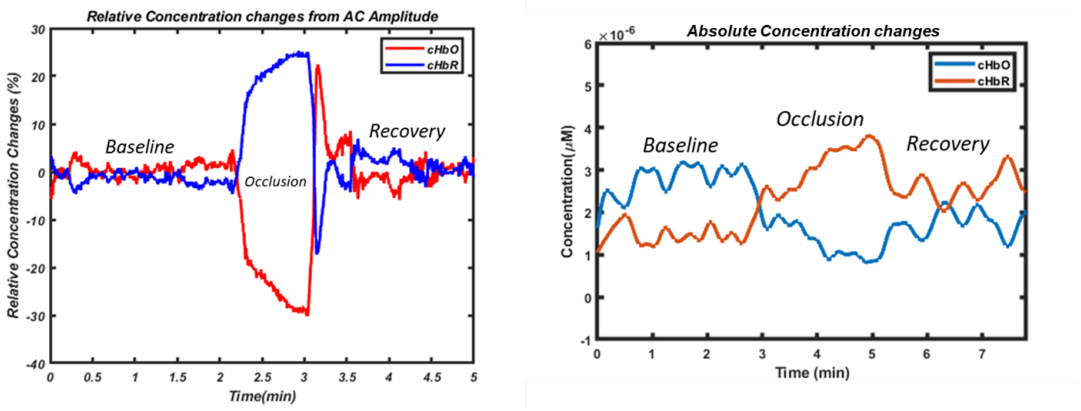

Figure 3.24: Arm cuff-occlusion concentration changes

I conclude this chapter with a brief discussion on the limitations of the mfFD-DOS system. Analog heterodyne demodulation requires a lot of active and passive RF components. It is crucial to maintain the SNR, isolation, insertion loss of these signal when using these RF components. This makes characterization of the instrument response and calibration critical. Because of the use of RF signals in the MHz range and amplifiers at different stages of the circuit, care should be taken to avoid electromagnetic interference. To get more

concentrations of more than two chromophores, more wavelengths are required increasing the complexity of the instrumentation.

Another significant limitation of the mfFD-DOS system is that, it can only measures the static optical properties. To get a complete picture of the metabolism of tissue, we need information on blood flow which is dynamic property. A separate modality - Diffuse correlation Spectroscopy is needed to get the blood flow estimate. I discuss a new method to overcome this issue in the following chapter.

Chapter 4: Frequency Domain Diffuse Correlation Spectroscopy

4.1 Introduction

[2]In the previous chapter, I discussed multi-frequency FD-DOS and its implementation using heterodyne demodulation. Diffuse Optics spectroscopy (DOS) quantitatively measures the static properties of the tissue, *i.e.,* tissue absorption coefficient (μ_a) and scattering coefficient (μ_s), and hence tissue oxygen saturation [35,37,38]. While quantitative measurement of tissue oxygen saturation provides a good estimate of oxygen consumption, another tissue property – tissue blood flow, is required to fully characterize tissue function, per tissue metabolism, health, and pathology. The complimentary diffuse optics technique of Diffuse Correlation Spectroscopy (DCS) measures tissue perfusion. [37].

Recalling from Chapter 2 - in DCS, a highly coherent near infrared light source illuminates the tissue and diffuses through the it via multiple trajectories or path-lengths. The ensemble back-scattered light is collected at a detector position, and recorded using single photon counting detectors. As light diffuses through tissue, multiple scattering and absorption events occur, resulting in the change of light intensity at the detector. However, since DCS uses a coherent light source, scattering from moving particles in tissue (typically red blood cells), causes temporal and spatial fluctuations in the detected intensity. The auto-correlation function $(g_2(\tau)$ of these fluctuating intensities is fit to the solution of Correlation Diffusion Equation to estimate tissue blood flow/perfusion [13, 14, 16]. Here, fast blood flow results in a rapid decay of the auto-correlation function, while a slower flow results in slower decay.

[2] *This chapter is adapted from [75, 76]. Permission included in Appendix A. Submitted for provisional patent: Us Provisional patent application 63/265,626*

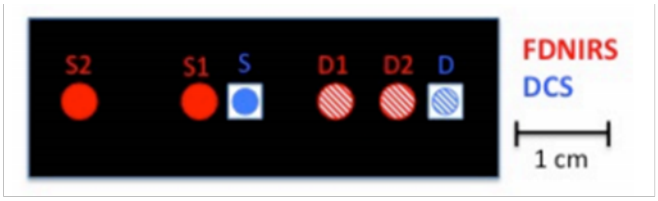

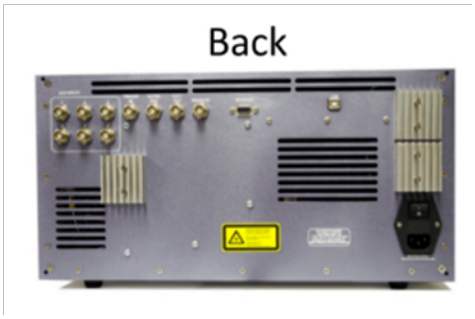

Figure 4.1: A hybrid multi-distance DOS and DCS probe and corresponding system. Figure adapted with permission from [19].

In practice, DCS or DOS are used separately in hemodynamic studies, leading to systematic measurement errors and unrealistic interpretations [9, 11, 43]. For instance, 'DOS only' measurements without the blood flow information, can interpret the cause of increased de-oxy hemoglobin as either increased oxygen metabolism or reduced blood supply. On the other hand, to estimate blood flow using DCS, static optical properties – absorption coefficient μ_a and scattering coefficient μ_s are required for the inverse model of Correlation Diffusion Equation [3]. It is a common practice to assume these optical properties for a nominal tissue type.

One solution to address these practical difficulties is to have simultaneous DOS and DCS measurements by using a hybrid probe as shown in Fig 4.1 [4, 19, 22, 25, 43, 65, 71, 110]. However, this somewhat simplistic yet effective solution suffers from the partial volume effects similar to multi-distance FD-DOS, discussed in Chapter 3. Since DOS and DCS fibers are typically located at different positions on the probe, the difference in measurement geometry leads to sampling of different tissue volumes by DOS and DCS instruments. This results in systematic errors in estimation of tissue oxygen saturation, blood flow, or both. Specifically, in the case of *in-vivo* measurements that are heterogeneous in nature, differences in sampling

volumes can produce significant measurement errors. Additionally, using a hybrid DOS and DCS significantly increases the cost $(2x)$ and portability $3x$ compared to a DOS-only or DCS-only approach. The increased size of the probe restricts its usage in spatially constrained areas like spine, neonates, and intrathoracic cavity. Recently a few methods like Time domain DCS [80, 97] and Interferometric NIRS [18] have been proposed to acquire static and dynamic optical properties simultaneously, typically with measurements at one source-detector separation. These methods however require complex instrumentation like custom pulsed laser sources, expensive enhanced detectors, and synchronized detection.

In this chapter, I introduce a new diffuse optical approach - Frequency Domain Diffuse Correlation Spectroscopy (FD-DCS) that aides in acquiring robust, quantitative measurements of tissue oxygen saturation and blood flow simultaneously. In FD-DCS, the multi-frequency aspect of multi-frequency FD-DOS is extended to DCS to acquire μ_a, μ_s and F from intensity auto-correlation functions measured at single source-detector separation. Specifically , the intensity of a highly coherent laser light source is modulated at RF frequencies $(\omega, 50MHz-400MHz)$ and a frequency dependent intensity auto-correlation function $g_2(\tau, \omega)$, is measured. A new general light propagation model - Frequency Domain Correlation Diffusion Equation (CDE) is developed and a multi-parametric fit of the measured frequency dependent auto-correlation function to the solution of frequency domain CDE will allow simultaneous estimation of μ_a, μ_s and F.

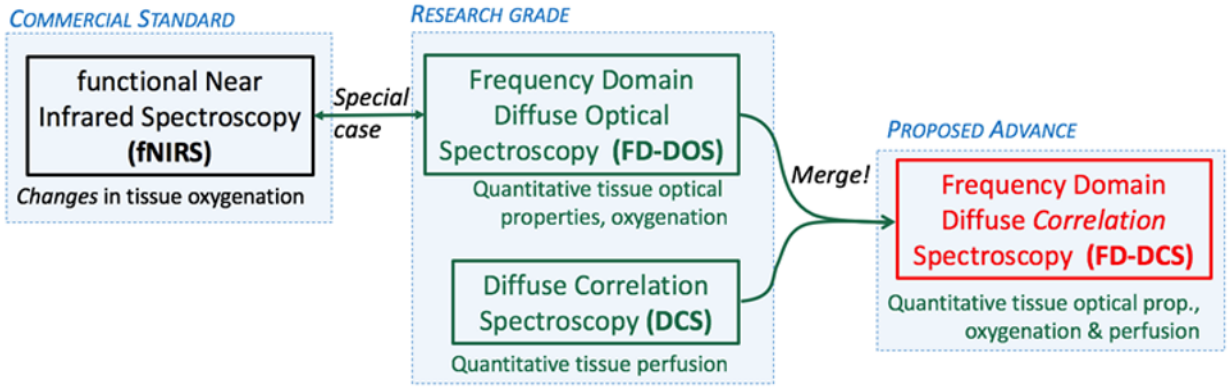

Figure 4.2: Frequency domain diffuse correlation spectroscopy approach

With simultaneous measurement of both static and optical properties at a single source-detector separation, FD-DCS eliminates the systematic errors caused due to the geometric variation in multi-distance measurements. Fig 3.3 confirms the differences of the spatial sampling volumes in the case of multi-distance and multi-frequency measurements. Multi-frequency measurements of optical signal at a single source-detector separation have similar tissue sensitivities. Also, it has been shown that tissue sampling volumes are relatively constant with modulation frequencies, for frequencies less than 600 MHz. [5]. FD-DCS eliminates the need for collocated sources and phase sensitive detectors, thus making the system portable and low cost. Higher speeds of data acquisitions can be achieved using FD-DCS as the flow and oxygenation information is implicit in the data set. These advantages make FD-DCS system a solution for some of the issues in traditional DOS and DCS systems. Furthermore, FD-DCS can be executed by simply replacing the source of a conventional fast DCS system with an intensity modulated coherent laser, the detector mechanism remains the same decreasing the build time and cost.

4.2 FD-DCS Model/Theory

Recalling from equation 2.22, the steady state time independent Correlation Diffusion Equation (CDE) is given by $[\nabla^2 D - \upsilon\mu_a - 2\upsilon\mu_s'\kappa_o^2 F\tau]G_1(\tau) = -\upsilon S_o$

Here, $G_1(\tau)$ is the electric field auto-correlation function, μ_a and μ_s' are the tissue absorption and scattering coefficients respectively, D is photon diffusion coefficient, υ is the speed of light in tissue, $\kappa_o = 2\pi/\lambda$ is the wave number of input light, τ is the correlation lag, S_o is the source power and F is the tissue blood flow index.

Also recall the Photon Diffusion Equation (PDE) (Equation 2.8) for a continuous wave source, given by $[\nabla^2 D - \upsilon\mu_a]\phi_{cw} = -\upsilon S_o$, where ϕ_{cw} is photon fluence rate for continuous wave source, and other terms are as defined above. We can view the Correlation Diffusion Equation (CDE) as an extension of the continuous wave Photon Diffusion Equation (PDE), but with the notable addition of a dynamic absorption term $2\upsilon\mu_s'\kappa_o^2 F\tau$. Further, the PDE for

an intensity modulated source can be extended from the continuous wave PDE by addition of the $i\omega$ term; $[\nabla^2 D - \upsilon\mu_a - i\omega]\phi_{ac} = -\upsilon S_{ac}$. Here, $\omega = 2\pi f$ and f is the frequency of modulation in [Hz] and $S_{ac} = S_o(1 + m.e^{i\omega t})$, m is the modulation depth of the source $(0 \leq m \leq 1)$.

Similarly, by adding $i\omega$ to the CDE, we can derive an expression for the Frequency domain Correlation Diffusion Equation(FD-CDE), which extends DCS to intensity modulated sources;

$$[\nabla^2 D - \upsilon\mu_a - 2\upsilon\mu_s'\kappa_o^2 F\tau - i\omega]G_1(\tau) = -\upsilon S_{ac} \tag{4.1}$$

The modulated intensity travels through the tissue as a wave and can be called Diffuse Correlation Density Wave(DCDW), similar to Diffuse Photon Density Wave(DPDW). The solution to the DCDW for semi-infinite homogeneous tissue is given by

$$G_1(\rho, \tau, \omega) = \frac{\upsilon}{4\pi D}\left[\frac{exp(-K_D(\tau,\omega)r_1)}{r_1} - \frac{exp(-K_D(\tau,\omega)r_b)}{r_b}\right] \tag{4.2}$$

Here,

ρ - Source - Detector Separation

$K_D(\tau, \omega) = [(\upsilon\mu_a - 2\upsilon\mu_s'\kappa_o^2 F\tau - i\omega)/D]^{1/2}$ - Frequency dependent dynamic wave vector

$r_1 = (l_{tr} + \rho^2)^{1/2}$; $r_b = ((2z_b + l_{tr})^2 + \rho^2)^{1/2}$

$l_{tr} \approx 1/\mu_s'$ - Transport mean free path

$Z_b = \frac{2}{3} l_{tr} \frac{1+R_{eff}}{1-R_{eff}}$ - Extrapolated zero boundary for index matched boundaries.

Numerical computation of the frequency dependent intensity auto-correlation function $g_{2_{FD}}(\rho, \tau, \omega)$ at $\rho = 2.5cm$ for a flow index of $F = 10^{-7} cm^2/sec$, $\beta = 0.5$, $\mu_a = 0.1cm^{-1}$ and $\mu_s' = 10cm^{-1}$ is shown in fig 4.3. This can be better understood by looking at fig 4.4 and fig 4.5. Fig 4.4 gives the traditional $g_2(\rho, \tau)$ with $\omega = 0$ and fig 4.5 is a the simulated $g_{2_{FD}}(\rho, \tau, \omega)$ intercept as a function of ω.

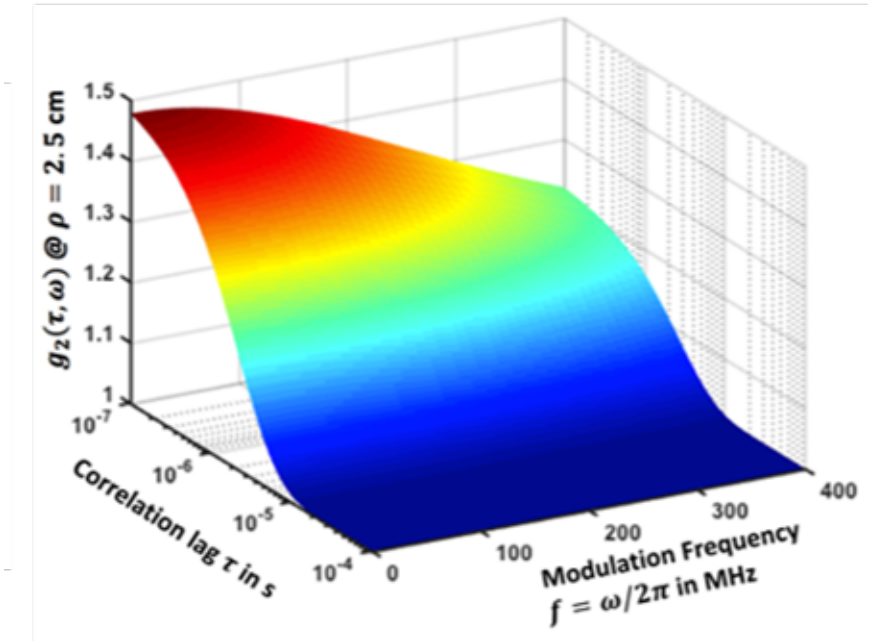

Figure 4.3: Surf plot of frequency dependent intensity auto-correlation function $g_{2_{FD}}(\rho, \tau, \omega)$ at $\rho = 2.5cm$ for a flow index of $F = 10^{-7}cm^2/sec$, $\beta = 0.5$, $\mu_a = 0.1cm^{-1}$ and $\mu_s' = 10cm^{-1}$

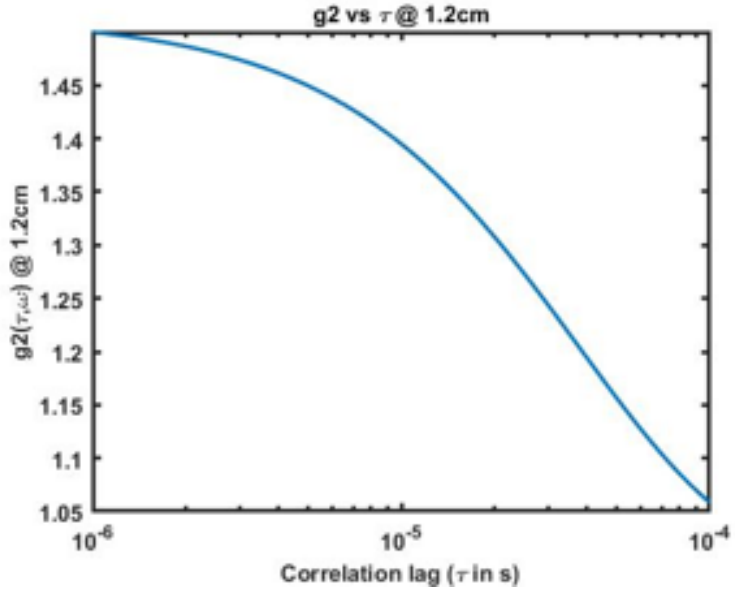

Figure 4.4: Frequency dependent intensity auto-correlation function $g_{2_{FD}}(\rho, \tau, \omega)$ at zero frequency

The frequency dependent solution of DCDW can be considered as the most general case of diffusion of coherent light through tissue with limiting cases being: (1) when $\tau =$ or $F = 0$

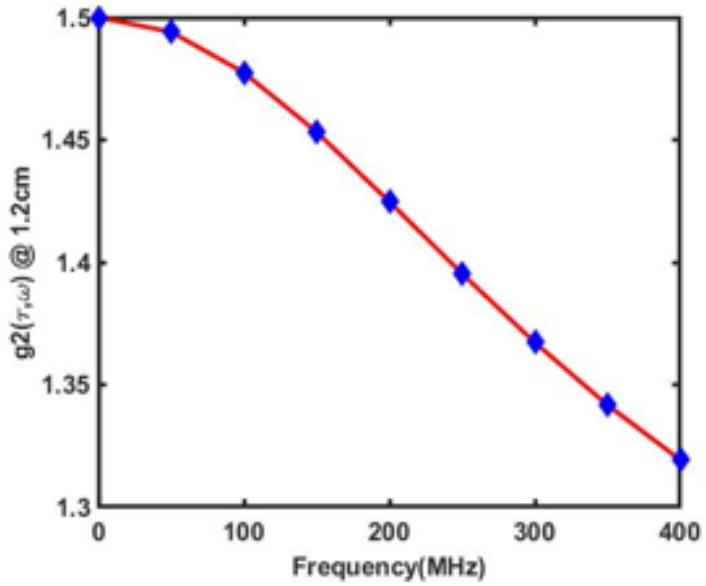

Figure 4.5: Intercept of $g_{2_{FD}}(\rho, \tau, \omega)$ as a function of modulating frequency (ω)

DCDW reduces to DPDW and the solution analogous to that of Frequency domain DOS, and (2) when $\omega = 0$ DCDW reduces to the Correlation Diffusion Equation (CDE).

We should note however that in FD-DOS, the AC component of the signal can be easily filtered from the DC component by using a DC blocking capacitor. Thus the solutions for FD-DOS typically only include expressions for the measured 'ac' fluence. However, this is not possible in DCS because, conventional DCS instruments record photon counts using a single photon counting avalanche photo diode. The recorded signal contains both AC and DC components, which needs to be accounted for via the modulation depth (m). One somewhat simplistic method to account for the modulation depth is to model the measured intensity auto-correlation function as

$$g_2(\tau, \rho, \omega) = 1 + \beta[(1 - m)|g_1(\rho, \tau, \omega = 0)|^2 + (m)|g_1(\rho, \tau, \omega = 0)|^2] \tag{4.3}$$

4.3 Instrumentation

Figure 4.6 provides a schematic of a practical implementation of FD-DCS. A long coherence, near infrared, wavelength stabilized laser (Thorlabs LD785-SEV300, $200 - 300mW$,

coherence length $\approx 10m$) was used as the light source. Use of the wavelength stabilized laser ensured that source coherence is sufficient for DCS measurements. The source light was collimated and coupled to custom fiber-optic probes (multimode) to illuminate the tissue sample. A constant current source (Thorlabs LDC205C) was used to drive the laser and a bias-tee was used to add an RF signal generated by a signal generator (HP 8648C – Synthesized RF Signal Generator). Source intensities were modulated at $0Hz$ (i.e., CW), and frequencies $50MHz$ to $400MHz$, in steps of $50MHz$. A free-space polarization sensitive NIR isolator was used to avoid back-reflections into the laser-diode cavity from the fiber coupling. A temperature controller (Thorlabs TED200C) was used to maintain the the laser diode temperature at room temperature. Isolator and temperature controller together help the laser diode to maintain the single frequency operation and thereby its coherence length.

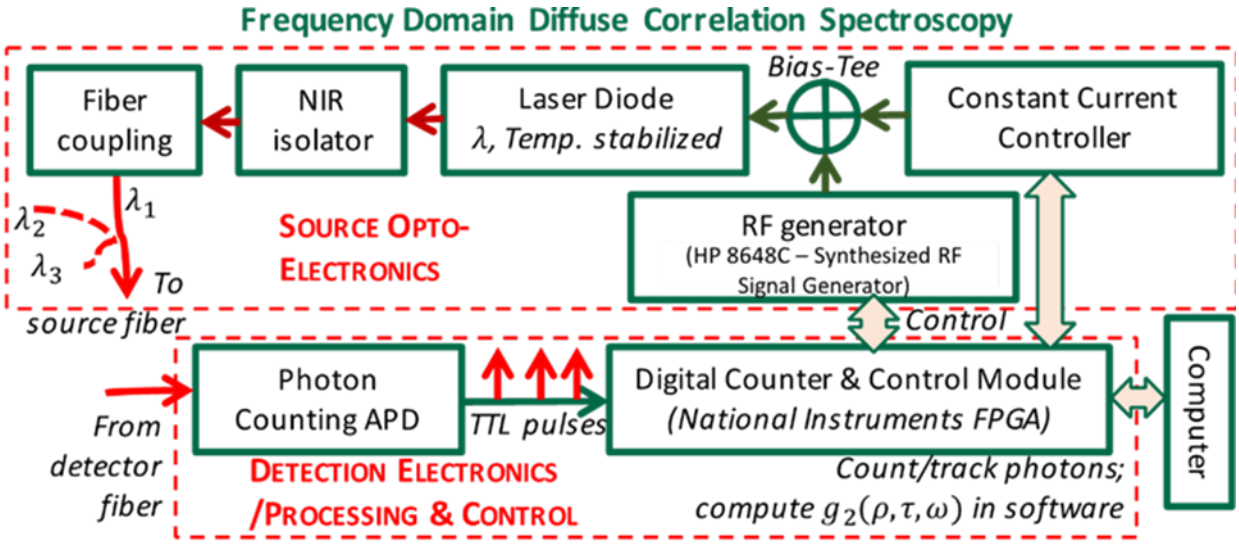

Figure 4.6: FD-DCS block diagram

Back-scattered light was collected at a detector position, $1.3cm$ away from the source on the sample using single-mode detector fibers and directed to single photon counting avalanche photo diodes, (Excelitas SPCM AQ4C, Quebec) typically used in DCS instruments. The APDs generate TTL pulses for every photon detected, which are counted using a NI counter/timer module (National Instruments PXI-6229, Austin, TX). Custom software (LabVIEW) ws used to acquire digital pulses at every modulation frequency using digital

counter/timer module (NI Instruments) with up to $20Hz$ acquisition rates to compute the DCS intensity auto-correlation function. Detection electronics, data acquisition and software control were similar to our recently developed fast diffuse correlation spectroscopy systems. To acquire μ_a,μ_s' and F intensity auto-correlation function was fit to the newly developed Frequency Domain Correlation Diffusion Equation model.

4.4 Experiments and Results

4.4.1 Validating Coherence Length of FD-DCS Light Source

FD-DCS introduces a significant change in the instrumentation of a DCS blood flow monitoring system, i.e., the intensity of the laser source is modulated at RF frequencies. The first experiment was to confirm that the light source maintained its coherence length at these modulation frequencies. The presence of the optical isolator after the laser the diode helps reduce back reflections from fibers/sample to the diode laser cavity. This is essential to maintaining single-frequency operation of the laser diode even when the laser intensity is not modulated. To verify that the single-frequency operation is maintained during intensity modulation, I characterized the line-width of the laser using a Fabry-Perot interferometer. Fabry-Perot interferometer, also known as multiple beam interferometer, detects the laser spectrum with high precision using interference from multiple beams generated from two highly reflective glass with partial transmission facing each other.

A Scanning Fabry-Perot interferometer (SA30-73, Thorlabs, Newton, NJ) was used to characterize the laser source. This instrument has a wavelength range of $630 - 824\ nm$, a free spectral range of $1.5GHz$, and resolution of less than $1MHz$. It therefore has sufficient range to observe the side lobes produced by modulating frequencies up to 700 MHz. The optical beam from the laser was collimated and steered into the interferometeric cavity. A controller (SA201, Thorlabs, Newton, NJ) was used to adjust the length of the cavity by adjusting supply voltage to the piezoelectric transducers present on the interferometer. The controller also generates an alternating voltage (triangle or saw-tooth) to scan the length

of the cavity accounting for one spectral range of the interferometer (Free spectral range of FSR). The transmitted light intensity was measured using a photo diode followed by a trans-impedance amplifier. A trigger/control signal from the controller was used to isolate one FSR for display on an oscilloscope for post processing.

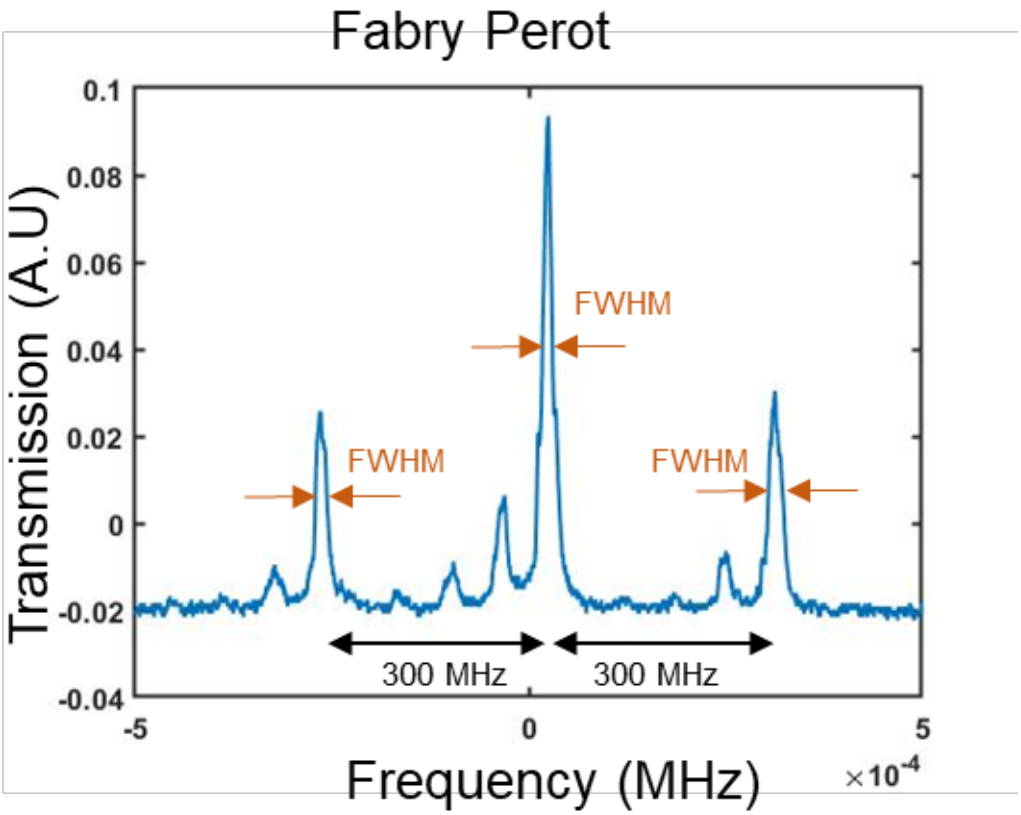

Figure 4.7: Fabry-Perot plot at 300 MHz intensity modulated laser source

Fig 4.7 shows the spectrum of the laser from a fabry-perot interferometer experiment with the laser source modulated at $300MHz$. The y-axis is the transmission intensity in arbitrary units. The x-axis represents one trigger period, equal to the free spectral range. A prominent central lobe and two side lobes are present clearly visible. The central peak represents the 'dc' operation of the laser, while the two side lobes represent the 'ac' components. Single-frequency operation can be confirmed by measuring the line width of the central and side lobes. Table 4.1 shows the line-width of the laser for all three lobes, measured as the full-width at half-max (FWHM) for different modulating frequencies. The line-width of the laser

Table 4.1: Line-width of intensity modulated laser source at multiple frequencies

Frequency (MHz)	Left Sidelobe (MHz)	Center Peak (MHz)	Right Sidelobe (MHz)
DC	-	100	-
50 MHz	110	230	110
100 MHz	100	400	100
150 MHz	100	170	100
200 MHz	110	320	125
250 MHz	160	110	140
300 MHz	125	100	160
350 MHz	90.9	166	125
400 MHz	110	160	111

stays relatively constant with modulating frequency, indicating that intensity modulating the laser source does not impact the coherence length.

4.4.2 Validation Experiments on Tissue Simulating Phantoms

I validated the FD-DCS instrument and model using tissue simulating phantoms to verify the accuracy of the device to estimate static and dynamic tissue optical properties, i.e., tissue absorption coefficient μ_a, tissue scattering coefficient μ_s, and blood flow index F. A liquid phantom, comprising of India ink, 20% intralipid and distilled water was used for this study.

Frequency dependent DCS intensity auto-correlation functions were recorded at each wavelength $g_2^m(\tau, \rho, \omega)$. Superscript m indicates measured data. The measured data was fit to the model describing frequency dependent intensity auto-correlation function $g_2^{th}(\tau, \rho, \omega)$, superscript th indicates theory, to estimate free parameters $mu_a(\lambda_1)$, $\mu_s(\lambda_1)$ and F. The fit was solved as a multivariate nonlinear optimization problem, wherein parameter $\chi^2 = \Sigma_{MxN}|g_2^{th}(\tau, \rho, \omega) - g_2^m(\tau, \rho, \omega)|^2$ was minimized over N correlation lags, and M modulation frequencies to estimate unknown parameters (fminsearch, MATLAB, Natick, MA). Additional fit parameters include β the speckle averaging factor and m the modulation depth. When translated to in-vivo experiments, concentrations C_{HbO}, C_{HbR} can be estimated from measured $\mu_a(\lambda)$ and molar extinction coefficients $\epsilon(\lambda)$. To elaborate, we solve the linear system

of equations given by $\mu_a(\lambda) = \epsilon_{HBR}(\lambda)C_{HbR} + \epsilon_{HbO}(\lambda)C_{HbO}$ where C_{HbO}, C_{HbR} corresponds to oxy- and deoxy- hemoglobin. Finally, tissue oxygen saturation is $StO_2 = C_{HbO}/(C_{HbO}+C_{HbR})$, and the metabolic rate of oxygen will be calculated from the oxygen concentrations and blood flow.

The prototype FD-DCS instrument was used to record $g_2(\tau, \rho, \omega)$ from the phantom with a custom fiber optic probe, with a source detector separation ($\rho = 1.2cm$), placed on the surface of the liquid (semi-infinite geometry). The integration time of the measurements was 100ms, while the average intensity across the modulation frequencies was $300KHz \pm 100KHz$. 180 intensity auto-correlation curves were averages (per frequency) to improve measurement signal to noise ratio. Fig 4.8 shows frequency dependent DCS intensity auto correlation functions measured from a representative liquid phantom with optical properties $\mu_a = 0.12cm^{-1}$ and $\mu_s' = 10cm^{-1}$ at $785nm$. The measured auto-correlation function data points are represented by circles, and each color/curve represents measurements made with different modulation frequencies from $0Hz$ to $400MHz$ in steps of $50MHz$. The x-axis represents correlation lag ($1\mu s$ to $100\mu s$) displayed on a log scale. The solid lines are fits of the data to the frequency dependent solution to the correlation diffusion equation (Equation). The nonlinear fitting estimated the phantom optical properties to be $\mu_a = 0.12cm^{-1}$ and $\mu_s' = 10cm^{-1}$. The optical properties were recovered within 5.3% error for μ_a and 9% μ_s'. The estimated blood flow index of $F = 2.88 \times 10^{-8}cm^2/s$ is in the rage of flow indices typically observed in these liquid phantoms.

The second tissue phantom experiment was to record/estimate the linearity and sensitivity of FD DCS to estimate changes in tissue optical properties. In a series of experimental sessions (4 steps each), the static and dynamic properties of the phantoms were systematically varied, while estimating μ_a, μ_s' and F from the measurements of $g_2(\tau, \rho, \omega)$. Specifically, μ_a was varied from 0.03 to $0.9cm^{-1}$ in steps of $0.02cm^{-1}$ by changing the concentration of India ink in the phantom. μ_s was varied from 60 to $140cm^{-1}$ in steps of $20cm^{-1}$ by changing the volume of intralipid in the phantom. F was held constant across all phantoms. As

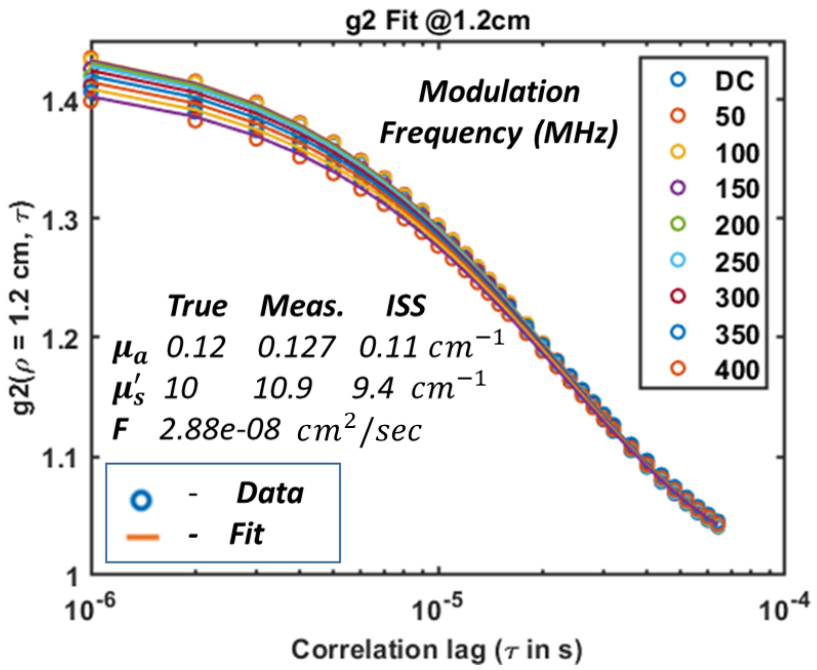

Figure 4.8: Representative frequency dependent intensity auto-correlation function measured at a source-detector separation $\rho = 1.2$cm, delay time $\tau = 1\mu s$ to $0.1ms$,wavelength $\lambda = 785nm$, modulating frequencies $\omega = 0 - 400MHz$ in steps of 50 MHz on a tissue simulating phantom of $\mu_a = 0.12cm^{-1}$ and $\mu_s' = 10cm^{-1}$. Optical properties are retrieved within $\approx 10\%$ error for a semi-infinite homogeneous tissue simulating phantom with a source-detector separation of 1.2 cm.

described above, 9 frequency dependent intensity auto-correlation functions were measured and averaged per frequency for all phantoms. Non-linear fitting of the measured data to Equation 4.3 yielded the estimates for μ_a, μ_s' and F. In all cases, the optical properties recovered using the FD-DCS instrument were compared to theoretical values. The relationship between measured and set tissue properties of the phantom will indicate the sensitivity of FD-DCS instrument to changes in μ_a and μ_s'.

Fig. 4.9 plots the phantom absorption coefficients (μ_a) estimated with FD-DCS on the y-axis, with the theoretical values along the x-axis. μ_s' and F were fixed for these phantoms. The solid diamond red markers indicate the estimated absorption coefficient, while the blue line is a linear fit to the data. The dashed black lines indicate the 95% confidence bounds of the linear regression. The slope of the regression line is 1.05 ($R^2 > 0.8$) indicating good 1:1 correspondence between measured and actual values of absorption coefficients. The results

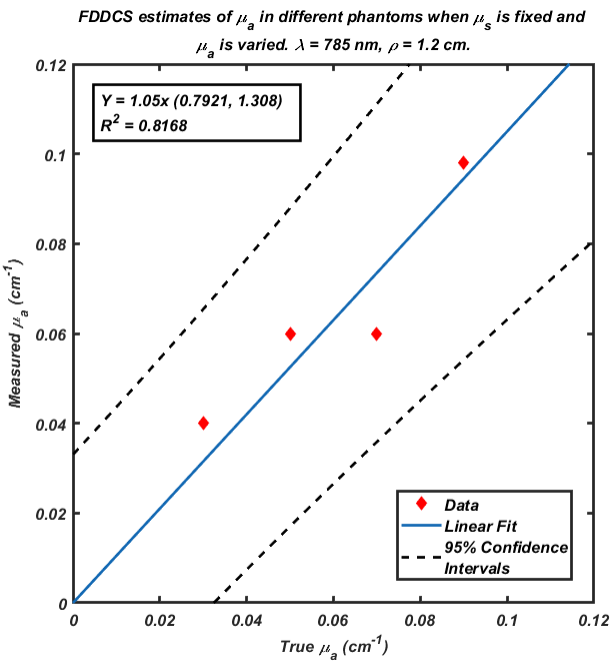

Figure 4.9: Sensitivity of FD-DCS system to absorption changes in tissue simulating phantoms when absorption coefficient is varied and scattering coefficient is kept constant

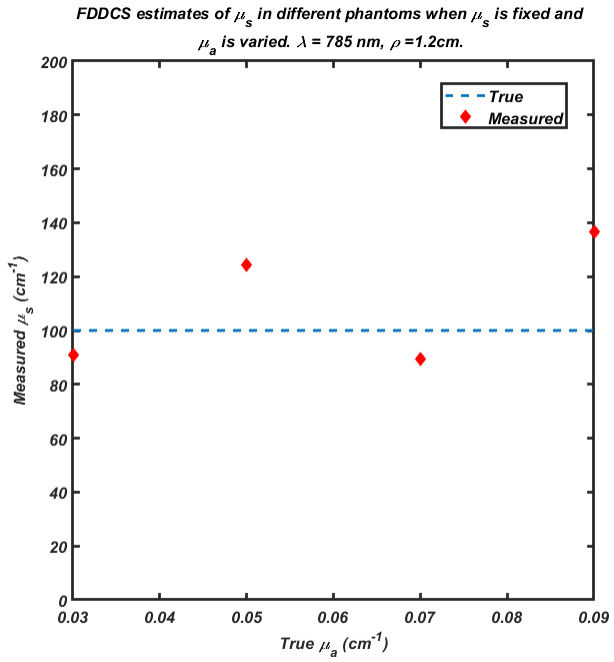

Figure 4.10: Sensitivity of FD-DCS system to scattering changes in tissue simulating phantoms when absorption coefficient is varied and scattering coefficient is kept constant

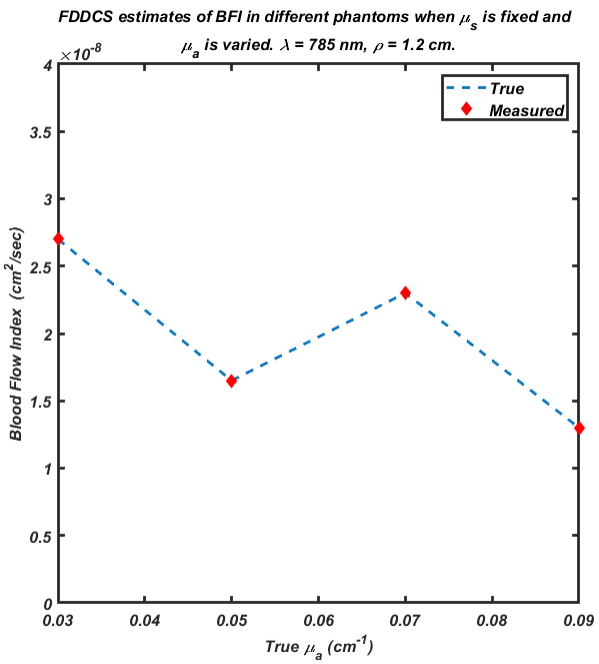

Figure 4.11: Sensitivity of FD-DCS system to BFI changes in tissue simulating phantoms when absorption coefficient is varied and scattering coefficient is kept constant

show that FD-DCS estimates of μ_a are linear. Figure 4.10 shows the estimates of μ_s by FD-DCS system for different phantoms when μ_a is varied and μ_s is fixed. As expected the phantom scattering coefficients are close to their true values. Figure 4.11 shows the estimates of BFI by FD-DCS system for different phantoms when μ_a is varied and μ_s is fixed. The blood flow index are in the order of $1e-8$ as expected and scattering coefficient for various phantoms in these phantoms were relatively constant.

Fig 4.12 demonstrates the sensitivity of FD-DCS system to scattering changes. Here, the scattering coefficient (μ_s) estimated with FD-DCS is on the y-axis, with the theoretical values along the x-axis. μ_a and F were fixed for these phantoms. The solid diamond red markers indicate the estimated absorption coefficient, while the blue line is a linear fit to the data. The dashed black lines indicate the 95% confidence bounds of the linear regression. The slope of the regression line is 1.12 ($R^2 > 0.89$) indicating good 1:1 correspondence between measured and actual values of absorption coefficients. The results show that FD-DCS estimates of μ_s are linear. Figure 4.13 shows the estimates of μ_a by FD-DCS system

for different phantoms when μ_s is varied and μ_a is fixed. Figure 4.14 shows the estimates of BFI by FD-DCS system for different phantoms when μ_s is varied and μ_a is fixed. The blood flow index are also in the order of $1e-8$ and scattering coefficient for various phantoms in these phantoms were relatively constant.

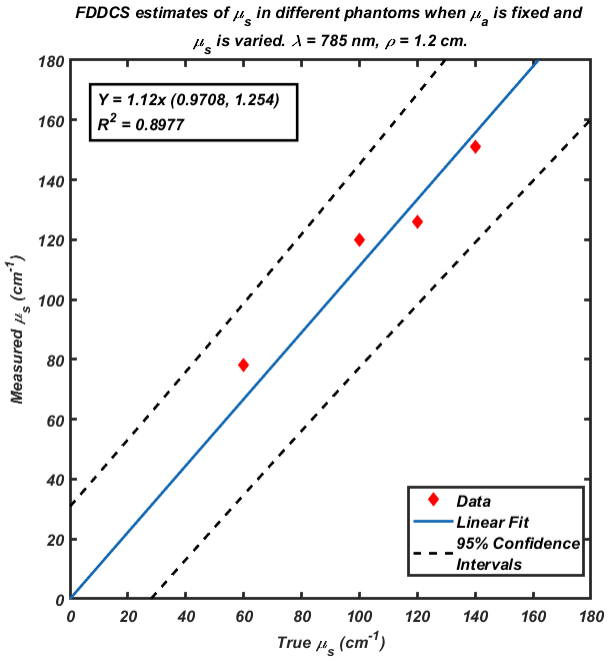

Figure 4.12: Sensitivity of FD-DCS system to scattering changes in tissue simulating phantoms when scattering coefficient is varied and absorption coefficient is kept constant

4.5 Discussion

The results indicate that the newly developed FD-DCS system can retrieve the static and dynamic optical properties. For phantom 1, absorption coefficient(mu_a) and scattering coefficient (mu_s) are retrieved with a maximum error of 9% while a commercial FD-DOS system (ISS Imagent) retrieved the properties with maximum error of 10%. F was retrieved in the order of $1e{-}8cm^2/sec$ with both FD-DCS system and conventional fast DCS system. The sensitivity of FD-DCS system to the absorption, scattering and flow changes were verified. Furthermore, the new general diffusion model includes the effect of source modulation depth.

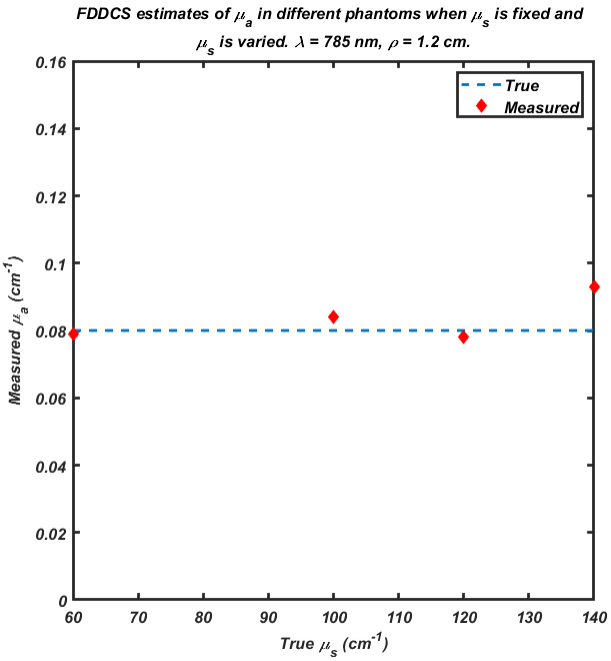

Figure 4.13: Sensitivity of FD-DCS system to absorption changes in tissue simulating phantoms when scattering coefficient is varied and absorption coefficient is kept constant

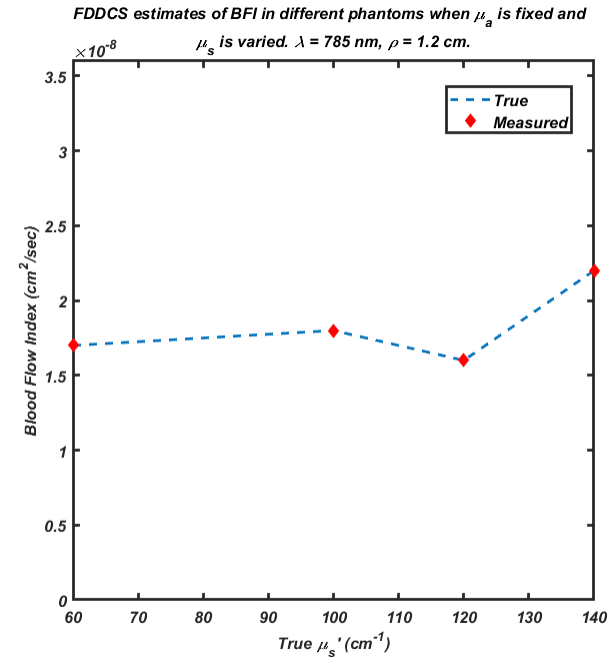

Figure 4.14: Sensitivity of FD-DCS system to BFI changes in tissue simulating phantoms when scattering coefficient is varied and absorption coefficient is kept constant

We note a few other considerations for the instrument/measurement. It is important that the source laser diode be operated within its linear range throughout the modulation frequencies in order to avoid the influence of harmonics. Practically, we accomplish this by characterizing the diode frequency characteristics using a Fabry Perot scanning interferometer. However, the sensitivity of the isolator, small misalignments due to presence of an elliptical laser beam (non-gaussian beam) may introduce errors in the measurement. The Fabry Perot measurements can also confirm that the coherence length of the laser is preserved while modulating the laser at RF frequencies. Resolving the above issues could improve the accuracy of the FD DCS measurements. Nevertheless, FD-DCS is a significant advance of optical technology to retrieve optical properties at single source detector distance in one measurement. With sufficient optimizations in the instrument and model, it can be a versatile instrument to monitor tissue static and dynamic optical properties at the bedside.

4.5.1 A More Rigorous Model for FD-DCS

In section 4.2 we proposed an empirical model to account for the influence of the modulation depth. While this model works to the first approximation, a more robust expression could help improve the accuracy of the FD-DCS instrument.

Here, I derive a rigorous expression for the intensity auto-correlation function directly from the electric fields. Recall that $G_1(\tau, \omega)$ is the un-normalized electric field auto-correlation function, and $G_2(\tau, \omega)$ is the un-normalized intensity auto-correlation function; only the latter is measured in practice.

The electric field reaching the detector is a superposition of electric field due to continuous wave and modulating source. Therefore,

$$E(t) = E_{dc}(t) + E_{ac}(t) \tag{4.4}$$

The temporal intensity auto-correlation function can be written as

$$G_2(\tau) = \langle I(t)I(t+\tau)\rangle_t \tag{4.5}$$

Inserting equation 4.4 in equation 4.5 ($I = E^2$) and expanding yields 16 terms.

$$\begin{aligned}
G_{2FD}(\tau) &= \langle I(t)I(t+\tau)\rangle_t \\
&= \langle E(t)E^*(t)E(t+\tau)E^*(t+\tau)\rangle_t \\
&= \langle (E_{dc}(t)+E_{ac}(t))(E^*_{dc}(t)+E^*_{ac}(t)) \\
&\quad (E_{dc}(t+\tau)+E_{ac}(t+\tau))(E^*_{dc}(t+\tau)+E^*_{ac}(t+\tau))\rangle_t \\
&= \langle (E_{dc}(t)E^*_{dc}(t)+E_{dc}(t)E^*_{ac}(t)+E_{ac}(t))E^*_{dc}(t)+E_{ac}(t))E^*_{ac}(t)) \\
&\quad (E_{dc}(t+\tau)E^*_{dc}(t+\tau)+E_{dc}(t+\tau)E^*_{ac}(t+\tau) \\
&\quad + E_{ac}(t+\tau))E^*_{dc}(t+\tau)+E_{ac}(t+\tau))E^*_{ac}(t+\tau))\rangle_t
\end{aligned} \tag{4.6}$$

$$\begin{aligned}
G_{2FD}(\tau) = \langle & E_{dc}(t)E^*_{dc}(t)E_{dc}(t+\tau)E^*_{dc}(t+\tau) + E_{dc}(t)E^*_{dc}(t)E_{dc}(t+\tau)E^*_{ac}(t+\tau) \\
&+ E_{dc}(t)E^*_{dc}(t)E_{ac}(t+\tau)E^*_{dc}(t+\tau) + E_{dc}(t)E^*_{dc}(t)E_{ac}(t+\tau)E^*_{ac}(t+\tau) \\
&+ E_{ac}(t)E^*_{dc}(t)E_{dc}(t+\tau)E^*_{dc}(t+\tau) + E_{ac}(t)E^*_{dc}(t)E_{dc}(t+\tau)E^*_{ac}(t+\tau) \\
&+ E_{ac}(t)E^*_{dc}(t)E_{ac}(t+\tau)E^*_{dc}(t+\tau) + E_{ac}(t)E^*_{dc}(t)E_{ac}(t+\tau)E^*_{ac}(t+\tau) \\
&+ E_{dc}(t)E^*_{ac}(t)E_{dc}(t+\tau)E^*_{dc}(t+\tau) + E_{dc}(t)E^*_{ac}(t)E_{dc}(t+\tau)E^*_{ac}(t+\tau) \\
&+ E_{dc}(t)E^*_{ac}(t)E_{ac}(t+\tau)E^*_{dc}(t+\tau) + E_{dc}(t)E^*_{ac}(t)E_{ac}(t+\tau)E^*_{ac}(t+\tau) \\
&+ E_{ac}(t)E^*_{ac}(t)E_{dc}(t+\tau)E^*_{dc}(t+\tau) + E_{ac}(t)E^*_{ac}(t)E_{dc}(t+\tau)E^*_{ac}(t+\tau) \\
&+ E_{ac}(t)E^*_{ac}(t)E_{ac}(t+\tau)E^*_{dc}(t+\tau) + E_{ac}(t)E^*_{ac}(t)E_{ac}(t+\tau)E^*_{ac}(t+\tau)\rangle_t
\end{aligned} \tag{4.7}$$

We note that 10 of these products (terms 2, 3, 4, 5, 8, 9, 12, 13, 14, and 15) average to zero. Thus $G_{2FD}(\tau)$ simplifies to

$$
\begin{aligned}
G_{2FD}(\tau) = \langle & E_{dc}(t)E^*_{dc}(t)E_{dc}(t+\tau)E^*_{dc}(t+\tau) \\
& + E_{ac}(t)E^*_{dc}(t)E_{dc}(t+\tau)E^*_{ac}(t+\tau) \\
& + E_{ac}(t)E^*_{dc}(t)E_{ac}(t+\tau)E^*_{dc}(t+\tau) \\
& + E_{dc}(t)E^*_{ac}(t)E_{dc}(t+\tau)E^*_{dc}(t+\tau) \\
& + E_{dc}(t)E^*_{ac}(t)E_{ac}(t+\tau)E^*_{ac}(t+\tau) \\
& + E_{ac}(t)E^*_{ac}(t)E_{ac}(t+\tau)E^*_{ac}(t+\tau)\rangle_t
\end{aligned}
\tag{4.8}
$$

Here, terms 1 and 6 in equation 4.8 are readily seen as representing the auto-correlation of dc and ac terms alone, while and terms 3 and 4 are cross terms. The terms 2 and 4 convert to intensity terms as shown below

$$
\begin{aligned}
G_{2FD}(\tau) \approx \langle I^2_{dc}\rangle_t + \beta\langle I^2_{dc}\rangle_t |g_{1dc}(\tau)|^2 + 2I_{dc}I_{ac} + 2\beta I_{dc}I_{ac}|g_{1dc}||g_{1ac}| \\
+\langle I^2_{ac}\rangle_t + \beta\langle I^2_{ac}\rangle_t |g_{1ac}(\tau)|^2
\end{aligned}
\tag{4.9}
$$

In FD-DCS the source is a modulating source and given by $S_{ac} = S_o(1+m.e^{i\omega t})$, implying $I = I_{ac} + I_{dc}$ and $I_{ac}/I_{dc} = m$. The normalized intensity auto-correlation function after substituting m in equation 4.9 is

$$
g_{2_{FD}}(\rho,\tau,\omega) = 1 + \beta\left[\frac{|g_{1dc}(\tau)|^2 + 2m|g_{1dc}||g_{1ac}| + m^2|g_{1ac}(\tau)|^2}{(1+m)^2}\right] \tag{4.10}
$$

We note here, that for a conventional CW-DCS, $g_{1ac} = 0$ and $m = 0$, in which case $g_{2_{FD}}(\rho,\tau,\omega = 0)$ reduces to $g_2(\rho,\tau) = 1 + \beta|g_{1dc}(\tau)|^2$, which is the well known Siegert relation [5, 38]

Chapter 5: Conclusion and Future Work

5.1 Conclusion

In this dissertation, I have used frequency domain diffuse optical methods to measure oxy- and de-oxy hemoglobin concentrations as well as blood flow. These new techniques minimize systematic errors, cost and form factor of conventional diffuse optics instruments. To measure the static optical properties, I have introduced a heterodyne demodulation method to perform multi-frequency Frequency Domain Diffuse Optical Spectroscopy (mfFD-DOS), which could be easily realized using off-the-shelf components. The new system not only reduces partial volume effects but can also be used to estimate optical properties at longer source-detector separations.

In addition, I have extended the multi-frequency aspect of the mfFD-DOS system to Diffuse Correlation Spectroscopy (DCS), to estimate both the static and dynamic optical properties using a new approach - 'Frequency Domain Diffuse Correlation Spectroscopy' (FD-DCS). I have developed a new theory/model, and have characterized and validated the approach in systematic experiments. FD-DCS can be a replacement to hybrid DOS - DCS systems and it reduces the partial volume effects. I hope the systems I introduced will impact the landscape of biomedical diffuse optics in monitoring blood oxygenation and blood flow and provide life-saving information.

Here, I layout some of the possible applications for these new instruments.

5.2 Future Work and Applications

5.2.1 Extension to Other Wavelengths

In chapter 4, I developed a new FD-DCS technique, derived a new mathematical model and conducted experiments to demonstrate its validity by performing systematic experiments using a 785 nm source. The FD-DCS system can be extended to other wavelengths in the NIR region to perform *in-vivo* experiments. Two wavelengths on either side of the isobestic point (wavelength where the molar extinction coefficients for oxy and de-oxy hemoglobin are equal) will enable the estimation of tissue optical properties and blood flow in a single measurement. A dual wavelength FD-DCS system would have similar wavelengths to mFFD-DOS system. Generally, any wavelength source above 820 nm with a single frequency output would be suitable to execute the system.

One limitation of selecting the wavelengths from the near infrared region is that the SNR drops drastically for Recently, Carp. et al [23] have performed diffuse correlation spectroscopy at wavelength $1064nm$ for better SNR and lower attenuation ($< 30\%$ compared to 785 nm). mfFD-DOS and FDDCS systems can both be readily implemented at these wavelengths to probe deeper tissues with a high SNR.

5.2.2 Functional Clinical Studies

Functional activation studies using diffuse optics and imaging techniques have gained momentum in the last decade [2]. Functional studies are systematic studies that measure the cerebral tissue response for simulated activation's for specific areas of the human body. Generally, these studies are performed to monitor response of different cortical activity of the brain corresponding to functional activity of different parts. mfFD-DOS and FD-DCS systems have the advantages of reducing the partial volume effects and decreasing the form factor and can be used to perform these functional activation studies.

5.2.3 Wearables Using Silicon Photonics

Substantial advancements have been made in the field of semiconductor industry that can allow the implementation of wearable devices using diffuse optics [93]. Recently, we have shown a fiberless DCS system [12] that eliminates the use of optical fibers and can be a wearable device for monitoring blood flow continuously. These devices can revolutionize the diagnosis and monitoring in medical field for point-of-care devices and at-home personal devices. mfFD-DOS and FD-DCS systems can be implemented to be wearable devices with the advancements in silicon photonics. These systems can make use of integrated photonics circuits to include the signal generation and acquisition electronics on one single IC.

5.2.4 Real Time Computations

Conventional diffuse optics devices post-process the data to infer the results. Stillwell et. al. [95] introduced a look-up- table approach to estimate and image the tissue concentrations real time. Extension of these techniques to the new FD-DCS system would help to get the complete picture of the tissue real time by estimating the concentration of oxy and de-oxy hemoglobin along with the blood flow index.

References

[1] Matthew B Applegate and Darren Roblyer. Multi-distance diffuse optical spectroscopy with a single optode via hypotrochoidal scanning. *Optics Letters*, 43(4):747–750, 2018.

[2] Hasan Ayaz, Wesley B Baker, Giles Blaney, David A Boas, Heather Bortfeld, Kenneth Brady, Joshua Brake, Sabrina Brigadoi, Erin M Buckley, Stefan A Carp, et al. Optical imaging and spectroscopy for the study of the human brain: status report. *Neurophotonics*, 9(S2):S24001, 2022.

[3] Wesley B Baker, Ashwin B Parthasarathy, David R Busch, Rickson C Mesquita, Joel H Greenberg, and AG Yodh. Modified beer-lambert law for blood flow. *Biomedical optics express*, 5(11):4053–4075, 2014.

[4] Wesley B Baker, Ashwin B Parthasarathy, Tiffany S Ko, David R Busch, Kenneth Abramson, Shih-Yu Tzeng, Rickson C Mesquita, Turgut Durduran, Joel H Greenberg, David K Kung, et al. Pressure modulation algorithm to separate cerebral hemodynamic signals from extracerebral artifacts. *Neurophotonics*, 2(3):035004, 2015.

[5] Wesley Boehs Baker. *Optical cerebral blood flow monitoring of mice to men*. University of Pennsylvania, 2015.

[6] Han Y Ban, David R Busch, Saurav Pathak, Frank A Moscatelli, Manabu Machida, John C Schotland, Vadim A Markel, and Arjun G Yodh. Diffuse optical tomography in the presence of a chest wall. *Journal of biomedical optics*, 18(2):026016, 2013.

[7] HY Ban, M Schweiger, VC Kavuri, JM Cochran, L Xie, DR Busch, J Katrašnik, S Pathak, SH Chung, Kijoon Lee, et al. Heterodyne frequency-domain multispectral diffuse optical tomography of breast cancer in the parallel-plane transmission geometry. *Medical physics*, 43(7):4383–4395, 2016.

[8] Krzysztof B Beć, Justyna Grabska, and Christian W Huck. Near-infrared spectroscopy in bio-applications. *Molecules*, 25(12):2948, 2020.

[9] Frédéric Bevilacqua, Joon S You, Carole K Hayakawa, and Vasan Venugopalan. Sampling tissue volumes using frequency-domain photon migration. *Physical Review E*, 69(5):051908, 2004.

[10] Irving J Bigio and Sergio Fantini. *Quantitative biomedical optics: theory, methods, and applications*. Cambridge University Press, 2016.

[11] Tiziano Binzoni, Angelo Sassaroli, Alessandro Torricelli, Lorenzo Spinelli, Andrea Farina, Turgut Durduran, Stefano Cavalieri, Antonio Pifferi, and Fabrizio Martelli. Depth sensitivity of frequency domain optical measurements in diffusive media. *Biomedical Optics Express*, 8(6):2990–3004, 2017.

[12] Arindam Biswas, Sadhu Moka, Andreas Muller, and Ashwin B Parthasarathy. Fast diffuse correlation spectroscopy with a low-cost, fiber-less embedded diode laser. *Biomedical Optics Express*, 12(11):6686–6700, 2021.

[13] DA Boas, MA O'Leary, B Chance, and AG Yodh. Scattering and wavelength transduction of diffuse photon density waves. *Physical Review E*, 47(5):R2999, 1993.

[14] David A Boas, LE Campbell, and Arjun G Yodh. Scattering and imaging with diffusing temporal field correlations. *Physical review letters*, 75(9):1855, 1995.

[15] David A Boas, Tom Gaudette, Gary Strangman, Xuefeng Cheng, John JA Marota, and Joseph B Mandeville. The accuracy of near infrared spectroscopy and imaging during focal changes in cerebral hemodynamics. *Neuroimage*, 13(1):76–90, 2001.

[16] David A Boas and Arjun G Yodh. Spatially varying dynamical properties of turbid media probed with diffusing temporal light correlation. *JOSA A*, 14(1):192–215, 1997.

[17] David Alan Boas. *Diffuse photon probes of structural and dynamical properties of turbid media: theory and biomedical applications*. University of Pennsylvania, 1996.

[18] Dawid Borycki, Oybek Kholiqov, Shau Poh Chong, and Vivek J Srinivasan. Interferometric near-infrared spectroscopy (inirs) for determination of optical and dynamical properties of turbid media. *Optics express*, 24(1):329–354, 2016.

[19] Erin M Buckley, Stefan Carp, Ivy Lin, Haruo Nakaji, Jay Dubb, Dennis Heuber, Mathieu Dehaes, Ellen Grant, David Boas, and Maria Angela Franceschini. A novel combined frequency-domain near-infrared spectroscopy and diffuse correlation spectroscopy system. In *Biomedical Optics*, pages BM3A–17. Optical Society of America, 2014.

[20] Erin M Buckley, Noah M Cook, Turgut Durduran, Meeri N Kim, Chao Zhou, Regine Choe, Guoqiang Yu, Susan Shultz, Chandra M Sehgal, Daniel J Licht, et al. Cerebral hemodynamics in preterm infants during positional intervention measured with diffuse correlation spectroscopy and transcranial doppler ultrasound. *Optics Express*, 17(15):12571–12581, 2009.

[21] David R Busch, Regine Choe, Mark A Rosen, Wensheng Guo, Turgut Durduran, Michael D Feldman, Carolyn Mies, Brian J Czerniecki, Julia Tchou, Angela DeMichele, et al. Optical malignancy parameters for monitoring progression of breast cancer neoadjuvant chemotherapy. *Biomedical optics express*, 4(1):105–121, 2013.

[22] Stefan A Carp, Parisa Farzam, Norin Redes, Dennis M Hueber, and Maria Angela Franceschini. Combined multi-distance frequency domain and diffuse correlation spectroscopy system with simultaneous data acquisition and real-time analysis. *Biomedical optics express*, 8(9):3993–4006, 2017.

[23] Stefan A Carp, Davide Tamborini, Dibbyan Mazumder, Kuan-Cheng Wu, Mitchell B Robinson, Kimberly A Stephens, Oleg Shatrovoy, Niyom Lue, Nisan Ozana, Megan H Blackwell, et al. Diffuse correlation spectroscopy measurements of blood flow using 1064 nm light. *Journal of Biomedical Optics*, 25(9):097003, 2020.

[24] Albert Cerussi, David Hsiang, Natasha Shah, Rita Mehta, Amanda Durkin, John Butler, and Bruce J Tromberg. Predicting response to breast cancer neoadjuvant chemotherapy using diffuse optical spectroscopy. *Proceedings of the National Academy of Sciences*, 104(10):4014–4019, 2007.

[25] Cecil Cheung, Joseph P Culver, Kasushi Takahashi, Joel H Greenberg, and AG Yodh. In vivo cerebrovascular measurement combining diffuse near-infrared absorption and correlation spectroscopies. *Physics in Medicine & Biology*, 46(8):2053, 2001.

[26] Regine Choe, Soren D Konecky, Alper Corlu, Kijoon Lee, Turgut Durduran, David R Busch Jr, Saurav Pathak, Brian J Czerniecki, Julia C Tchou, Douglas L Fraker, et al. Differentiation of benign and malignant breast tumors by in-vivo three-dimensional parallel-plate diffuse optical tomography. *Journal of biomedical optics*, 14(2):024020, 2009.

[27] Regine Choe, Mary E Putt, Peter M Carlile, Turgut Durduran, Joseph M Giammarco, David R Busch, Ki Won Jung, Brian J Czerniecki, Julia Tchou, Michael D Feldman, et al. Optically measured microvascular blood flow contrast of malignant breast tumors. *PloS one*, 9(6):e99683, 2014.

[28] SH Chung, AE Cerussi, C Klifa, HM Baek, O Birgul, G Gulsen, SI Merritt, D Hsiang, and BJ Tromberg. In vivo water state measurements in breast cancer using broadband diffuse optical spectroscopy. *Physics in Medicine & Biology*, 53(23):6713, 2008.

[29] SH Chung, AE Cerussi, SI Merritt, J Ruth, and BJ Tromberg. Non-invasive tissue temperature measurements based on quantitative diffuse optical spectroscopy (dos) of water. *Physics in Medicine & Biology*, 55(13):3753, 2010.

[30] Jeffrey M Cochran, David R Busch, Anaïs Leproux, Zheng Zhang, Thomas D O'Sullivan, Albert E Cerussi, Philip M Carpenter, Rita S Mehta, Darren Roblyer, Wei Yang, et al. Tissue oxygen saturation predicts response to breast cancer neoadjuvant chemotherapy within 10 days of treatment. *Journal of biomedical optics*, 24(2):021202, 2018.

[31] JM Cochran, SH Chung, A Leproux, WB Baker, DR Busch, AM DeMichele, J Tchou, BJ Tromberg, and AG Yodh. Longitudinal optical monitoring of blood flow in breast tumors during neoadjuvant chemotherapy. *Physics in Medicine & Biology*, 62(12):4637, 2017.

[32] M Cope, DT Delpy, EOR Reynolds, S Wray, JVdZP Wyatt, and P Zee. Methods of quantitating cerebral near infrared spectroscopy data. In *Oxygen Transport to Tissue X*, pages 183–189. Springer, 1988.

[33] JP Culver, R Choe, MJ Holboke, L Zubkov, T Durduran, A Slemp, V Ntziachristos, B Chance, and AG Yodh. Three-dimensional diffuse optical tomography in the parallel plane transmission geometry: Evaluation of a hybrid frequency domain/continuous wave clinical system for breast imaging. *Medical physics*, 30(2):235–247, 2003.

[34] Hamid Dehghani, Matthew E Eames, Phaneendra K Yalavarthy, Scott C Davis, Subhadra Srinivasan, Colin M Carpenter, Brian W Pogue, and Keith D Paulsen. Near infrared optical tomography using nirfast: Algorithm for numerical model and image reconstruction. *Communications in numerical methods in engineering*, 25(6):711–732, 2009.

[35] Turgut Durduran, Regine Choe, Wesley B Baker, and Arjun G Yodh. Diffuse optics for tissue monitoring and tomography. *Reports on progress in physics*, 73(7):076701, 2010.

[36] Turgut Durduran, Regine Choe, Guoqiang Yu, Chao Zhou, Julia C Tchou, Brian J Czerniecki, and Arjun G Yodh. Diffuse optical measurement of blood flow in breast tumors. *Optics letters*, 30(21):2915–2917, 2005.

[37] Turgut Durduran and Arjun G Yodh. Diffuse correlation spectroscopy for non-invasive, micro-vascular cerebral blood flow measurement. *Neuroimage*, 85:51–63, 2014.

[38] Turgut Durduran, Guoqiang Yu, Mark G Burnett, John A Detre, Joel H Greenberg, Jiongjiong Wang, Chao Zhou, and Arjun G Yodh. Diffuse optical measurement of blood flow, blood oxygenation, and metabolism in a human brain during sensorimotor cortex activation. *Optics letters*, 29(15):1766–1768, 2004.

[39] Turgut Durduran, Chao Zhou, Erin M Buckley, Meeri N Kim, Guoqiang Yu, Regine Choe, J William Gaynor, Thomas L Spray, Suzanne M Durning, Stefanie E Mason, et al. Optical measurement of cerebral hemodynamics and oxygen metabolism in neonates with congenital heart defects. *Journal of biomedical optics*, 15(3):037004, 2010.

[40] Turgut Durduran, Chao Zhou, Brian L Edlow, Guoqiang Yu, Regine Choe, Meeri N Kim, Brett L Cucchiara, Mary E Putt, Qaisar Shah, Scott E Kasner, et al. Transcranial optical monitoring of cerebrovascular hemodynamics in acute stroke patients. *Optics express*, 17(5):3884–3902, 2009.

[41] Adam T Eggebrecht, Silvina L Ferradal, Amy Robichaux-Viehoever, Mahlega S Hassanpour, Hamid Dehghani, Abraham Z Snyder, Tamara Hershey, and Joseph P Culver. Mapping distributed brain function and networks with diffuse optical tomography. *Nature photonics*, 8(6):448–454, 2014.

[42] Sergio Fantini, Dennis Hueber, Maria Angela Franceschini, Enrico Gratton, Warren Rosenfeld, Phillip G Stubblefield, Dev Maulik, and Miljan R Stankovic. Non-invasive optical monitoring of the newborn piglet brain using continuous-wave and frequency-domain spectroscopy. *Physics in Medicine & Biology*, 44(6):1543, 1999.

[43] Parisa Farzam, Erin M Buckley, Pei-Yi Lin, Katherine Hagan, P Ellen Grant, Terrie Eleanor Inder, Stefan A Carp, and Maria Angela Franceschini. Shedding light on the neonatal brain: probing cerebral hemodynamics by diffuse optical spectroscopic methods. *Scientific reports*, 7(1):1–10, 2017.

[44] Christopher G Favilla, Rickson C Mesquita, Michael Mullen, Turgut Durduran, Xiangping Lu, Meeri N Kim, David L Minkoff, Scott E Kasner, Joel H Greenberg, Arjun G Yodh, et al. Optical bedside monitoring of cerebral blood flow in acute ischemic stroke patients during head-of-bed manipulation. *Stroke*, 45(5):1269–1274, 2014.

[45] Marco Ferrari, Makii Muthalib, and Valentina Quaresima. The use of near-infrared spectroscopy in understanding skeletal muscle physiology: recent developments. *Philosophical Transactions of the Royal Society A: Mathematical, Physical and Engineering Sciences*, 369(1955):4577–4590, 2011.

[46] Joshua B. Fishkin, Olivier Coquoz, Eric R. Anderson, Matthew Brenner, and Bruce J. Tromberg. Frequency-domain photon migration measurements of normal and malignant tissue optical properties in a human subject. *Appl. Opt.*, 36(1):10–20, Jan 1997.

[47] Joshua B Fishkin, Peter TC So, Albert E Cerussi, Sergio Fantini, Maria Angela Franceschini, and Enrico Gratton. Frequency-domain method for measuring spectral properties in multiple-scattering media: methemoglobin absorption spectrum in a tissuelike phantom. *Applied Optics*, 34(7):1143–1155, 1995.

[48] Rodrigo M Forti, Christopher G Favilla, Jeffrey M Cochran, Wesley B Baker, John A Detre, Scott E Kasner, Michael T Mullen, Steven R Messé, W Andrew Kofke, Ramani Balu, et al. Transcranial optical monitoring of cerebral hemodynamics in acute stroke patients during mechanical thrombectomy. *Journal of Stroke and Cerebrovascular Diseases*, 28(6):1483–1494, 2019.

[49] Maria Angela Franceschini, K Thomas Moesta, Sergio Fantini, Gerhard Gaida, Enrico Gratton, Helge Jess, William W Mantulin, Marcel Seeber, Peter M Schlag, and Michael Kaschke. Frequency-domain techniques enhance optical mammography: initial clinical results. *Proceedings of the National Academy of Sciences*, 94(12):6468–6473, 1997.

[50] Maria Angela Franceschini, Vlad Toronov, Mattia E Filiaci, Enrico Gratton, and Sergio Fantini. On-line optical imaging of the human brain with 160-ms temporal resolution. *Optics express*, 6(3):49–57, 2000.

[51] E Gratton and WW Mantulin. Mj vandeven, jb fishkin, mb maris, and b. chance. In *The possibility of a near-infrared optical imaging system using frequencydomain methods", In Proceedings of the Third International Conference on Peace through Mind@ Brain Science*, pages 183–189, 1990.

[52] Angela R Harrivel, Daniel H Weissman, Douglas C Noll, and Scott J Peltier. Monitoring attentional state with fnirs. *Frontiers in human neuroscience*, 7:861, 2013.

[53] Louis G Henyey and Jesse Leonard Greenstein. Diffuse radiation in the galaxy. *The Astrophysical Journal*, 93:70–83, 1941.

[54] DM Hueber, MA Franceschini, HY Ma, Q Zhang, JR Ballesteros, S Fantini, D Wallace, V Ntziachristos, and B Chance. Non-invasive and quantitative near-infrared haemoglobin spectrometry in the piglet brain during hypoxic stress, using a frequency-domain multidistance instrument. *Physics in Medicine & Biology*, 46(1):41, 2001.

[55] Steven L Jacques. Time-resolved reflectance spectroscopy in turbid tissues. *IEEE Transactions on Biomedical Engineering*, 36(12):1155–1161, 1989.

[56] Steven L Jacques and Brian W Pogue. Tutorial on diffuse light transport. *Journal of biomedical optics*, 13(4):041302, 2008.

[57] Franck Jaillon, Jun Li, Gregor Dietsche, Thomas Elbert, and Thomas Gisler. Activity of the human visual cortex measured non-invasively by diffusing-wave spectroscopy. *Optics Express*, 15(11):6643–6650, 2007.

[58] Dorota B Jakubowski, Albert E Cerussi, Frédéric P Bevilacqua, Natasha Shah, David Hsiang, John A Butler, and Bruce J Tromberg. Monitoring neoadjuvant chemotherapy in breast cancer using quantitative diffuse optical spectroscopy: a case study. *Journal of biomedical optics*, 9(1):230–238, 2004.

[59] Frans F Jöbsis. Noninvasive, infrared monitoring of cerebral and myocardial oxygen sufficiency and circulatory parameters. *Science*, 198(4323):1264–1267, 1977.

[60] Frans F Jobsis-vander Vliet. Discovery of the near-infrared window into the body and the early development of near-infrared spectroscopy. *Journal of biomedical optics*, 4(4):392–396, 1999.

[61] Frans F Jobsis-vander Vliet and Paul Joebsis. Biochemical and physiological basis of medical near-infrared spectroscopy. *Journal of biomedical optics*, 4(4):397–402, 1999.

[62] Justin Jung, Raeef Istfan, and Darren Roblyer. Effect of modulation frequency bandwidth on measurement accuracy and precision for digital diffuse optical spectroscopy (ddos). In *Design and Quality for Biomedical Technologies VII*, volume 8936, pages 113–119. SPIE, 2014.

[63] Justin Jung, Raeef Istfan, and Darren Roblyer. Note: A simple broad bandwidth undersampling frequency-domain digital diffuse optical spectroscopy system. *Review of Scientific Instruments*, 85(7):076108, 2014.

[64] Hasan Onur Keles, Randall L Barbour, and Ahmet Omurtag. Hemodynamic correlates of spontaneous neural activity measured by human whole-head resting state eeg+ fnirs. *Neuroimage*, 138:76–87, 2016.

[65] Meeri N Kim, Turgut Durduran, Suzanne Frangos, Brian L Edlow, Erin M Buckley, Heather E Moss, Chao Zhou, Guoqiang Yu, Regine Choe, Eileen Maloney-Wilensky, et al. Noninvasive measurement of cerebral blood flow and blood oxygenation using near-infrared and diffuse correlation spectroscopies in critically brain-injured adults. *Neurocritical care*, 12(2):173–180, 2010.

[66] Vincent J Kitsmiller, Matthew M Dummer, Klein Johnson, Garrett D Cole, and Thomas D O'Sullivan. Frequency domain diffuse optical spectroscopy with a near-infrared tunable vertical cavity surface emitting laser. *Optics express*, 26(16):21033–21043, 2018.

[67] Sarah Lloyd-Fox, Anna Blasi, and CE Elwell. Illuminating the developing brain: the past, present and future of functional near infrared spectroscopy. *Neuroscience & Biobehavioral Reviews*, 34(3):269–284, 2010.

[68] Milan Malinsky, Michael Jermyn, Brian W Pogue, and Hamid Dehghani. An online modeling and image reconstruction tool for optical imaging based on nirfast. In *Biomedical Optics*, page BSuD27. Optical Society of America, 2010.

[69] Donna M Mancini, Lizann Bolinger, Hao Li, Keith Kendrick, Britton Chance, and John R Wilson. Validation of near-infrared spectroscopy in humans. *Journal of Applied Physiology*, 77(6):2740–2747, 1994.

[70] Troy O McBride, Brian W Pogue, Shudong Jiang, Ulf L Österberg, and Keith D Paulsen. A parallel-detection frequency-domain near-infrared tomography system for hemoglobin imaging of the breast in vivo. *Review of Scientific Instruments*, 72(3):1817–1824, 2001.

[71] Rickson C Mesquita, Olufunsho K Faseyitan, Peter E Turkeltaub, Erin M Buckley, Amy Thomas, Meeri N Kim, Turgut Durduran, Joel H Greenberg, John A Detre, Arjun G Yodh, et al. Blood flow and oxygenation changes due to low-frequency repetitive transcranial magnetic stimulation of the cerebral cortex. *Journal of Biomedical Optics*, 18(6):067006, 2013.

[72] Penaz Parveen Sultana Mohammad. *Quantitative measurement of cerebral hemodynamics during activation of auditory cortex with single-and multi-distance near infrared spectroscopy*. University of South Florida, 2018.

[73] Penaz Parveen Sultana Mohammad, Sittiprapa Isarangura, Ann Eddins, and Ashwin B Parthasarathy. Comparison of functional activation responses from the auditory cortex derived using multi-distance frequency domain and continuous wave near-infrared spectroscopy. *Neurophotonics*, 8(4):045004, 2021.

[74] Penaz Parveen Sultana Mohammad, Sadhu Moka, and Ashwin B Parthasarathy. Comparison of continuous wave and frequency domain functional near infrared spectroscopy estimates of focal hemodynamic changes with finite element simulations. In *Optics and the Brain*, pages JW3A–38. Optical Society of America, 2020.

[75] Sadhu Moka, Penaz PS Mohammad, Abdul Mohaimen Safi, Ann Eddins, and Ashwin B Parthasarathy. Estimation of static and dynamic tissue optical properties using frequency domain diffuse correlation spectroscopy. In *Optical Tomography and Spectroscopy*, pages OM4D–2. Optica Publishing Group, 2022.

[76] Sadhu Moka, Abdul Mohaimen Safi, Penaz Parveen Sultana Mohammad, Ann Eddins, and Ashwin B Parthasarathy. Frequency domain diffuse correlation spectroscopy: a new method for simultaneous estimation of static and dynamic tissue optical properties. In *Multiscale Imaging and Spectroscopy III*, volume 11944, pages 52–57. SPIE, 2022.

[77] Sadhu Moka, Abdul Mohaimen Safi, Penaz PS Mohammad, and Ashwin B Parthasarathy. Broadband frequency domain diffuse optical spectroscopy with heterodyne demodulation. In *Optics and the Brain*, pages JW3A–16. Optica Publishing Group, 2020.

[78] Rami Nachabe, Benno HW Hendriks, Adrien E Desjardins, Marjolein van der Voort, Martin B van der Mark, and Henricus JCM Sterenborg. Estimation of lipid and water concentrations in scattering media with diffuse optical spectroscopy from 900 to 1600 nm. *Journal of biomedical optics*, 15(3):037015, 2010.

[79] Keun-Sik No, Richard Y Kwong, Pai H Chou, and Albert E Cerussi. Design and testing of a miniature broadband frequency domain photon migration instrument. *Journal of biomedical optics*, 13(5):050509, 2008.

[80] M Pagliazzi, S Konugolu Venkata Sekar, L Colombo, E Martinenghi, J Minnema, R Erdmann, D Contini, A Dalla Mora, A Torricelli, A Pifferi, et al. Time domain diffuse correlation spectroscopy with a high coherence pulsed source: in vivo and phantom results. *Biomedical optics express*, 8(11):5311–5325, 2017.

[81] Michael S Patterson, Britton Chance, and Brian C Wilson. Time resolved reflectance and transmittance for the noninvasive measurement of tissue optical properties. *Applied optics*, 28(12):2331–2336, 1989.

[82] Tuan H Pham, Olivier Coquoz, Joshua B Fishkin, Eric Anderson, and Bruce J Tromberg. Broad bandwidth frequency domain instrument for quantitative tissue optical spectroscopy. *Review of scientific instruments*, 71(6):2500–2513, 2000.

[83] Antonio Pifferi, Johannes Swartling, Ekaterine Chikoidze, Alessandro Torricelli, Paola Taroni, Andrea Li Bassi, Stefan Andersson-Engels, and Rinaldo Cubeddu. Spectroscopic time-resolved diffuse reflectance and transmittance measurements of the female breast at different interfiber distances. *Journal of biomedical optics*, 9(6):1143–1151, 2004.

[84] Brian W Pogue and Michael S Patterson. Frequency-domain optical absorption spectroscopy of finite tissue volumes using diffusion theory. *Physics in medicine & biology*, 39(7):1157, 1994.

[85] Brian W Pogue, Markus Testorf, Troy McBride, Ulf Osterberg, and Keith Paulsen. Instrumentation and design of a frequency-domain diffuse optical tomography imager for breast cancer detection. *Optics express*, 1(13):391–403, 1997.

[86] Darren Roblyer, Thomas D O'Sullivan, Robert V Warren, and Bruce J Tromberg. Feasibility of direct digital sampling for diffuse optical frequency domain spectroscopy in tissue. *Measurement Science and Technology*, 24(4):045501, 2013.

[87] Nadège Roche-Labarbe, Stefan A Carp, Andrea Surova, Megha Patel, David A Boas, P Ellen Grant, and Maria Angela Franceschini. Noninvasive optical measures of cbv, sto2, cbf index, and rcmro2 in human premature neonates' brains in the first six weeks of life. *Human brain mapping*, 31(3):341–352, 2010.

[88] Nadege Roche-Labarbe, Angela Fenoglio, Harsha Radhakrishnan, Marcia Kocienski-Filip, Stefan A Carp, Jay Dubb, David A Boas, P Ellen Grant, and Maria Angela Franceschini. Somatosensory evoked changes in cerebral oxygen consumption measured non-invasively in premature neonates. *Neuroimage*, 85:279–286, 2014.

[89] Saeed Samaei, Piotr Sawosz, Michał Kacprzak, Żanna Pastuszak, Dawid Borycki, and Adam Liebert. Time-domain diffuse correlation spectroscopy (td-dcs) for noninvasive, depth-dependent blood flow quantification in human tissue in vivo. *Scientific reports*, 11(1):1–10, 2021.

[90] Felix Scholkmann, Stefan Kleiser, Andreas Jaakko Metz, Raphael Zimmermann, Juan Mata Pavia, Ursula Wolf, and Martin Wolf. A review on continuous wave functional near-infrared spectroscopy and imaging instrumentation and methodology. *Neuroimage*, 85:6–27, 2014.

[91] Natasha Shah, Albert E Cerussi, Dorota Jakubowski, David Hsiang, John Butler, and Bruce J Tromberg. The role of diffuse optical spectroscopy in the clinical management of breast cancer. *Disease markers*, 19(2-3):95–105, 2004.

[92] AM Siegel, JJA Marota, and David A Boas. Design and evaluation of a continuous-wave diffuse optical tomography system. *Optics express*, 4(8):287–298, 1999.

[93] S. Y. Siew, B. Li, F. Gao, H. Y. Zheng, W. Zhang, P. Guo, S. W. Xie, A. Song, B. Dong, L. W. Luo, C. Li, X. Luo, and G.-Q. Lo. Review of silicon photonics technology and platform development. *Journal of Lightwave Technology*, 39(13):4374–4389, 2021.

[94] Hany Soliman, Anoma Gunasekara, Mary Rycroft, Judit Zubovits, Rebecca Dent, Jacqueline Spayne, Martin J Yaffe, and Gregory J Czarnota. Functional imaging using diffuse optical spectroscopy of neoadjuvant chemotherapy response in women with locally advanced breast cancer. *Clinical cancer research*, 16(9):2605–2614, 2010.

[95] Roy A Stillwell, Vincent J Kitsmiller, Alicia Y Wei, Alyssa Chong, Lyla Senn, and Thomas D O'Sullivan. A scalable, multi-wavelength, broad bandwidth frequency-domain near-infrared spectroscopy platform for real-time quantitative tissue optical imaging. *Biomedical optics express*, 12(11):7261–7279, 2021.

[96] Gary E Strangman, Zhi Li, and Quan Zhang. Depth sensitivity and source-detector separations for near infrared spectroscopy based on the colin27 brain template. *PloS one*, 8(8):e66319, 2013.

[97] Jason Sutin, Bernhard Zimmerman, Danil Tyulmankov, Davide Tamborini, Kuan Cheng Wu, Juliette Selb, Angelo Gulinatti, Ivan Rech, Alberto Tosi, David A Boas, et al. Time-domain diffuse correlation spectroscopy. *Optica*, 3(9):1006–1013, 2016.

[98] Glen M Tellis, Rickson C Mesquita, and AG Yodh. Use of diffuse correlation spectroscopy to measure brain blood flow differences during speaking and nonspeaking tasks for fluent speakers and persons who stutter. *Perspectives on Fluency and Fluency Disorders*, 21(3):96–106, 2011.

[99] Alyssa Torjesen, Raeef Istfan, and Darren Roblyer. Ultrafast wavelength multiplexed broad bandwidth digital diffuse optical spectroscopy for in vivo extraction of tissue optical properties. *Journal of biomedical optics*, 22(3):036009, 2017.

[100] Bruce J Tromberg, Olivier Coquoz, Joshua B Fishkin, Eric R Anderson, David Pham, Matthew Brenner, and Lars O Svaasand. Frequency-domain photon migration (fdpm) measurements of normal and malignant cell and tissue optical properties. In *Biomedical Optical Spectroscopy and Diagnostics*, page AP13. Optica Publishing Group, 1996.

[101] Bruce J Tromberg, Lars Othar Svaasand, Tsong-Tseh Tsay, Richard Campbell Haskell, and Michael W Berns. Optical property measurements in turbid media using frequency-domain photon migration. In *Future Trends in Biomedical Applications of Lasers*, volume 1525, pages 52–58. SPIE, 1991.

[102] Sheng-Hao Tseng, Alexander Grant, and Anthony Joseph Durkin. In vivo determination of skin near-infrared optical properties using diffuse optical spectroscopy. *Journal of biomedical optics*, 13(1):014016, 2008.

[103] Arno Villringer and Britton Chance. Non-invasive optical spectroscopy and imaging of human brain function. *Trends in neurosciences*, 20(10):435–442, 1997.

[104] Udo M Weigel, Rubén B Revilla, Nestor H Oliverio, Alberto A González, Jose C Cifuentes, Peyman Zirak, Ricardo Saiz, Daniel Mitrani, Jordi Ninou, Oscar Casellas, et al. A new, modular frequency domain diffuse optical monitor in the digital domain. In *Biomedical Optics*, pages JM3A–36. Optica Publishing Group, 2012.

[105] Martin Wolf, Marco Ferrari, and Valentina Quaresima. Progress of near-infrared spectroscopy and topography for brain and muscle clinical applications. *Journal of biomedical optics*, 12(6):062104, 2007.

[106] Yunsong Yang, Hanli Liu, Xingde Li, and Britton Chance. Low-cost frequency-domain photon migration instrument for tissue spectroscopy, oximetry, and imaging. *Optical Engineering*, 36(5):1562–1569, 1997.

[107] Arjun Yodh and Britton Chance. Spectroscopy and imaging with diffusing light. *Physics today*, 48(3):34–41, 1995.

[108] Sean C Youn. Characterization of diffuse optical tomography scans using nirfast. 2015.

[109] Bing Yu, Elizabeth S Burnside, Gale A Sisney, Josephine M Harter, Changfang Zhu, Al-Hafeez Dhalla, and Nirmala Ramanujam. Feasibility of near-infrared diffuse optical spectroscopy on patients undergoing image-guided core-needle biopsy. *Optics express*, 15(12):7335–7350, 2007.

[110] Guoqiang Yu, Turgut Durduran, Gwen Lech, Chao Zhou, Britton Chance, Emile R Mohler, and Arjun G Yodh. Time-dependent blood flow and oxygenation in human skeletal muscles measured with noninvasive near-infrared diffuse optical spectroscopies. *Journal of biomedical optics*, 10(2):024027, 2005.

[111] Meryem A Yücel, Juliette Selb, Christopher M Aasted, Pei-Yi Lin, David Borsook, Lino Becerra, and David A Boas. Mayer waves reduce the accuracy of estimated hemodynamic response functions in functional near-infrared spectroscopy. *Biomedical optics express*, 7(8):3078–3088, 2016.

[112] Bernhard B Zimmermann, Bin Deng, Bhawana Singh, Mark Martino, Juliette J Selb, Qianqian Fang, Amir Y Sajjadi, Jayne A Cormier, Richard H Moore, Daniel B Kopans, et al. Multimodal breast cancer imaging using coregistered dynamic diffuse optical tomography and digital breast tomosynthesis. *Journal of Biomedical Optics*, 22(4):046008, 2017.

[113] Bernhard B Zimmermann, Qianqian Fang, David A Boas, and Stefan A Carp. Frequency domain near-infrared multiwavelength imager design using high-speed, direct analog-to-digital conversion. *Journal of biomedical optics*, 21(1):016010, 2016.

Appendix A: Copyright Permissions

The permission below is for the reproduction of Figure 2.1

Thank you for your order with RightsLink / Elsevier

no-reply@email.copyright.com <no-reply@email.copyright.com>
Mon 10/17/2022 8:30 PM
To: Sadhu Moka <sundarsingh@usf.edu>

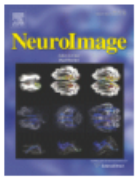

Thank you for your order!

Dear Mr. Sadhu Moka,

Thank you for placing your order through Copyright Clearance Center's RightsLink® service.

Order Summary

Licensee:	Mr. Sadhu Moka
Order Date:	Oct 17, 2022
Order Number:	5411630151560
Publication:	NeuroImage
Title:	A review on continuous wave functional near-infrared spectroscopy and imaging instrumentation and methodology
Type of Use:	reuse in a thesis/dissertation
Order Ref:	0143
Order Total:	0.00 USD

View or print complete details of your order and the publisher's terms and conditions.

Sincerely,

Copyright Clearance Center

The permission below is for the reproduction of Figure 2.2 and 3.2

Re: [External]Copyright permission to use figures

Baker, Wesley <BAKERW@chop.edu>
Wed 10/12/2022 7:07 PM
To: Sadhu Moka <sundarsingh@usf.edu>;wbb5uva@gmail.com <wbb5uva@gmail.com>
Cc: Ashwin Parthasarathy <ashwinbp@usf.edu>
Hi,

Please feel free to use any figures you like from my thesis.

Thanks,
Wes

From: Sadhu Moka <sundarsingh@usf.edu>
Sent: Tuesday, October 11, 2022 11:41 AM
To: Baker, Wesley <BAKERW@chop.edu>; wbb5uva@gmail.com <wbb5uva@gmail.com>
Cc: Ashwin Parthasarathy <ashwinbp@usf.edu>
Subject: [External]Copyright permission to use figures

You don't often get email from sundarsingh@usf.edu. Learn why this is important

Dr. Baker,

Hope you are doing well.
I'm a Ph.D. candidate in Dr. Ashwin's lab. I'm writing my dissertation ('Frequency Domain Diffuse Optics Spectroscopies for quantitative measurement of Tissue Optical Properties') and hope to graduate this December. I wanted to see if I could use some figures from your dissertation. I attached the ones I chose that aren't published by any other journal.

Please let me know either way.

Thank you,
Sadhu Moka
Ph.D Candidate, Department of Electrical Engineering
Translational Optics Imaging and Spectroscopy Laboratory
http://tropics.eng.usf.edu/
University of South Florida
Cell: 813-947-9747
E mail : sundarsingh@usf.edu

From: Assistant General Counsel / Copyright Advisor <copyright@upenn.libanswers.com>
Sent: Wednesday, September 21, 2022 2:26 PM
To: Sadhu Moka <sundarsingh@usf.edu>
Subject: [Copyright] Copyright permission to use figures

--# Type your reply above this line #--

Sep 21 2022, 02:26pm via Email
Good afternoon Sadhu Moka,

Unfortunately, I am not the correct contact for this inquiry, but as a courtesy to you I looked at the attached link you sent to see if I can share some information with you about how you might be able to obtain the permission that you are seeking. The default arrangement at Penn is that graduate students retain the copyright to their dissertations provided the work is creative and original to them (not copied from somewhere else). From your note it was not clear to me what figures you were referring to and if the figures were created by the author, or if the author, Wesley Boehs Baker, received permission to use them and include them within his dissertation from a third-party copyright holder. I would suggest reaching out to Dr. Baker directly (wbb5uva@gmail.com<mailto:wbb5uva@gmail.com>) to find out if he is the creator and/or copyright-holder of those figures and seek or his permission if he is. If he is not the copyright-holder, hopefully he can point you in the right direction. If you need some resources on seeking permission or drafting a permission's letter, Penn's standard guide is available at this link - https://guides.library.upenn.edu/copyright/permission.

The permission below is for the reproduction of Figure 2.4 and 3.1

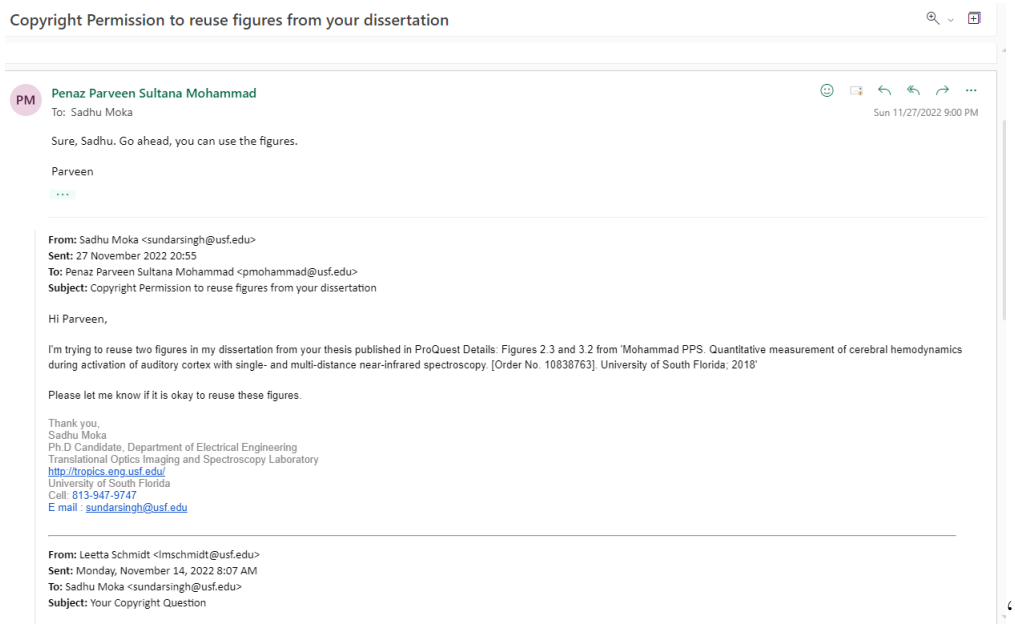

Copyright Permission to reuse figures from your dissertation

PM **Penaz Parveen Sultana Mohammad**
To: Sadhu Moka
Sun 11/27/2022 9:00 PM

Sure, Sadhu. Go ahead, you can use the figures.

Parveen

...

From: Sadhu Moka <sundarsingh@usf.edu>
Sent: 27 November 2022 20:55
To: Penaz Parveen Sultana Mohammad <pmohammad@usf.edu>
Subject: Copyright Permission to reuse figures from your dissertation

Hi Parveen,

I'm trying to reuse two figures in my dissertation from your thesis published in ProQuest Details: Figures 2.3 and 3.2 from 'Mohammad PPS. Quantitative measurement of cerebral hemodynamics during activation of auditory cortex with single- and multi-distance near-infrared spectroscopy. [Order No. 10838763]. University of South Florida; 2018'

Please let me know if it is okay to reuse these figures.

Thank you,
Sadhu Moka
Ph.D Candidate, Department of Electrical Engineering
Translational Optics Imaging and Spectroscopy Laboratory
http://tropics.eng.usf.edu/
University of South Florida
Cell: 813-947-9747
E mail : sundarsingh@usf.edu

From: Leetta Schmidt <lmschmidt@usf.edu>
Sent: Monday, November 14, 2022 8:07 AM
To: Sadhu Moka <sundarsingh@usf.edu>
Subject: Your Copyright Question

The permission below is for the reproduction of Figure 2.9

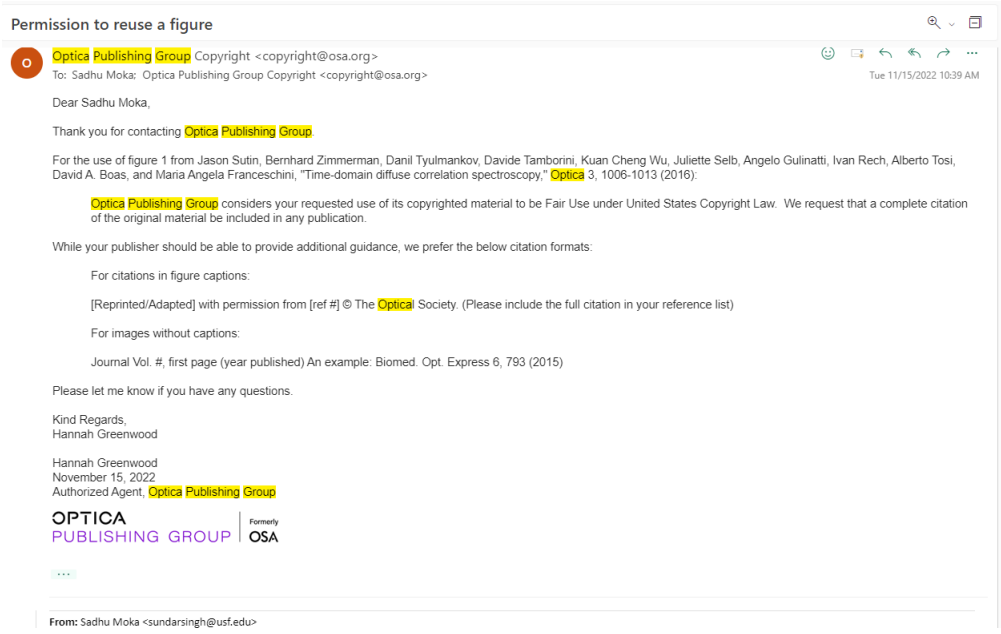

Permission to reuse a figure

Optica Publishing Group Copyright <copyright@osa.org>
To: Sadhu Moka; Optica Publishing Group Copyright <copyright@osa.org>
Tue 11/15/2022 10:39 AM

Dear Sadhu Moka,

Thank you for contacting Optica Publishing Group.

For the use of figure 1 from Jason Sutin, Bernhard Zimmerman, Danil Tyulmankov, Davide Tamborini, Kuan Cheng Wu, Juliette Selb, Angelo Gulinatti, Ivan Rech, Alberto Tosi, David A. Boas, and Maria Angela Franceschini, "Time-domain diffuse correlation spectroscopy," Optica 3, 1006-1013 (2016):

> Optica Publishing Group considers your requested use of its copyrighted material to be Fair Use under United States Copyright Law. We request that a complete citation of the original material be included in any publication.

While your publisher should be able to provide additional guidance, we prefer the below citation formats:

> For citations in figure captions:
>
> [Reprinted/Adapted] with permission from [ref #] © The Optical Society. (Please include the full citation in your reference list)
>
> For images without captions:
>
> Journal Vol. #, first page (year published) An example: Biomed. Opt. Express 6, 793 (2015)

Please let me know if you have any questions.

Kind Regards,
Hannah Greenwood

Hannah Greenwood
November 15, 2022
Authorized Agent, Optica Publishing Group

OPTICA PUBLISHING GROUP | Formerly OSA

...

From: Sadhu Moka <sundarsingh@usf.edu>

The permission below is for the reproduction of content in chapter 3 and Chapter 4

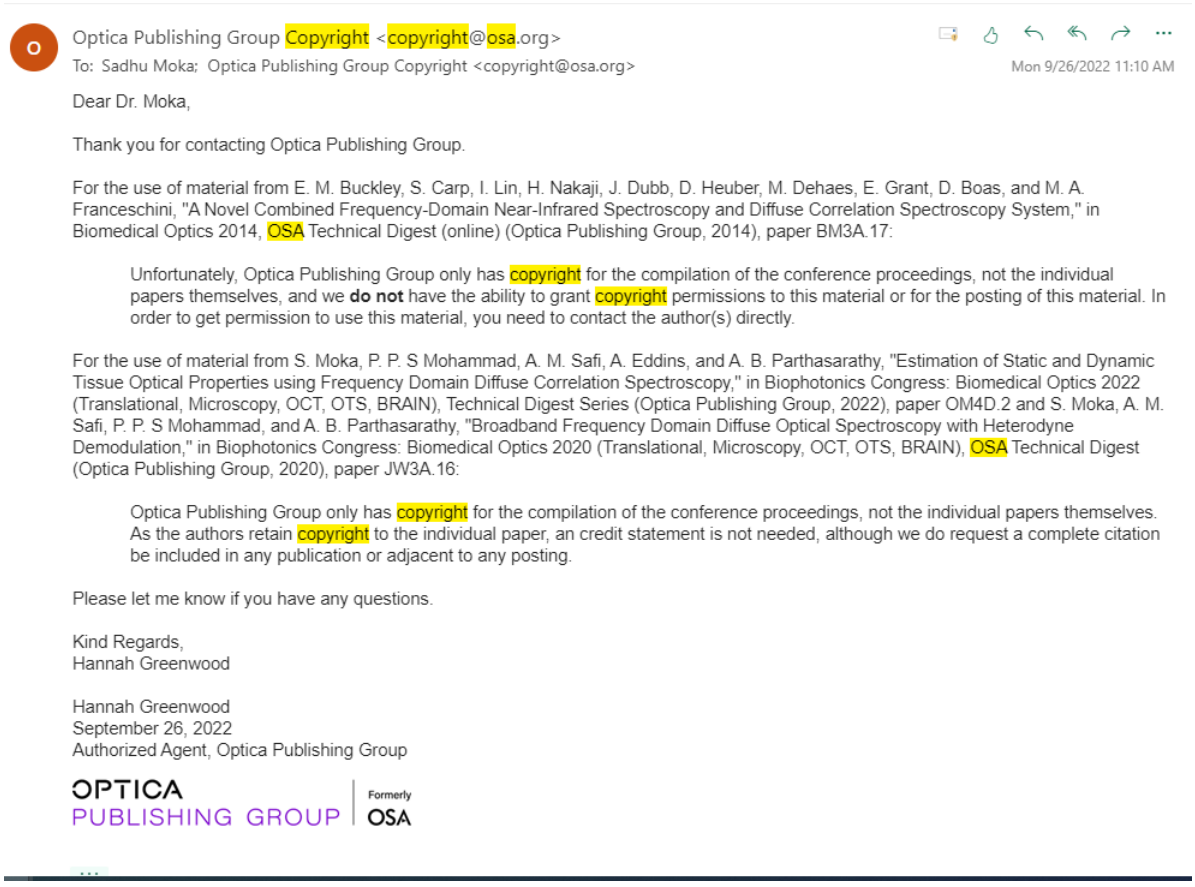

Optica Publishing Group Copyright <copyright@osa.org>
To: Sadhu Moka; Optica Publishing Group Copyright <copyright@osa.org>
Mon 9/26/2022 11:10 AM

Dear Dr. Moka,

Thank you for contacting Optica Publishing Group.

For the use of material from E. M. Buckley, S. Carp, I. Lin, H. Nakaji, J. Dubb, D. Heuber, M. Dehaes, E. Grant, D. Boas, and M. A. Franceschini, "A Novel Combined Frequency-Domain Near-Infrared Spectroscopy and Diffuse Correlation Spectroscopy System," in Biomedical Optics 2014, OSA Technical Digest (online) (Optica Publishing Group, 2014), paper BM3A.17:

> Unfortunately, Optica Publishing Group only has copyright for the compilation of the conference proceedings, not the individual papers themselves, and we **do not** have the ability to grant copyright permissions to this material or for the posting of this material. In order to get permission to use this material, you need to contact the author(s) directly.

For the use of material from S. Moka, P. P. S Mohammad, A. M. Safi, A. Eddins, and A. B. Parthasarathy, "Estimation of Static and Dynamic Tissue Optical Properties using Frequency Domain Diffuse Correlation Spectroscopy," in Biophotonics Congress: Biomedical Optics 2022 (Translational, Microscopy, OCT, OTS, BRAIN), Technical Digest Series (Optica Publishing Group, 2022), paper OM4D.2 and S. Moka, A. M. Safi, P. P. S Mohammad, and A. B. Parthasarathy, "Broadband Frequency Domain Diffuse Optical Spectroscopy with Heterodyne Demodulation," in Biophotonics Congress: Biomedical Optics 2020 (Translational, Microscopy, OCT, OTS, BRAIN), OSA Technical Digest (Optica Publishing Group, 2020), paper JW3A.16:

> Optica Publishing Group only has copyright for the compilation of the conference proceedings, not the individual papers themselves. As the authors retain copyright to the individual paper, an credit statement is not needed, although we do request a complete citation be included in any publication or adjacent to any posting.

Please let me know if you have any questions.

Kind Regards,
Hannah Greenwood

Hannah Greenwood
September 26, 2022
Authorized Agent, Optica Publishing Group

OPTICA PUBLISHING GROUP | Formerly OSA

The permission below is for the reproduction of content in chapter 4

RE: Permission to reuse material

Karleena Burdick <karleenab@spie.org>
Mon 9/19/2022 3:32 PM

To: Sadhu Moka <sundarsingh@usf.edu>

Dear Sadhu Moka,

Thank you for seeking permission from SPIE to reprint material from our publications. SPIE shares the copyright with you, so as author you retain the right to reproduce your paper in part or in whole.

Publisher's permission is hereby granted under the following conditions:
(1) the material to be used has appeared in our publication without credit or acknowledgment to another source; and
(2) you credit the original SPIE publication. Include the authors' names, title of paper, volume title, SPIE volume number, and year of publication in your credit statement.

Please let me know if I may be of any further assistance.

Best,
Karleena Burdick
Editorial Assistant, Publications
SPIE – the international society for optics and photonics
karleenab@spie.org
1 360 685 5515
SPIE.

From: Sadhu Moka <sundarsingh@usf.edu>
Sent: Monday, September 19, 2022 9:59 AM
To: reprint_permission <reprint_permission@spie.org>
Subject: Permission to reuse material

Hello,

I wanted to reach out to seek permission to reuse the following publications in my dissertation(will be published by ProQuest)

Sadhu Moka, Abdul Mohaimen Safi, Penaz Parveen Sultana Mohammad, Ann Eddins, Ashwin B. Parthasarathy, "Frequency domain diffuse correlation spectroscopy: a new method for simultaneous estimation of static and dynamic tissue optical properties," Proc. SPIE 11944, Multiscale Imaging and Spectroscopy III, 1194409 (4 March 2022); https://doi.org/10.1117/12.2610115

Proceedings Volume 11944, Multiscale Imaging and Spectroscopy III; 1194409
(2022) https://doi.org/10.1117/12.2610115
Event: SPIE BiOS, 2022, San Francisco, California, United States

Thank you,
Sadhu Moka
Ph.D Candidate, Department of Electrical Engineering
Translational Optics Imaging and Spectroscopy Laboratory

The permission below is for the reproduction of Figure 4.1

Re: Copy right permission to reuse a figure

Buckley, Erin M <ebuckley6@gatech.edu>
Thu 10/13/2022 11:08 AM
To: Sadhu Moka <sundarsingh@usf.edu>
Cc: Ashwin Parthasarathy <ashwinbp@usf.edu>

No problem on my end as long as you cite our paper!

Erin M. Buckley, PhD (she/her/hers)
Assistant Professor
Wallace H. Coulter Department of Biomedical Engineering at Georgia Tech & Emory
Department of Pediatrics, Emory University
Health Sciences Research Building, Room E106
1760 Haygood Dr NE
Atlanta, GA 30322
Office: (404) 727-4323
Fax: (404) 727-9873
Website: https://sites.gatech.edu/buckley/

From: Sadhu Moka <sundarsingh@usf.edu>
Date: Thursday, October 13, 2022 at 11:07 AM
To: "Buckley, Erin M" <erin.buckley@bme.gatech.edu>
Cc: Ashwin Parthasarathy <ashwinbp@usf.edu>
Subject: Copy right permission to reuse a figure

Hello Dr. Buckley,

Hope you are doing well.
I'm a Ph.D. candidate in Dr. Ashwin's lab. I'm writing my dissertation ('Frequency Domain Diffuse Optics Spectroscopies for quantitative measurement of Tissue Optical Properties') and hope to graduate this December. I wanted to see if I could use figures 1 and 2 from your Paper

E. M. Buckley, S. Carp, I. Lin, H. Nakaji, J. Dubb, D. Heuber, M. Dehaes, E. Grant, D. Boas, and M. A. Franceschini, "A Novel Combined Frequency-Domain Near-Infrared Spectroscopy and Diffuse Correlation Spectroscopy System," in Biomedical Optics 2014, OSA Technical Digest (online) (Optica Publishing Group, 2014), paper BM3A.17:

I've attached the figure that I was hoping to use. Please let me know either way.

Thank you,
Sadhu Moka
Ph.D Candidate, Department of Electrical Engineering
Translational Optics Imaging and Spectroscopy Laboratory
http://tropics.eng.usf.edu/
University of South Florida
Cell: 813-947-9747
E mail : sundarsingh@usf.edu

From: Optica Publishing Group Copyright <copyright@osa.org>
Sent: Monday, September 26, 2022 11:10 AM
To: Sadhu Moka <sundarsingh@usf.edu>; Optica Publishing Group Copyright <copyright@osa.org>
Subject: RE: Copy right permission to reuse a figure

Dear Dr. Moka,

Thank you for contacting Optica Publishing Group.

For the use of material from E. M. Buckley, S. Carp, I. Lin, H. Nakaji, J. Dubb, D. Heuber, M. Dehaes, E. Grant, D. Boas, and M. A. Franceschini, "A Novel Combined Frequency-Domain Near-Infrared Spectroscopy and Diffuse Correlation Spectroscopy System," in Biomedical Optics 2014, OSA Technical Digest (online) (Optica Publishing Group, 2014), paper BM3A.17:

> Unfortunately, Optica Publishing Group only has copyright for the compilation of the conference proceedings, not the individual papers themselves, and we **do not** have the ability to grant copyright permissions to this material or for the posting of this material. In order to get permission to use this material, you need to contact the author(s) directly.

Appendix B: IRB Approval Pages

IRB approval for experiments performed in chapter 3 and 4 is given below.

UNIVERSITY of SOUTH FLORIDA

APPROVAL

January 14, 2021 This letter supersedes the letter dated November 23, 2020

Ashwin Parthasarathy
4202 E Fowler Ave
ENB 118
Tampa, FL 33620

Dear Dr. Ashwin Parthasarathy:

On 11/17/2020, the IRB reviewed and approved the following protocol:

Application Type:	Continuing Review
IRB ID:	Pro00039832_CR000001
Review Type:	Committee
Title:	Noninvasive monitoring of tissue hemodynamics with diffuse optical techniques
Funding:	None
IND, IDE, or HDE:	None
Approved Protocol and Consent(s)/Assent(s):	• Omnibus_IRB_V2_2_CleanCopy.pdf; • Omnibus Informed Consent V3 Clean Copy.pdf; Approved study documents can be found under the 'Documents' tab in the main study workspace. Use the stamped consent found under the 'Last Finalized' column under the 'Documents' tab.

The IRB approved the protocol from 11/17/2020 to 11/17/2021. Within 45 days of 11/17/2021, submit a continuing review/study closure request in BullsIRB by clicking Create Modification/CR.

If continuing review approval is not granted before the expiration date of 11/17/2021, approval of this protocol expires on that date.

In conducting this protocol you are required to follow the requirements listed in the INVESTIGATOR MANUAL (HRP-103).

Institutional Review Boards / Research Integrity & Compliance
FWA No. 00001669
University of South Florida / 3702 Spectrum Blvd., Suite 165 / Tampa, FL 33612 / 813-974-5638

UNIVERSITY of SOUTH FLORIDA

APPROVAL

November 30, 2021

Ashwin Parthasarathy
4202 E Fowler Ave
ENB 118
Tampa, FL 33620

Dear Dr. Ashwin Parthasarathy:

On 11/16/2021, the IRB reviewed and approved the following protocol:

Application Type:	Continuing Review
IRB ID:	Pro00039832_CR000002
Review Type:	Committee
Title:	Noninvasive monitoring of tissue hemodynamics with diffuse optical techniques
Funding:	None
IND, IDE, or HDE:	None
Approved Protocol and Consent:	• Omnibus_IRB_V2_2_CleanCopy.pdf; • Omnibus Informed Consent V3 Clean Copy.pdf; Approved study documents can be found under the 'Documents' tab in the main study workspace. Use the stamped consent found under the 'Last Finalized' column under the 'Documents' tab.

The IRB approved the protocol from 11/17/2021 to 11/17/2022. Within 45 days of 11/17/2022, submit a continuing review/study closure request in BullsIRB by clicking Create Modification/CR.

If continuing review approval is not granted before the expiration date of 11/17/2022, approval of this protocol expires on that date.

In conducting this protocol you are required to follow the requirements listed in the INVESTIGATOR MANUAL (HRP-103).

Appendix C: mfFDDOS Phantom Results

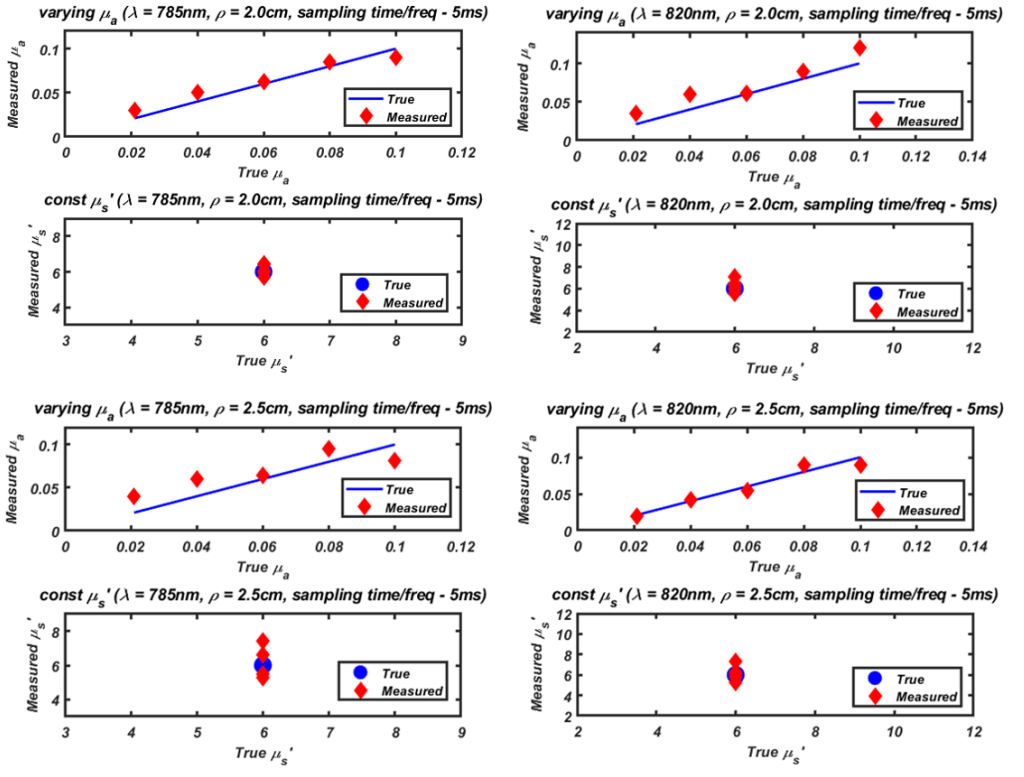

Figure C.1: Sensitivity of mfFD-DOS system to measuring absorption changes at 5ms sampling time. True absorption coefficient (varied) and scattering coefficient(constant) compared with measured values at source wavelength ($\lambda = 785nm \ \ and \ \ 820nm$), source detector separation ($\rho = 2.0cm \ \ and \ \ 2.5cm$) and a 5ms sampling time per modulating frequency

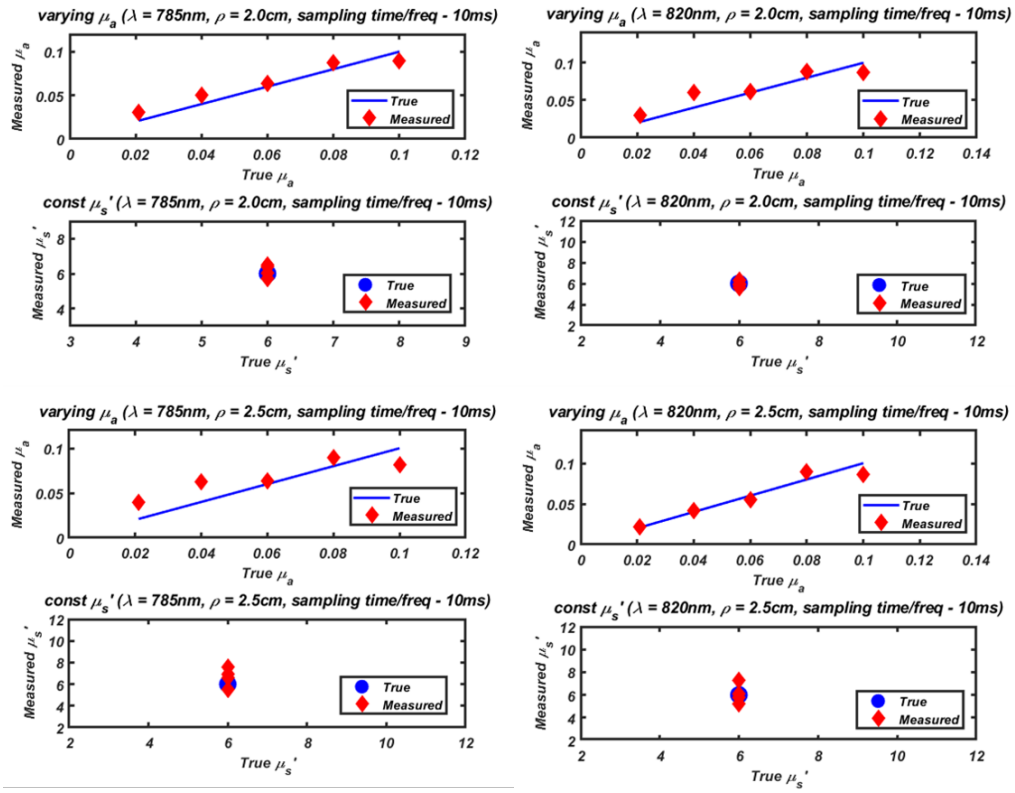

Figure C.2: Sensitivity of mfFD-DOS system to measuring absorption changes at 10ms sampling time. True absorption coefficient (varied) and scattering coefficient(constant) compared with measured values at source wavelength ($\lambda = 785nm \ \ and \ \ 820nm$), source detector separation ($\rho = 2.0cm \ \ and \ \ 2.5cm$) and a 10ms sampling time per modulating frequency

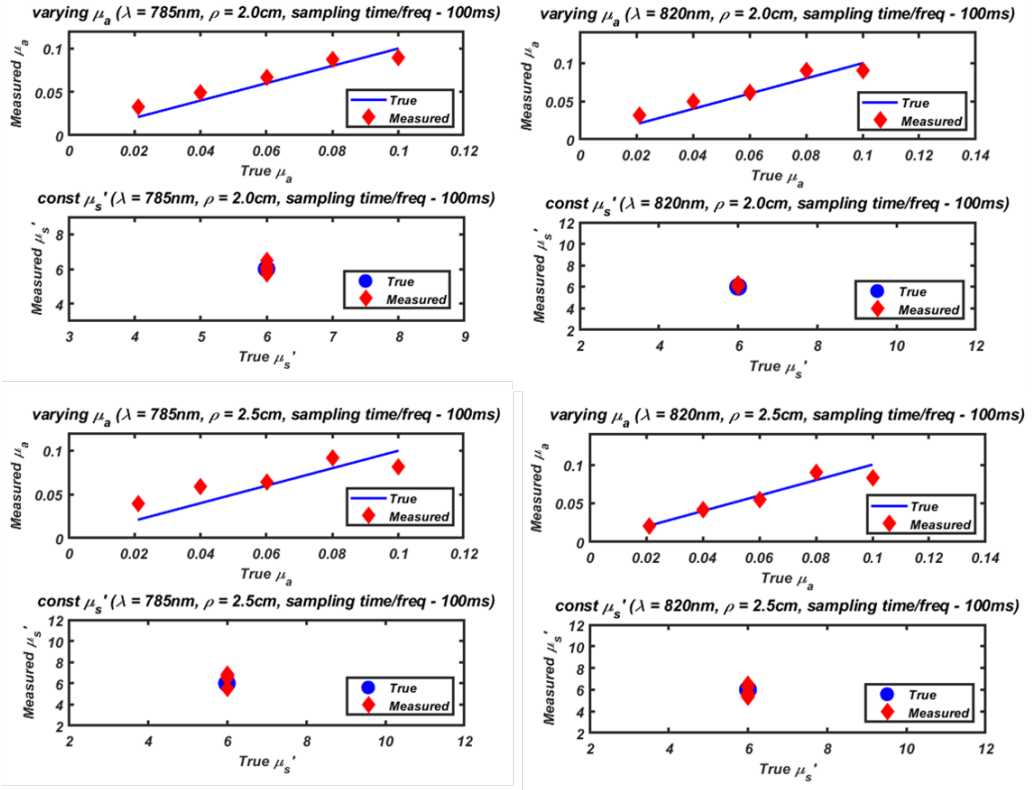

Figure C.3: Sensitivity of mfFD-DOS system to measuring absorption changes at 100ms sampling time. True absorption coefficient (varied) and scattering coefficient(constant) compared with measured values at source wavelength ($\lambda = 785nm \ \ and \ \ 820nm$), source detector separation ($\rho = 2.0cm \ \ and \ \ 2.5cm$) and a 100ms sampling time per modulating frequency

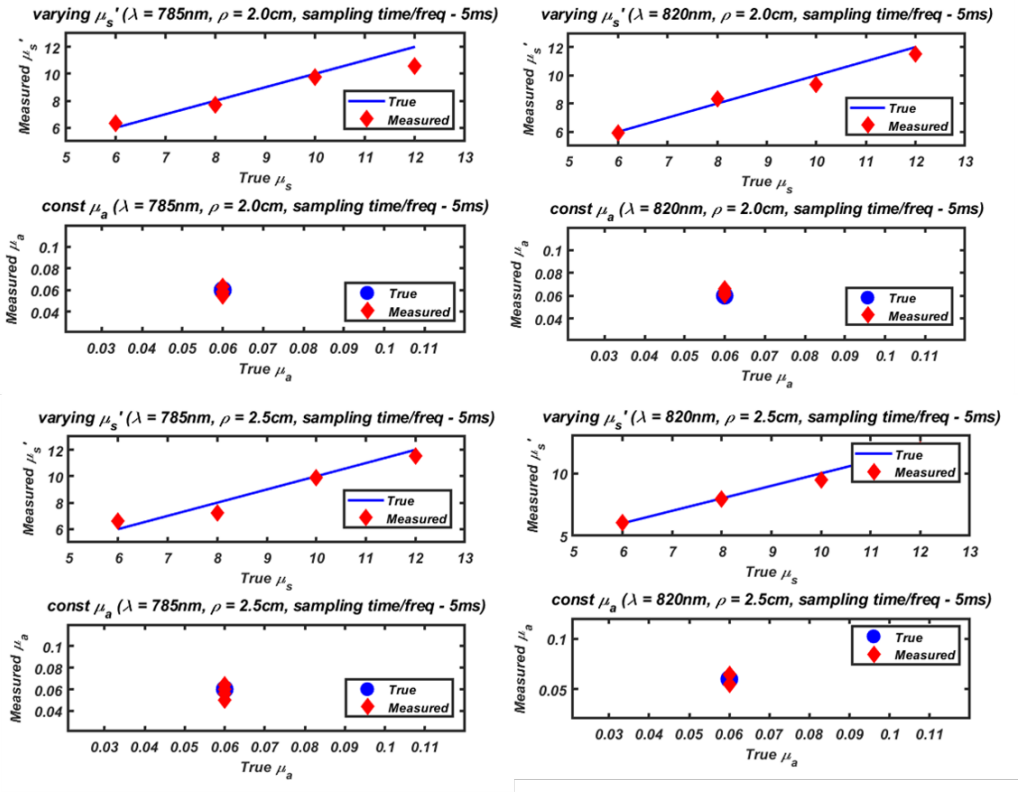

Figure C.4: Sensitivity of mfFD-DOS System to measuring scattering Changes at 5ms sampling time. True scattering coefficient (varied) and absorption coefficient(constant) compared with measured values at source wavelength ($\lambda = 785nm \ \ and \ \ 820nm$), source detector separation ($\rho = 2.0cm \ \ and \ \ 2.5cm$) and a 5ms sampling time per modulating frequency

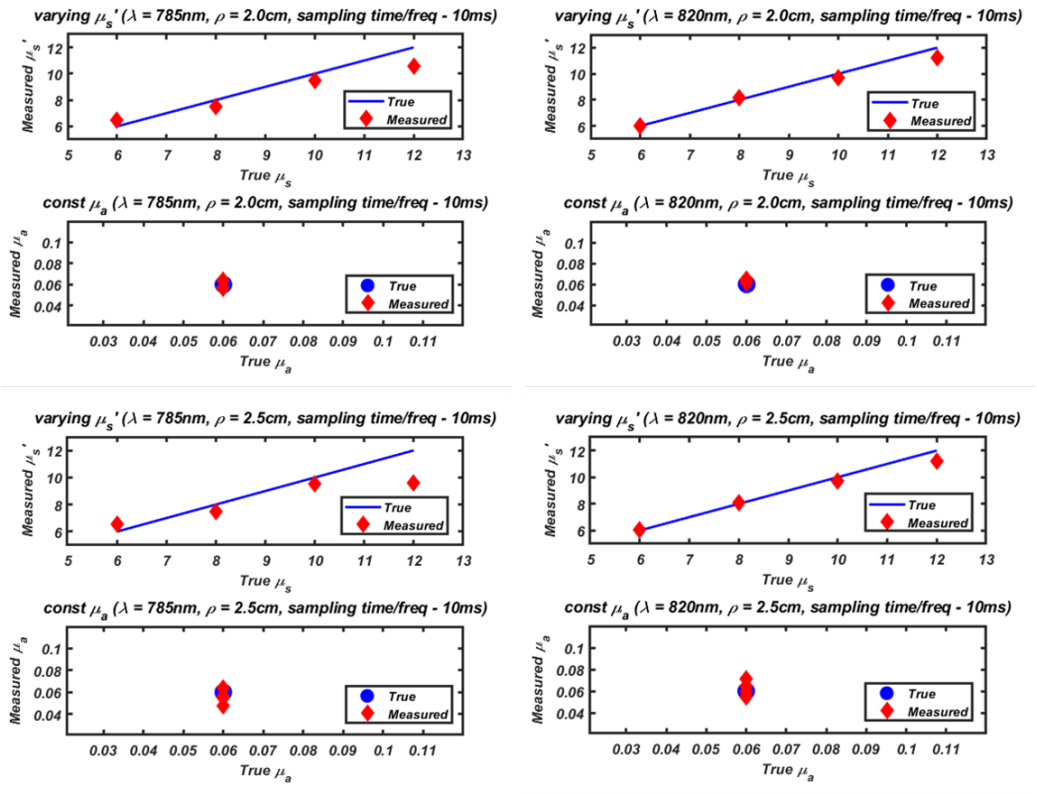

Figure C.5: Sensitivity of mfFD-DOS system to measuring scattering changes at 10ms sampling time. True scattering coefficient (varied) and absorption coefficient(constant) compared with measured values at source wavelength ($\lambda = 785nm \ \ and \ \ 820nm$), source detector separation ($\rho = 2.0cm \ \ and \ \ 2.5cm$) and a 10ms sampling time per modulating frequency

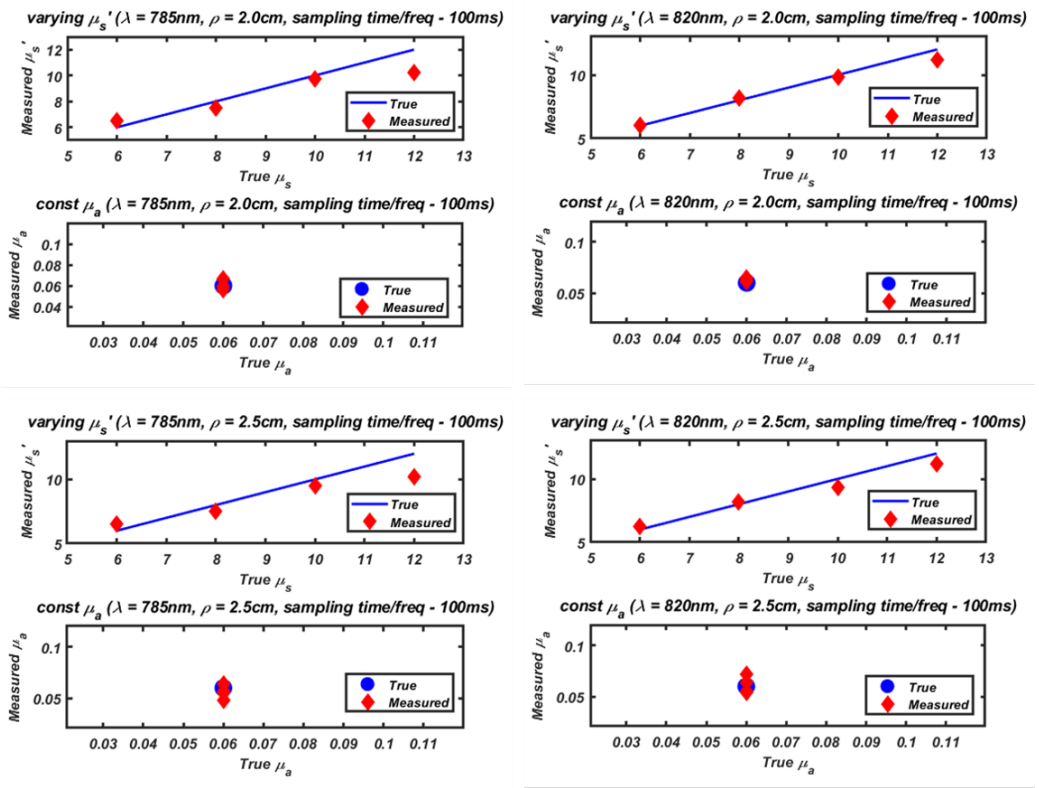

Figure C.6: Sensitivity of mfFD-DOS system to measuring scattering changes at 100ms sampling time. True scattering coefficient (varied) and absorption coefficient(constant) compared with measured values at source wavelength ($\lambda = 785nm \ \ and \ \ 820nm$), source detector separation ($\rho = 2.0cm \ \ and \ \ 2.5cm$) and a 100ms sampling time per modulating frequency

About the Author

Sadhu Moka is a doctoral candidate in Electrical Engineering at University of South Florida, graduating in Fall 2022. He has a Masters degree in Electrical Engineering from University of South Florida and another Masters degree in Digital Systems and Computer Electronics from Jawaharlal Nehru Technological University Hyderabad, India. He received his bachelors degree in Electronics and Communications Engineering from Jawaharlal Nehru Technological University Kakinada, India.

During his time at TROPICS Laboratory in USF, he has worked on development and advancement of biomedical instrumentation using diffuse optics for clinical and research use. In particular, he worked on applying frequency domain techniques on diffuse optics to improve the existing techniques. His skillset include Electro-optics, RF system design, system Engineering and development, optical alignment techniques, finite element simulations. His work has been recognized by several international and national awards including - best student paper award at SPIE Photonics West 2022, finalist for best student paper award at Optica Biophotonics Congress 2022, Dissertation Completion Fellowship, TiE University Global Business Hackathon Winner 2021, NSF I-Corps Fellow 2020, American Society for Engineering Education in 25 years Award 2019

He has also served as a teaching assistant at USF for the course EE Science II which deals with electro-magnetic theory. For his excellence in teaching, he has won the USF Provost's Award for Outstanding Teaching by a Graduate TA - Honorable Mention. Outside laboratory setting, He loves to play guitar, involve in church activities and volunteer for production, audio engineering. He also has a passion for photography and videography and loves to explore various places and cultures.